Biological Ion Transporters as Gating Devices for Chemomechanical and Chemoelectrical Energy Conversion

by

Vishnu Baba Sundaresan

Dissertation submitted to the Faculty of the
Virginia Polytechnic Institute and State University
in partial fulfillment of the requirements for the degree of

Doctor of Philosophy

in

Mechanical Engineering

Donald J. Leo, Chair
Daniel J. Inman
John Cuppoletti
Pavlos Vlachos
Lisa M Weiland
Mark Paul

15^{th} May 2007
Blacksburg, Virginia

Keywords: Chemomechanical energy conversion, chemoelectrical energy conversion, SUT4 cotransporter, ATPase enzymes, ATP

Copyright by Vishnu Baba Sundaresan, 2007

To Amma, Appa and Vivek

Biological Ion Transporters as Gating Devices for Chemomechanical and Chemoelectrical Energy Conversion

Vishnu Baba Sundaresan, Ph.D. Candidate
Virginia Polytechnic Institute and State University, 2007
Advisor: Donald J. Leo

Abstract

This dissertation presents a new class of engineered devices, fabricated from synthetic materials and protein transporters extracted from cell membranes of plants, that use chemomechanical and chemoelectrical energy conversion processes to perform mechanical and electrical work.

The ***chemomechanical energy conversion*** concept is implemented in a protein based actuator. The chemical energy is applied as an electrochemical gradient of protons across a membrane assembly formed from phospholipids and SUT4 -a proton-sucrose cotransporter. The membrane assembly forms a physical barrier between two chambers in the actuator. The SUT4 proteins in the membrane assembly balances the applied electrochemical gradient by a concentration gradient of sucrose across the membrane. The sucrose gradient simultaneously generates an osmotic flow which deforms a flexible wall in a constrained chamber of the actuator, thus exhibiting mechanical strain. The sucrose concentration balanced by the protein transporter is used as the control variable for fluid flow through the membrane. The transport properties of the membrane assembly has been characterized for the control variable in the system. The reaction kinetics based model for solute transport through the cotransporter is modified to compute the equilibrium constant for solute binding and fluid translocation rate through the membrane. The maximum initial flux rate through the membrane is computed to be 2.51 ± 0.6 μl/μg.cm^2.min for an applied pH4.0/pH7.0 concentration gradient across the membrane. The flux rate can be modulated by varying the sucrose concentration in the actuator. The prototype actuator has been

fabricated using the characterized membrane assembly. A maximum deformation of 60μm at steady state is developed by the actuator for 20 mM sucrose concentration in the system.

The ***chemoelectrical energy conversion*** concept is based on the electrogenic proton pumps in plasma and vacuolar membranes of a plant cell. A prototype device referred to as a BioCell demonstrates the chemoelectric energy conversion using V-type ATPase extracted from plant cell membranes. The enzyme in the bilayer lipid membrane hydrolyzes ATP and converts the chemical energy from the reaction into a charge gradient across the membrane. Silver-silver chloride electrodes on both the sides of the membrane convert the charge established by the proton pumps into cell voltage. The redox reactions at the surface of the electrodes result in a current through the external load connected to the terminals of the BioCell. The single cell behaves like a constant current power source and has an internal resistance of 10-22kΩ. The specific power from the cell of the membrane assembly is estimated to be around 2μW/cm^2. The demonstration of chemoelectrical energy conversion shows the possibility to use ATP as an alternative source of electrical power to design novel chemo-electro-mechanical devices.

Acknowledgments

I would like to express my deep gratitude to my academic advisor, Prof. Donald J Leo for his extraordinary patience, encouragement and support. I would also like to thank Dr. Daniel J Inman, Dr. Pavlos Vlachos, Dr. John Cuppoletti, Dr. Lisa Mauck-Weiland and Dr. Mark Paul for their advice and serving as committee members. I would like to thank all of my colleagues, current and past for making CIMSS a home away from home. I would also like to particularly thank Mrs. Beth Howell and my current graduate student colleagues David Hopkinson, Andy Sarles, Austin, Justin, Pablo and former colleagues Dr. Kevin Farinholt and Dr. Henry Sodano for their help. I would also like to acknowledge the financial support from DARPA-DSO under the Nastic Materials Grant for funding this work through contract (ARO Grant No. W911-NF-04-1-0421). Lastly but not the least - *amma, appa, athai, athimbar, vivek, and abi* - thank you for your motivation, care, love and prayers and for having my academic aspirations on the top of your list.

Vishnu Baba Sundaresan

Virginia Polytechnic Institute and State University
15th May 2007

Contents

Abstract **iii**

Acknowledgments **v**

List of Tables **ix**

List of Figures **x**

Nomenclature **xvi**

1 Prologue **1**

1.1 Structure of a cell 4

1.2 Cell membranes 5

1.3 Solute transport in biological systems 8

1.3.1 Simple diffusion 9

1.3.2 Solute transport through ion transporters 9

1.3.3 Cotransport and antiport 17

1.4 Chemomechanical energy conversion 17

1.4.1 Ion transport in mechanical transduction 18

1.4.2 Chemomechanical actuation using protein transporters 19

1.5 Chemoelectrical energy conversion 21

1.6 Contributions 23

1.7 Document overview 24

2 Chemomechanical Energy Conversion **25**

2.1 Planar BLM supported on porous substrates 26

2.1.1 Lipid self-assembly - Painting technique . . . 28
2.1.2 Liposome fusion . . . 28
2.1.3 Langmuir-Blodgett method . . . 29
2.1.4 Chemical methods . . . 30
2.2 Protein based actuator . . . 30
2.3 Thermodynamics of facilitated cotransport . . . 32
2.4 Kinetic model for facilitated ion transport . . . 37
2.5 Sensitivity of the membrane assembly to solute concentration . . . 39
2.6 Chapter summary . . . 42

3 Transport Experiments 44
3.1 Component selection for the actuator . . . 45
3.1.1 Protein: SUT4 proton-sucrose cotransporter . . . 45
3.1.2 Lipids and Substrates . . . 48
3.2 Membrane assembly fabrication . . . 49
3.2.1 Self-assembly of the bilayer lipid membrane . . . 51
3.2.2 Self-assembly of SUT4 in bilayer lipid membrane . . . 52
3.2.3 Electrical model of the bilayer lipid membrane . . . 53
3.3 pH gradient driven transport . . . 55
3.3.1 Porous polycarbonate membranes . . . 55
3.3.2 Lead silicate glass plates . . . 60
3.3.3 Rate constants for fluid flux . . . 68
3.4 ATP driven transport for actuation . . . 71
3.4.1 Mechanism of ATP driven transport . . . 71
3.4.2 Materials used . . . 73
3.4.3 Experimental setup . . . 74
3.4.4 Results - ATP powered transport . . . 75
3.5 Chapter summary . . . 79

4 Actuation Experiments 81
4.1 Polycarbonate membrane as supporting substrate . . . 81
4.1.1 Actuator configuration . . . 81
4.1.2 Experimental setup . . . 83

4.1.3 Results and discussion . . . 84
4.2 Lead silicate glass as supporting substrate . . . 86
4.2.1 Actuator configuration . . . 86
4.2.2 Results and discussion . . . 88
4.3 Comparing transport and actuation results . . . 91
4.4 Analysis of deformation results . . . 93
4.5 Chapter summary . . . 96
4.6 Actuation Experiments - Detailed results . . . 97

5 Chemoelectrical energy conversion 99
5.1 Prototype energy conversion device . . . 99
5.2 Fabrication and characterization . . . 101
5.3 Cell configuration . . . 102
5.4 Baseline Power measurements . . . 105
5.5 Power characterization of a full cell . . . 107
5.6 Chapter Summary . . . 110

6 Summary and Conclusion 113
6.1 Research Summary . . . 113
6.2 Result Summary . . . 114
6.2.1 Actuation experiments . . . 114
6.2.2 Chemoelectrical energy conversion . . . 115
6.3 Contributions . . . 116
6.4 Future directions . . . 117

Bibliography 118

A Capacitance meter 129
A.1 Sensor configuration . . . 130
A.2 Capacitance based level sensing . . . 130
A.3 Experimental setup . . . 132

B Copyright approval 135

Vita 137

List of Tables

3.1 Equilibrium concentration of sucrose in the two chambers of the actuator for pH4 vs. pH7 applied across the membrane assembly 48

3.2 Flux rate through membrane assembly for different substrates 68

3.3 Translocation rate through different membrane assemblies 70

3.4 System parameters for ATPase experiments 77

4.1 Polycarbonate substrate based actuator - dimensions 82

4.2 Lead silicate glass plate substrate based actuator - details 87

4.3 Volume change in the top chamber computed from transport and actuation experiments for glass plate substrate with 2μm pores 93

4.4 Analysis of the deformation data from the two prototypes 95

4.5 Energy density of the second prototype actuator 95

List of Figures

1.1 Energy density of various actuators shown on stress-strain graph 1

1.2 Plant as actuators - shown here are movies that demonstrate the rapid response of Mimosa sensitiva and Venus flytrap plant. The leaves of mimosa sensitiva close on coming in contact with a heat source to prevent moisture loss. The Venus flytrap leaf detects the insect's motion using the sensory hairs on the leaf and it shuts close. 2

1.3 The vacuole is the most prominent feature in a plant cell and is separated from the cell cytoplasm by a membrane. Similar membranes separate other cellular organelles and adjacent cells. This image was obtained from Wikipedia and is in the public domain. 5

1.4 Structure of a phospholipid molecule. The hydrocarbon tail is attached to a polar head through the phosphate group. The lipid molecules assemble into a monolayer on the surface of an aqueous medium with the tail pointing away from the fluid medium. 6

1.5 Polymorphic forms of a phospholipid molecule 7

1.6 Ion transport - different processes 8

1.7 Protein types: Integral membrane proteins and peripheral proteins - based on the nature of their insertion in a lipid membrane 10

1.8 Ion transporter incorporated in a BLM - 1SU4 12

1.9 Ligand-gated transport 14

1.10 Voltage-gated transport 15

1.11 Cotransport and Antiport - based on direction of ion transport 17

1.12 An ionic polymer transducer(IPT) and a polymer hydrogel shown above bend and change shape due to ion and fluid transport respectively 18

1.13 Demonstration of volumetric expansion of a synthetic capsule formed from lipid membranes with ion transporters expending ATP 20
1.14 Arrangement of spherical capsules in a structure to result in shape change . 21
1.15 V-type ATPase in the tonoplast membrane of a plant cell and its application in a BioCell. The proton pumping enzyme is shown with the membrane peripheral(V_0) and membrane integral(V_1) units. The protein develops an electrochemical proton gradient from chemical energy stored in ATP. 23

2.1 Mueller Rudin method of forming a planar BLM 27
2.2 The protein based actuator 31
2.3 Thermodynamic variables to model facilitated cotransport driven by electrochemical gradients 33
2.4 Four state carrier model with one diffusing solute 37

3.1 SUT4 protein exists in plant cell membrane with other proteins. The gradient established by active transporters is used by SUT4 for sucrose transport. . . 46
3.2 Mechanism of sucrose transport through SUT4 protein. (a) Flux of sucrose molecules through SUT4 due to an imposed pH and sucrose gradient. (b) Mean sucrose flux for different pH imposed in the extracellular medium published by Weise et. al [106] shows the dependence of flux on imposed pH gradient 47
3.3 Phospholipids - POPS and POPE used for BLM self-assembly and protein reconstitution 49
3.4 Porous polycarbonate membrane and Lead silicate glass plate used as supporting substrates for the membrane assembly 50
3.5 Porous lead silicate glass plate shown with the exposed circular port and clamped in the fixture 52
3.6 Planar BLM in the porous substrate modeled as a RC in parallel. The access electrolyte is modeled as a resistor and the measured value represents a 2R-1C network model 53
3.7 Fixture to characterize the membrane assembly on polycarbonate substrate 55
3.8 Measured impedance on the PC membrane assembly from 5 Hz to 1 MHz . 56

3.9 Z-plot for the measured impedance data for the BLM. From the 2R-1C model, the capacitance and conductance of the BLM in the pores are 6.008 nF/cm^2 and 173.212 μS/cm^2 respectively 57
3.10 Normalized flux through membrane assembly on PC. 58
3.11 Normalized flux through the membrane on PC for different sucrose concentration 59
3.12 Experimental setup - Lead silicate glass supported membrane assembly . . 60
3.13 Amount of lipids added vs. Measured impedance (n-decane microlens fills in the region between the hydrophobic tails is shown in the inset) 61
3.14 Nyquist plot of two of the trials reported for 10 μl lipids on the substrate. . 62
3.15 Measured impedance with and without SUT4 in BLM on lead silicate glass substrate with 50 μm pores. Computed capacitance and conductance of the BLM are 6.5 nF/cm^2 and 150 μS/cm^2 63
3.16 Normalized flux through membrane assembly - time response(Lead silicate glass with 50μm pores) 64
3.17 Normalized flux through the membrane for different sucrose concentration (Lead silicate glass with 50μm pores) 64
3.18 Effect of protein density and BLM area on fluid transport 66
3.19 Normalized flux through membrane assembly - time response(Lead silicate glass with 2μm pores) 67
3.20 Normalized flux through the membrane on 2 μm pores for different sucrose concentration 67
3.21 Reciprocal plots from experimental data for the membrane assembly with SUT4 formed on PC membranes & lead silicate glass 69
3.22 Sensitivity of the membrane formed on different substrates to concentration gradient of sucrose 70
3.23 Principle of ATP-hydrolysis powered fluid transport 72
3.24 Experimental setup for measuring ATP hydrolysis driven transport through the membrane assembly 75
3.25 Measured impedance on the substrate for different membrane assemblies . . 76
3.26 Fluid flux through the membrane assembly in ATPase driven transport experiments - Baseline trials 77

3.27 Fluid flux through the membrane assembly in ATPase driven transport experiments 78
3.28 Flux rate through the membrane as a function of the amount of ATPase reconstituted in the membrane 79

4.1 Microhydraulic actuator element- schematic & prototype 82
4.2 Experimental arrangement to measure deformation 83
4.3 Measured deformation in the actuator for different baseline cases 85
4.4 Measured deformation in the actuator for different baseline cases 86
4.5 Measured deformation for different concentrations of sucrose developed by the actuator with polycarbonate supporting substrate 87
4.6 Second prototype actuator - components and configuration 88
4.7 Measured deformation in the second prototype actuator for different baseline cases 89
4.8 Representative deformation time histories measured in the actuator with 2 μm pores in lead silicate glass plates for different test cases 90
4.9 Measured deformation in the second prototype actuator for different concentrations of sucrose 91
4.10 Reciprocal plot from concentration and volumetric flux obtained from actuation data 92
4.11 Pressure in the top chamber and force exerted by fluid transport 94
4.12 Measured deformation in the second prototype actuator for different baseline cases and for different concentrations of sucrose 97
4.13 Measured deformation in the second prototype actuator for different baseline cases and for different concentrations of sucrose 98

5.1 Chemoelectrical energy conversion of adenosine triphosphate using ATPase in BioCell shown with the location of the membrane assembly in the cell. The components for the prototype BioCell fabricated is shown alongside. The top chamber in the picture is shown with polycarbonate membrane attached to the bottom. 100
5.2 Experimental setup - Electrical load analysis of BioCell 102

5.3 Plot (a): Impedance data measured using Ag/AgCl electrodes across pH7 buffer, pH7 buffer with polycarbonate membrane with 200 nm pores and 5-20% porosity, pH7 buffer with polycarbonate membrane carrying BLM and pH7 buffer with polycarbonate membrane carrying BLM reconstituted with ATPase proteins. Plot (b):Equivalent electrical circuit for the different components in the cell as interpreted from the impedance data 103
5.4 Equivalent electrical circuit for the different components in the cell as interpreted from the impedance data 104
5.5 Measurement of power output for different loads applied in the following order - 4.7 kΩ, 10 kΩ, 22 kΩ, 33 kΩ,39 kΩ, 55 kΩ, 100 kΩ, 150 kΩ. shows the VI behavior under different resistive loads of a full cell compared with that of the same electrode removed from the cell and kept in pH7.0 buffer. . 106
5.6 Measurement of power output for different loads applied in the following order - 4.7 kΩ, 10 kΩ, 22 kΩ, 33 kΩ,39 kΩ, 55 kΩ, 100 kΩ, 150 kΩ from different trials. 107
5.7 Power characterization plots. Current-voltage characteristics of the BioCell for different electrical loads compared with baseline data. 108
5.8 Power characterization plots. Plot of power developed by the BioCell from different trials compared with baseline data 109
5.9 ATPase pumps in BLM as a constant power source 109
5.10 Scanning electron micrographs of new Ag/AgCl electrodes used in the BioCell for characterizing a BLM with ATPase as an electrical power source. The SEM images at 200X and at 1kX show a clear surface and the composition of the new electrodes from EDS in (c) show only Ag and Cl as the constituent elements 111
5.11 Scanning electron micrographs of old Ag/AgCl electrodes used in the BioCell for characterizing a BLM with ATPase as an electrical power source. (a) (b) The SEM images at 200 X and at 1 kX show visible degradation on surface of electrodes (c) The EDS data at the bright regions shows traces of Phosphorus and Magnesium which are introduced into the electrode surface due to ATP hydrolysis reaction 112

A.1 Circuit equivalent: Capacitance based liquid level meter 131
A.2 Experimental setup: Capacitance meter calibration 132
A.3 Capacitance values from the meter 133
A.4 Capacitance meter:Result 134

Nomenclature

A_c	Area of the coverplate
D	Diffusion coefficient
G	Gibbs Free energy
G_{m}	Flexural rigidity of the coverplate material
K	Equilibrium constant for solute binding reaction
$L_{x,y}$	Coupling ratio for flux of species x due to the chemical potential of y across the membrane
R	Relative gas constant
T	Temperature
ΔP	Change in pressure in top chamber
$\Delta\mu_y$	Chemical potential of species y
$\Delta\psi$	Membrane potential
Δx	Deformation
α_w	Number of cycles of operation of transporter to balance gradients across the membrane
$\dot{\alpha}$	Translocation rate of solute through the membrane
$\dot{\alpha}_w$	Translocation rate of fluid through the membrane
$\dot{\phi}$	Flux rate through the membrane
$\dot{\phi}_{\max}$	Flux rate through the membrane
γ_y	Activity of species y
ν	Convective velocity
ϕ_s	Flux of solute through the membrane
c	Concentration
c_*^y	Concentration of species y on side $*$ of the membrane

d	Membrane thickness
f	Body force
k	Partition coefficient
n_w	Stoichiometry of water to sucrose diffusing through the membrane
q	Charge on species
r_c	Radius of the coverplate
r'_c	Arbitrary radius on the coverplate
t	Time
u	Drift velocity
x	Spatial coordinate

Chapter 1

Prologue

Actuators translate an applied stimulus into controllable force and motion. Actuation occurs due to processes involving the conversion of an applied form of energy into force and motion. Hard active materials such as piezoelectric wafers, magnetostrictive materials and shape memory alloys exhibit actuation due to internal domain transformation. Soft active materials like polymer transducers, hydrogels, etc., exhibit strain due to ion migration for an applied stimulus. In general, active materials can be grouped based on the the stress-

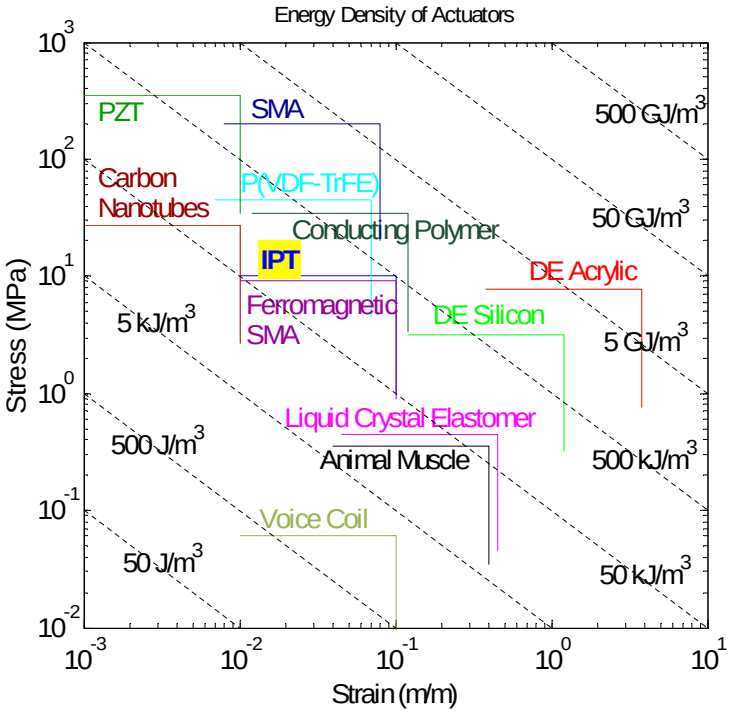

Figure 1.1: Energy density of various actuators shown on stress-strain graph

strain characteristic shown in Figure 1.1 and the stress-strain developed by an actuator material is likely to be dependent on the actuation mechanism. It may be observed that actuators with higher blocked stress (viz., piezoelectric, electrostriction, etc.,) exhibit small free strain and vice versa. Shape memory alloys(SMAs) generate moderate stress and strain and have comparably higher energy density, but thermal actuation required for SMA is not favorable for many engineering applications.

Plants and animals exhibit motion, apply force on their surrounding objects and can be considered as actuators. The rapid motion to an external stimulus in these naturally occurring systems is comparable to the actuation speed in actuator materials. Plants do not generate rapid motion with the exception of a very few species. The rapid response to external stimulus is used in plants for self-defense (*Mimosa sensitiva*), pollen dispersal in (*Impatiens capensis*) and nutrient absorption in insectivorous plants. These biological systems that generate rapid motion convert chemical energy stored in cells into force and motion. The movies shown in Figure 1.2 are obtained from 'Plants In Motion' website maintained by Prof. Roger Hangarter[74] and are presented here with his consent to emphasize the actuation rates observed in plants. For copyright purposes, his written consent is provided in Appendix B. The snapping action demonstrated by an insectivorous plant -

Click here Click here

Figure 1.2: Plant as actuators - shown here are movies that demonstrate the rapid response of Mimosa sensitiva and Venus flytrap plant. The leaves of mimosa sensitiva close on coming in contact with a heat source to prevent moisture loss. The Venus flytrap leaf detects the insect's motion using the sensory hairs on the leaf and it shuts close.

Venus flytrap - shown in Figure 1.2(b) is used as an example to explain the cellular processes causing the rapid response. The ciliary hairs in the trap leaves serve as the sensory system that initiates the trap closure. The mechanism for the snapping action of Venus flytrap has been investigated since Darwin[19] and there are conflicting claims on the internal mechanism that drives the process. Brown[13], Lichtner and Williams [56] proposed that action potentials across the cell membrane generated by the mechanical stimulus in the ciliary hairs initiate the closing action. The trap leaves continue to apply force on the insect through biochemical processes that complete the closure. According to Batalin[6], the second step through the biochemical pathway takes 7 hours to be complete. Williams and Bennet[109] proposed that H^+-ATPase reaction initiated the trap closure. The softening of the cell wall is brought about by the acidification resulting from the H^+ transport consuming 29% of the ATP available in the trap leaves. They claim that acidification due to proton transport caused sudden loss of cell turgor pressure produces the shape change. Sibaoka[86] added calcium transport driven by ATP hydrolysis as the driving mechanism. The membrane potential due to calcium uniport generates the internal stimulus for loss in turgor pressure. Hodick and Siebers[40] reject the loss in turgor pressure as the driving mechanism for trap closure. Their model presents a mechanism where the extensible cells of the leaves are kept compressed in the open position and are only triggered to close by membrane transport. Hill and Findlay[38], Morillon et. al[62] suggest osmotic regulation due to solute-water cotransport as the driving mechanism for trap closure. With a number of reports using internal biological processes as the motive force for shape change, a recent report by Forterre et. al[27] attribute elastic deformation of a pre-strained surface as the driving mechanims for trap closure. The report explains that the biological processes pre-strain the leaf over days by cell transport mechanism and the ciliary hairs trigger the change in shape of the leaf from convex to concave, thus generating the required rapid response. The actual mechanism is still elusive for a common consensus among plant biologists and has given rise to variety of theories that can be used for fabricating an actuator. The fluid transport resulting from biological processes causing cell expansion and contraction can be used in an engineered system to generate force and motion. Furthermore, the rate of motion observed in these naturally occurring systems serve as the motivation to use cell membrane transport processes for designing actuators.

The different processes that cause actuation in plants uses the energy from absorbed

nutrients. The metabolic pathway converts the absorbed nutrients into sugars that can be readily processed and converted into ATP. The synthesis of ATP occurs inside the cell and the chemical energy available with ATP is used for ion transport across cell the membrane that stimulates growth and response to an external stimulus. The transport of ions and molecules occurs through selective pathways, which are proteins that remain embedded in the membranes of living cells. *This dissertation presents a new class of engineered devices, fabricated from synthetic materials and protein transporters extracted from cell membranes of plants, that use chemomechanical and chemoelectrical energy conversion processes to perform mechanical and electrical work.* The proteins extracted from the cell membrane are the fundamental actuation elements in the actuator. The rest of the chapter discusses the composition and functional role of the cell membrane and the protein transporters in a plant or animal cell and introduces the chemomechanical and chemoelectrical energy conversion concept developed in this work.

1.1 Structure of a cell

The different cellular organelles are shown in Figure 1.3. The most prominent feature of a plant cell is the vacuole, which serves as storage space within the cell for excesses in the cell cytoplasm. The vacuole is separated from the cell cytoplasm by a well-defined boundary. All the cell organelles float in the cytoplasm and remain encapsulated by a similar membrane. Membranes that form the outer cover of a cell in plants have multiple layers of cellulose and chitin which contribute to mechanical strength and structural form. Membranes of inter-cellular organelles have cholesterol and other proteins that provide structural form. Ion transport across the cell boundary and across the membranes in the inter-cellular organelles take place through paths formed across the cell membrane called ion channels and ion pumps. All of the energy conversion processes for membrane transport in a cell occur at the cell membrane in the ion pumps and channels. The ion channels and pumps are macromolecules synthesized within the cell. An overview of the cell membrane and the uniqueness of ion transport through selective pathways in the membrane will ease the discussion of utilizing biological energy conversion processes for actuation.

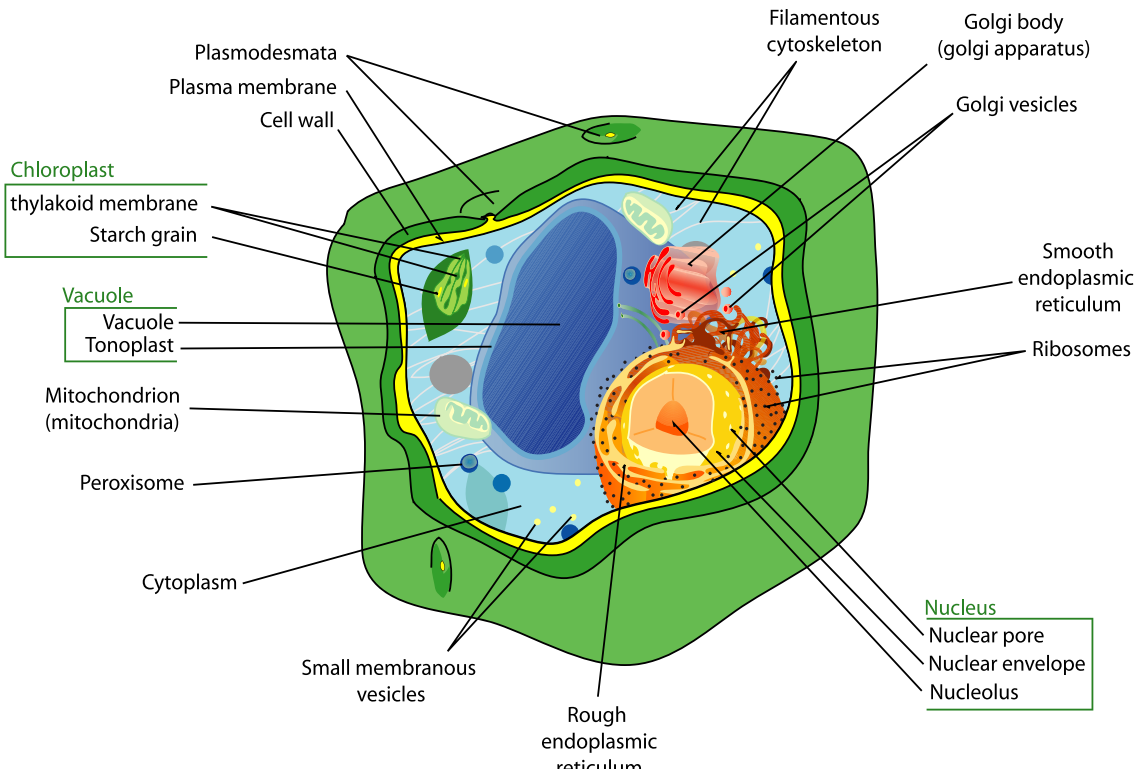

Figure 1.3: The vacuole is the most prominent feature in a plant cell and is separated from the cell cytoplasm by a membrane. Similar membranes separate other cellular organelles and adjacent cells. This image was obtained from Wikipedia and is in the public domain.

1.2 Cell membranes

The cell membrane is a laminated arrangement of amphiphilic molecules [25] compacted by turgor forces acting from inside. The amphiphilic molecules are formed from neutral hydrocarbon compounds called lipids. Organic acids or esters commonly having C_{16} or C_{18} carbon atoms are the most commonly occurring lipids in nature. The lipid molecules are immiscible in water and dissolve only in organic solvents. A simple lipid molecule cannot form into a membrane in an aqueous solution due to the absence of polar groups. When simple lipids have a polar group attached to the hydrocarbon chain, it results in a single molecule with hydrophobic and hydrophilic ends. This makes it amphiphilic and its affinity to hydrophilic and hydrophobic species. The lipids which have a phosphate group attached to the hydrocarbon chain forms a chemical bond with other polar groups. These lipids with an interconnecting phosphate ion and having a hydrophobic and a hydrophilic end as shown in Figure 1.4[75] are referred to as *phospholipids*. Phospholipids are the most abundantly available

lipids in cell membranes. Due to their affinity to polar and non-polar species, phospholipids are referred to as amphiphathic (or) amphiprotic molecules. A schematic representation of

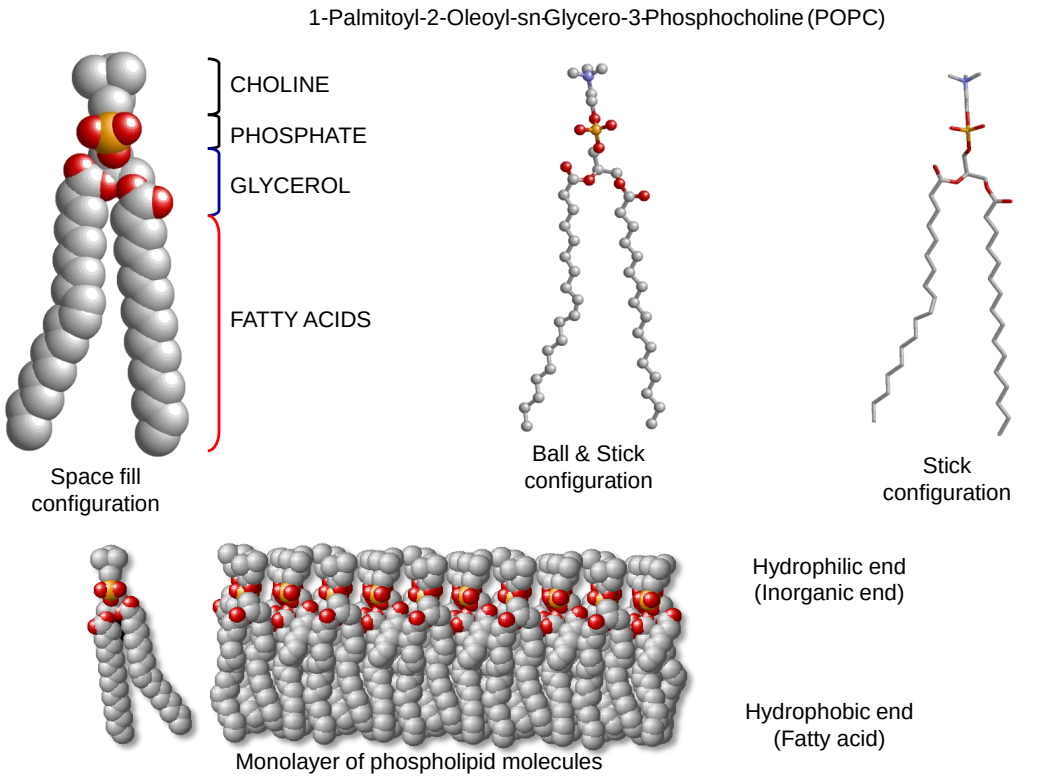

Figure 1.4: Structure of a phospholipid molecule. The hydrocarbon tail is attached to a polar head through the phosphate group. The lipid molecules assemble into a monolayer on the surface of an aqueous medium with the tail pointing away from the fluid medium.

the most commonly occurring phospholipid in nature is shown in Figure 1.4. The name is derived from the different chemical groups that form the phosphilipid molecule. The head group -choline can be substituted with a -serine group or an -ethanolamine group and will result in 1-Palmitoyl-2-Oleoyl-sn-Glycero-3-[Phospho-L-Serine](POPS) or 1-Palmitoyl-2-Oleoyl-sn-Glycero-3-Phosphoethanolamine(POPE). The phospholipid molecule exists in three polymorphic forms - fluid phase, gel phase and crystalline phase[51] as shown in Figure 1.5. The phospholipid is shortest in its fluid phase and longest in crystalline phase. In the intermediate gel phase, the phospholipid molecule is 28 $\mathring{A}$ long. The phospholipid molecules spread into a monolayer when sandwiched between a hydrophobic and hydrophilic medium. In a polar solvent, the phospholipids align themselves in such a way that the hydrophilic

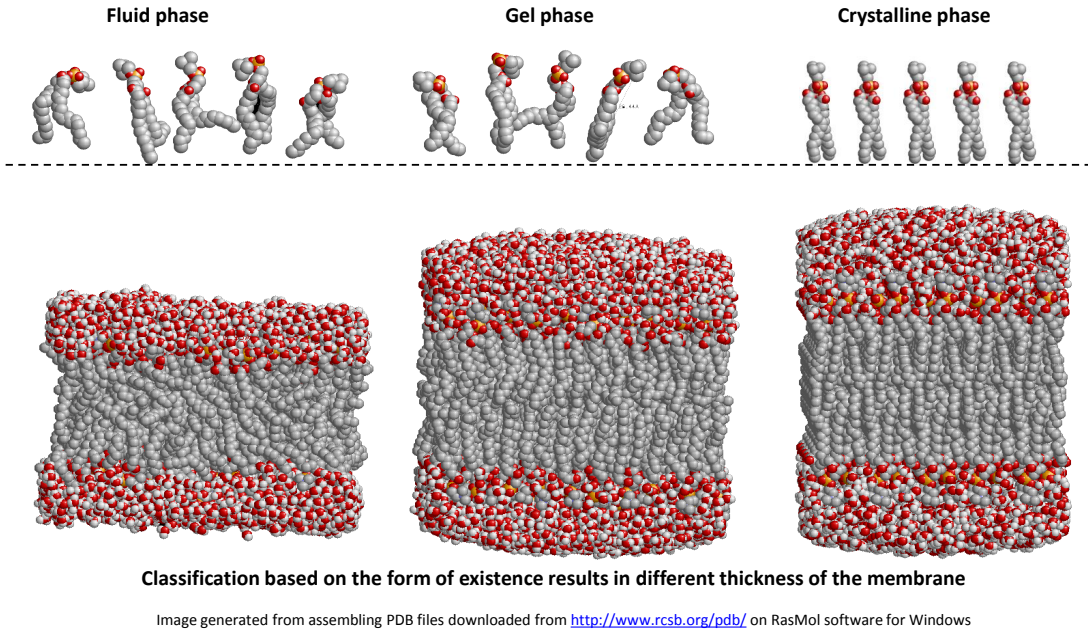

Figure 1.5: Polymorphic forms of a phospholipid molecule

groups come in to contact with water. The soft organelles of the cell consists of an assembly of amphiphilic phospholipid molecules to form a bilayer also referred to as a bilayer lipid membrane (BLM). The thickness of the BLM is dependent on the phase of existence of the phospholipid molecule. The occurrence of a form is dependent on the environment temperature and pressure at which the molecule exists. In an aqueous medium, the phospholipids arrange themselves on the surface at smaller concentrations and aggregate into micelles above the Critical Micellar Concentration(cmc)[58]. Agitating the phospholipids in an aqueous medium produces hollow spherical structures called *liposomes* [4]. Formation of liposomes is accelerated in the presence of an electric field [3] and the process is known as 'electroformation'. Liposomes are very similar to plant and animal cells or inter-cellular organelles, but lacks the reinforcing and functional components. The liposome shell is a BLM where the hydrophilic ends are in contact with the aqueous interior and exterior regions of the hollow spherical capsule. The phospholipid molecules in a BLM are held together by van der Waals force and the alignment of hydrophobic and hydrophilic ends maximizes the weak forces of interaction in the BLM to form a stable membrane. When the liposomes are spread on a pore with a very small aperture, they spread into a planar BLM. Mueller

et. al[63], Tien et. al [99] showed that spreading phospholipids mixed in an organic solvent across the edges of a pore also results in the formation of a planar BLM. The BLM formed as a capsule shell or as a planar membrane is similar in configurations as shown in Figure 1.5 [75]. The BLM in cell membranes exist in fluid phase at room temperature and forms the framework for supporting ion transporter proteins in their functional form. The amphipathic nature of the phospholipid facilitates hydrophobic molecules to be inserted into the cell membrane. The different methods to form a cell membrane for the actuator will be discussed in detail later in the document.

1.3 Solute transport in biological systems

The cell membrane formed from lipid molecules form the physical boundary of the cell contents. The phospholipid membrane is impervious to ions and neutral species. In spite of its impervious nature, the cell membrane conducts ions and species through the membrane. Ion transport across cell membranes of plants and animals occur through different schemes and can be classified into different types: simple diffusion, facilitated diffusion and active transport as shown in Figure 1.6.

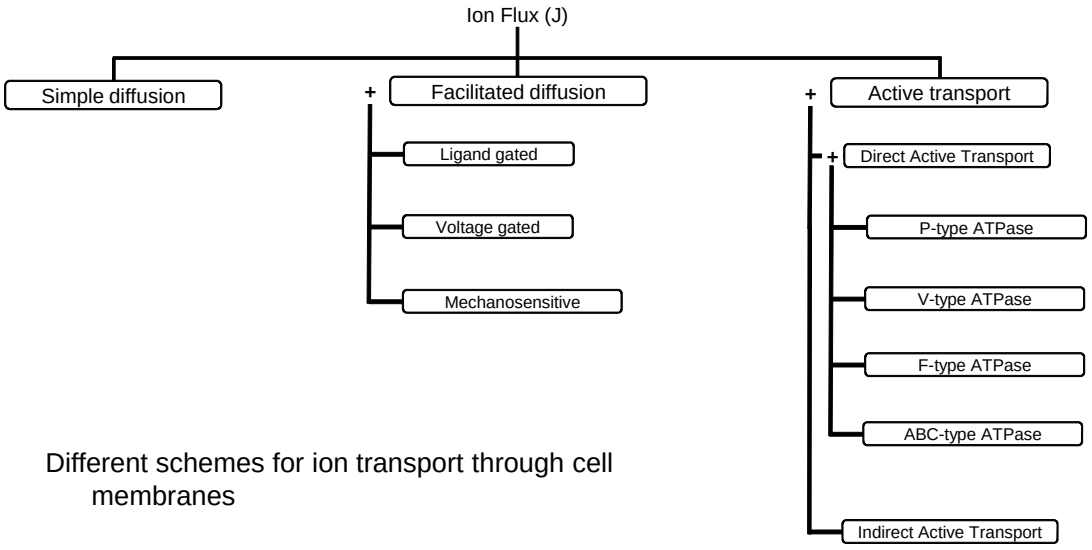

Figure 1.6: Ion transport - different processes

1.3.1 Simple diffusion

The simplest of ion transport processes is diffusion where ions disperse in the medium or through a semi-permeable membrane to equilibrate concentration gradients. The diffusing specie is mobile in the medium or is permeable to the membrane through which simple diffusion can occur. The applied concentration gradient is the source chemical potential that directs the random motion of particles in the medium down the gradient[18]. The governing equation for simple diffusion in a medium is given by

$$\frac{\partial c}{\partial t} = D\frac{\partial^2 c}{\partial x^2}, \qquad t > 0 \tag{1.1}$$

where c is the concentration of the solute at a given spatial coordinate and time $c(x,t)$ and D is the diffusion coefficient. The evolution of concentration in the spatial and temporal coordinate is given by the Green's function[107],

$$c(x,t) = \frac{c(x_0,t_0)}{\sqrt{4\pi Dt}} e^{-\frac{x^2}{4Dt}} \qquad t > 0 \tag{1.2}$$

where $c(x_0,t_0)$ is the concentration of the diffusing specie at position x_0 and time t_0. The flux of species ϕ at position x and a time t can be obtained using Fick's first law:

$$\phi(x,t) = -D\frac{\partial c(x,t)}{\partial x} \tag{1.3}$$

In addition to the concentration gradient, if there exists a hydraulic pressure causing a convective velocity ν and an electrical field exerting a body force f resulting in a drift velocity u, the total flux[107] is a sum of the diffusive flux, convective flux and given by

$$\phi(x,t) = -D\frac{\partial c(x,t)}{\partial x} + \nu c + ucf \tag{1.4}$$

Steady state flux for simple diffusion of a permeable solute for an applied concentration gradient across the membrane of thickness d is

$$\phi = \frac{D\,k}{d}(c_s^1 - c_s^2) \tag{1.5}$$

The parameter k is the partition coefficient of the membrane and c_1^s, c_2^s are solute concentrations on the both the sides of the membrane.

1.3.2 Solute transport through ion transporters

The membrane formed from phospholipid molecules is impermeable to ions. But the membrane offers a flexible system to accommodate a organic molecules that can participate in

ion transport. The proteins are synthesized in the cytoplasmic side of a living cell and inserted into the cell membrane. The lipid molecules in the cell membrane forms a leak-proof seal around the transporter. Ion transport across cell membrane is vital for life functions of the cell. Few of the important functions of ion transport are:

- Primary role of nutrient absorption and transport
- Inter-cellular signaling
- Maintaining ionic concentration at functional levels
- Maintaining the shape of the cell

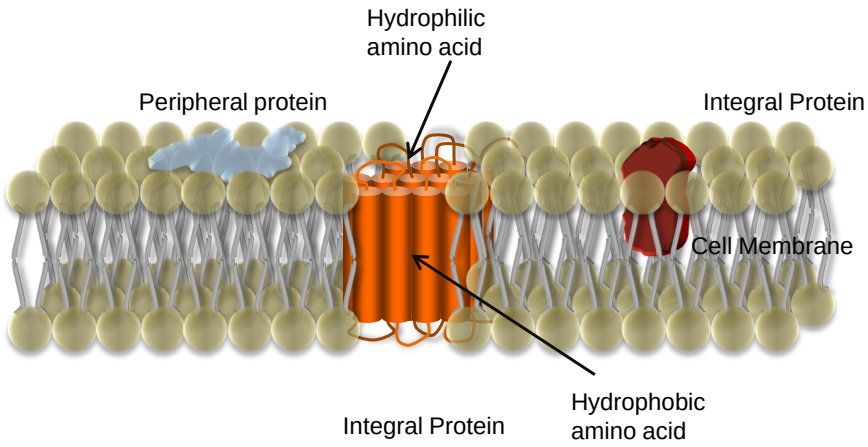

Figure 1.7: Protein types: Integral membrane proteins and peripheral proteins - based on the nature of their insertion in a lipid membrane

Transport of ions into and out of the cell occur through protein molecules, called ion transporters embedded in the cell membrane . Early research on membrane proteins led to a classification of proteins based on their location in the cell membrane. The classification based on the location of protein transporters is presented in this document due to its significance in the development of an engineered device. Membrane proteins are classified into integral membrane proteins and peripheral proteins as illustrated in schematic shown in Figure 1.7. Proteins are formed from hydrophobic and hydrophilic amino acid chains. Integral membrane proteins are arranged in the lipid bilayer where the middle segments of the protein are hydrophobic amino acids and the ends are made of hydrophilic amino acids.

The hydrophobic section is as thick as the hydrophobic region of the cell membrane. The arrangement of the membrane bound integral membrane protein and the amphipathic nature of the protein ensures that the protein cannot move out of the BLM. With the structural mapping of the protein molecule, similarities in physical arrangement of the amino acid chains and chemical structure are recently used to classify the protein structure. Sophisticated Molecular imaging techniques like Nuclear Magnetic Resonance (NMR) imaging, X-ray Photoelectron Spectroscopy(XPS) and X-Ray Crystallography have played an important role in visualizing the three-dimensional structure of the protein transporter. The sophisticated methods available also led to the grouping of transporters based on 'homology' - their confirmation.

Structure of an ion transporter:

Ion transporters in the cell membrane are an ordered arrangement of amino acids covalently connected together by polypeptide bonds. The structure of a protein present in nature is devolved and constructed back in a modular manner. The arrangement of amino acids with the covalent bonds that form the molecular structure of a protein transporter is referred to as the *configuration*. The mechanism of constructing the configuration of a protein transporter is done using the concept of orders of protein structure. The four orders of protein structure are constructed from 20 basic amino acid groups. These 'magic 20' [65] amino acid groups are the only ones specified in the genetic code of a protein transporter. Ordered by increasing size, the different groups are *glycine, alanine, valine, leucine, isoleucine, methionine, phenylalanine, tyrosine, tryptophan, aspartic acid, glutamic acid, lysine, arginine, histidine, asparagine, glutamine, serine, threonine, cysteine and proline*. The basic 20 units are assembled into a polypeptide chain and is referred to as the primary structure. The polypeptide chain is folded into an α-helix, a β-pleated sheet or the random coil which are referred to as the secondary structure. The compact structure resulting from the arrangement of many secondary structures is referred to as the tertiary structure. Many proteins are complete with tertiary structure. But many functional proteins have multiple protein sub-units that are attached by non-covalent bonds. These non-covalently linked molecules provide surface contact for molecules that bind to the protein and participate in biochemical reactions and assist in ion transport. The combination of tertiary structure subunits to form oligomeric, multimeric or multisubunit functional complex is referred to as quaternary structure. An accurate representation of a sucrose transporter(1SU4) is shown assembled

in a sectioned 1-Palmitoyl-2-Oleoyl-sn-Glycero-3-Phosphocholine (POPC) BLM in Figure 1.8. The different chemical bonds and their spatially arrangement of molecules have been determined for this transporter using XPS technique.

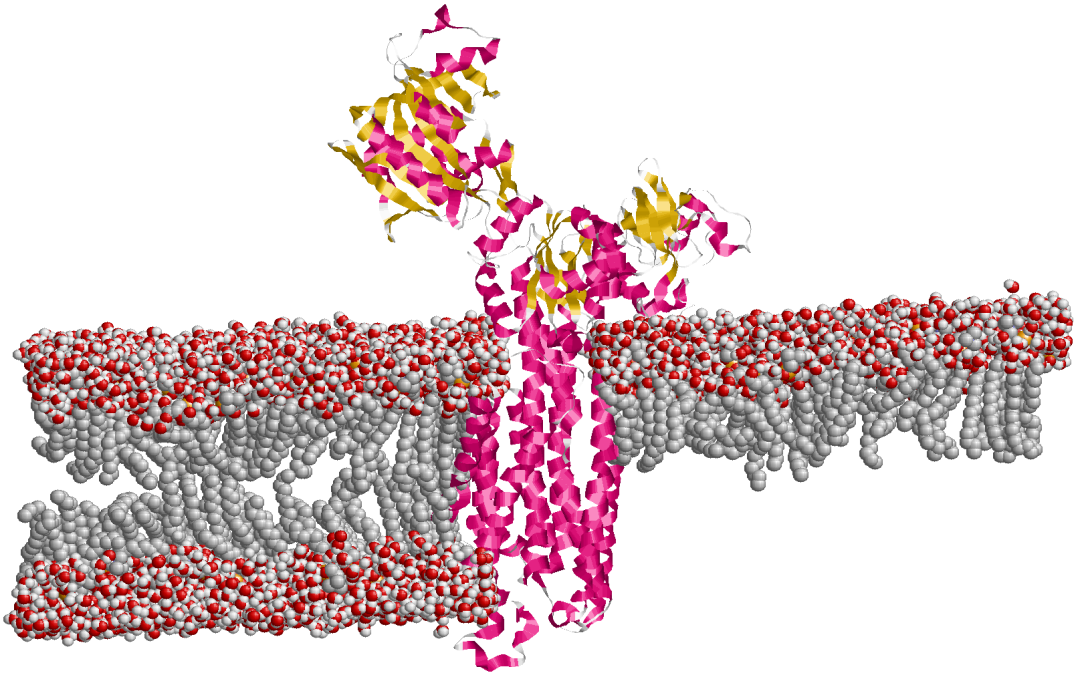

Image generated from assembling PDB files downloaded from http://www.rcsb.org/pdb/ on RasMol software for Windows

Figure 1.8: Ion transporter incorporated in a BLM - 1SU4

During ion transport, molecules and species squeeze through the molecular configuration of the protein. As a solute enters the protein transporter, the individual molecules of the transporter change their spatial arrangement without disturbing the configuration to ferry the solute from one side of the membrane to the other. The different possible spatial arrangement of the protein units are called *conformers*. The change from one conformer to the other without changing the configuration allows the protein to accommodate the transporter ion without breaking the covalent bonds. The change in confirmation is considered to occur via rotation about single bonds in the protein structure. The energy required for the conducting pore in the protein to change between conformers is absorbed from its environment when available to move the transported ion across the membrane.

The energy required for a protein transporter to switch between two conformers is modeled using thermodynamics[25]. Assuming that the protein exists in two of the possible

states: open(A) and closed(B),

$$\mathrm{A} \rightleftharpoons \mathrm{B}$$

and the energy available in each of the states are given by the molar concentrations of $[A]$ and $[B]$, as

$$G_a = G_a^{\mathrm{o}} + RT \ln [A]$$
$$G_b = G_b^{\mathrm{o}} + RT \ln [B]$$

The difference in energy between the two states to translocate the transported species is

$$\Delta G = G_b - G_a = \Delta G_{ab}^{o} + RT \ln \frac{[B]}{[A]}$$

For the two conformers at equilibrium with concentrations $[A]'$,$[B]'$, the energy required to switch states is

$$\Delta G_{ab}^{o} = -RT \ln K'$$

where $K' = [B]'/[A]'$. The additional energy required for the protein to change confirmation at non-equilibrium concentration is given by

$$\Delta G = -RT \ln K_{eq} + RT \ln \frac{[B]}{[A]} \tag{1.6}$$

This equation gets augmented with any additional external forces that should be overcome for ion transport and can be expressed as

$$\Delta G = -RT \ln K_{eq} + RT \ln \frac{[B]}{[A]} + f_i \tag{1.7}$$

Any external source that provides this energy to the protein to change its confirmation will drive ion transport. Thus based on external stimulus that provides this additional energy, transport of ions through the protein transporter can be grouped into two broad categories: active and passive transport.

Passive transport

Passive transport is the conduction of ions and species through the transporters for an established gradient and is also referred to as **facilitated diffusion**. The gated channel proteins participating in facilitated diffusion demands merit for discussion in this document as the transport of species is driven by a chemical, electrical or mechanical stimulus. Accordingly, facilitated diffusion is classified into ligand gated, voltage gated and stretch activated transport.

Ligand-gated transport:

The biochemical reactions introduces species that serve as a chemical signal to ligand-gated ion transporters. The signaling ligand binds to the transporter subunit and this chemical binding provides the additional energy to the pore forming subunits to change its confirmation. Thus the channel pore becomes conductive to a selective species down its concentration gradient. The flux of species across the membrane is dependent on the affinity of the transported species to transporter and switching rate of the transporter. The principle of ligand-gated transport through cell membranes is illustrated in Figure 1.9.

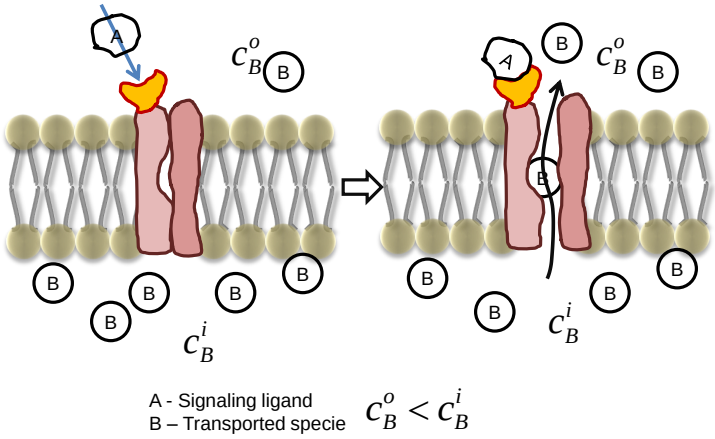

Figure 1.9: Ligand-gated transport

Voltage-gated transport:

Voltage-gated transport results from a transmembrane electrochemical gradient established across the membrane with the transporter. The genesis for membrane potential is the difference in number of charged species on both the sides of the membrane due to biochemical reactions inside the cell and cellular signaling from neighboring cells. The mechanism of voltage-gated ion transport is illustrated in Figure 1.10. The schematic shows that the transport of ions through voltage-gated transporter proteins depolarizes the membrane. The protein subunit forming the channel pore opens and becomes conductive to a selective ion or neutral molecule for a threshold transmembrane potential. The electrostatic energy available across a membrane of thickness d for a charged specie z for a membrane potential $\Delta\Phi$ is given by:

$$E_m = zd\Delta\Phi \tag{1.8}$$

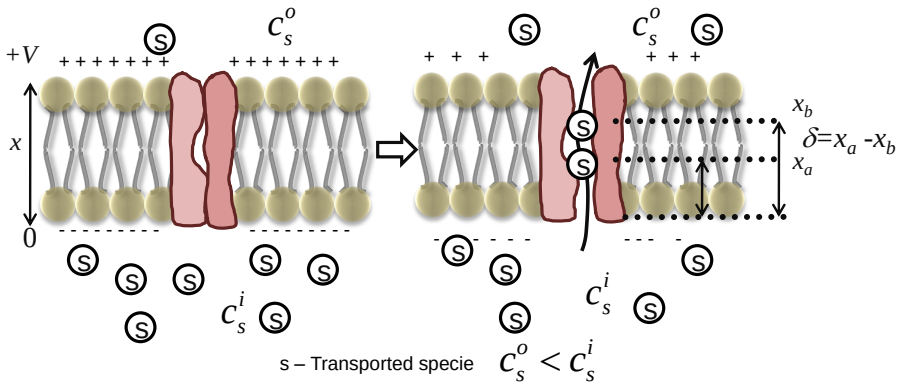

Figure 1.10: Voltage-gated transport

This energy is used for transporting a selective solute that can neutralize the electrostatic gradient across the membrane. Other charged species that are not selective still contribute to the voltage independent part of the external force that needs to be overcome by the transporter. The expression for energy required to transport a species can be found by combining Equations 1.8 and 1.7 and is

$$E_m = -RT \ln K_{eq} + RT \ln \frac{[B]}{[A]} + \Delta E_{vi}^o \tag{1.9}$$

where ΔE_{vi}^o is the voltage independent component that needs to be additionally overcome by the protein to change its conformers for transport. The protein transporter is not strictly conductive to a specific specie and other molecules having a similar charge and comparable size are ferried across the protein transporter. This effect is used by plants and animal cells for cellular signaling, turgor regulation and other mechanisms that require a biological system to generate a rapid response.

Apart from these two major categories of facilitated diffusion, few membrane proteins proteins are stretch-activated and temperature-gated. In the case of stretch-activated proteins, the channel pore opens and enters a conductive state above a threshold membrane strain. Ion transport through channels that open and close due to membrane stretch is also referred to as mechanosensitive ion transport and [44]. In the case of temperature-gated transport, the additional energy required for the conductive pore in a protein to open is provided by the heat in the system.

Aquaporins:

Aquaporins are water conducting channels in plant and animal cells[60]. Aquaporins are diverse in plants and have been classified into three plant-specific subfamilies. The types of

aquaporin vary in their location in the cell membrane. The homologous subfamilies are:

- Plasma membrane Intrinsic Protein(PIP)
- Tonoplast Intrinsic Protein(TIP)
- Nodulin 26-like Membrane Intrinsic Protein

The flux of water and small solutes through these water channels is several fold greater than most proteins in the cell membrane. The structural mechanism of gating in plants is also understood with recent X-ray studies into the structure of the protein channel. The higher flux of species through an aquaporin and recent reports on gated transport also makes this an interesting candidate for actuator development.

Active transport

Active transport[28] is the transport of ions against a resisting force- usually a concentration gradient or electrical potential. The energy required for overcoming the resisting force is provided by a biochemical reaction that releases energy stored in ATP. An ATP molecule splits into adenosine diphosphate(ADP) and a phosphate ion(Pi) and releases energy to the transporter as follows

$$ATP + H_2O \rightleftharpoons ADP + PO_4^{-3} \quad ; \Delta F^o \approx \text{-31,000 J/mol} \tag{1.10}$$

where $\Delta G^{\text{o}} = RT \ln \left(\frac{[ADP]'[PO_4^{-3}]'}{[ATP]'} \right)$ kJ/mol is the free energy of the reaction at standard concentration. The energy available from ATP hydrolysis at non-standard conditions is given as follows[82]:

$$\triangle G = \triangle G^o + RT \ln \left(\frac{[ADP][PO_4^{-3}]}{[ATP]} \right) \text{ J/mol} \tag{1.11}$$

This action is also referred to as 'pumping' and the transporter proteins involved in active transport are referred to as ion pumps. Combining the energy released to the protein by ATP with the energy required to change the confirmation of the protein in equation (1.7), the energetics of ATP power transport can be written as

$$\triangle G^o + RT \ln \left(\frac{[ADP][PO_4^{-3}]}{[ATP]} \right) = -RT \ln K_{eq} + RT \ln \frac{[B]}{[A]} + f_i \tag{1.12}$$

This section detailed the transporter protein embedded in the cell membrane and the genesis of ion and solute transport from one side of the membrane to the other. The classification of ion transport discussed has been extended to two other types in biochemistry.

1.3.3 Cotransport and antiport

In addition to the above classification, ion transport can be cotransport or antiport based on the direction of ions transported through the protein. In cotransport (also referred to as symport), another ion or a neutral molecule is transported across the membrane in the same direction. In antiport, the gradient established by one molecule is exchanged for another molecule through protein channel. The illustration in Figure 1.11 shows the transport of both A and B across the membrane in the same direction. The flux of species through the transporter is estimated by modeling the affinity of the transporter protein to the solute as a first order chemical reaction with a finite equilibrium constant. A detailed discussion on the available models and applying the existing models to characterize transport for ligand-gated diffusion will be presented in Chapter 3 of this document.

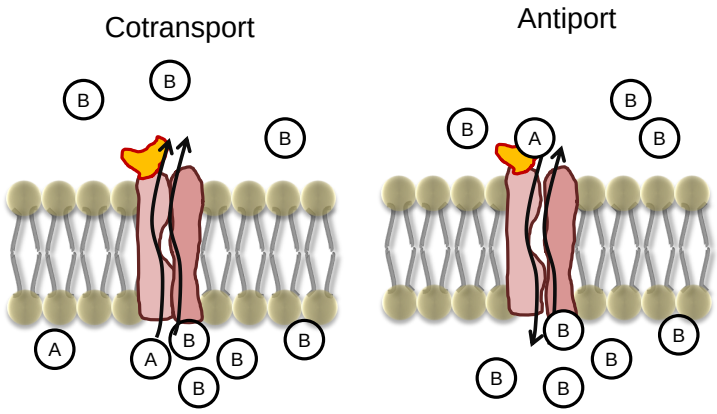

Figure 1.11: Cotransport and Antiport - based on direction of ion transport

1.4 Chemomechanical energy conversion

Actuation concepts have been developed using soft polymers, hard piezo electric materials, shape memory alloys and the like as depicted in Figure 1.1. The naturally occurring actuators have gone unnoticed due to the complexity and lack of knowledge associated with the internal mechanisms that results in actuation. The state of the art in biochemistry and molecular biology has been advancing and sophisticated techniques are available to analyze a single transporter in a lab bench. Research on extracting ion transporters from cell membranes is advancing and molecular biologists are breaking new grounds in purify-

ing membrane proteins. This dissertation attempts to bridge the technology gap between engineers and molecular biologists and combines the exclusive expertise available with two groups at Virginia Tech and at the University of Cincinnati to build an engineered device using biosynthetic components. The energy conversion devices developed in this work uses ion transport and associated fluid transport observed in cell membranes to convert the chemical energy available at a membrane interface into mechanical and electrical work. The ion transporters extracted from plant cell membranes serve as the active material in this novel concept.

1.4.1 Ion transport in mechanical transduction

The biological processes discussed in the preceding sections emphasizes the importance of ion transport through cell membranes for life functions in a living cell. The chemomechanical energy conversion concept uses ion transport in an engineered structure for actuation. Using ion transport for actuation has been demonstrated in Ionic Polymer Transducers(IPT) and hydrogels. Ionic polymer transducers[2, 79, 84] and hydrogels shown in Figure 1.12 use ion and fluid transport for actuation. The actuator element consists of an ionic polymer with mobile cations in the polymer matrix. The polymer is impregnated with water[70] or with an ionic liquid[7] and formed into films with conductive electrodes applied to both the sides. Ion migration within the constrained volume for an applied electric field from the cathode to the anode results in bending the flexible IPT. The fundamental mechanisms involves in ion transport and mathematical models for transduction are documented in various dissertations and journals [70, 9, 52, 26].

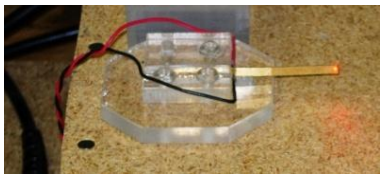

An ionic polymer transducer with Nafion as the active core

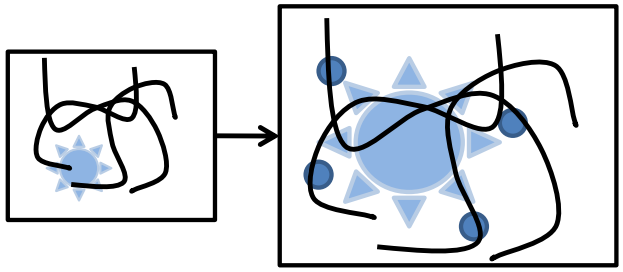

Expansion in hydrogels due to a chemical stimulus

Figure 1.12: An ionic polymer transducer(IPT) and a polymer hydrogel shown above bend and change shape due to ion and fluid transport respectively

Hydrogel resembles a hollow spherical capsule with a permeable membrane and have been been tailored to exhibit volume and shape change response for different chemical or physical stimuli like pH[1, 97], temperature[96], light[94],electric field[98], glucose[48] and recently protein blocks and peptides. Bulk fluid transport through the membrane is used for volumetric expansion and capsules packed into a structure have been demonstrated to do mechanical work.

The energy conversion concept developed in this work differs from existing concepts that use ion transport mechanism at the component level. The following section describes the chemomechanical actuation concept that uses protein transporter extracted from living cells as the active component.

1.4.2 Chemomechanical actuation using protein transporters

A membrane selectively permeable to ions, neutral molecules and water due to the presence of biological ion transporters in a lipid membrane is the active component of the chemomechanical actuator. Using two functionally different protein transporters, there can be two possible concepts to cause volumetric expansion in a capsule and in an actuator structure. The movie in Figure 1.13 demonstrates a possible concept to generate volumetric change using ion transport and assisted water movement expending ATP . This approach assumes the availability of a a protein transporter that uses *active transport* to move a proton and sucrose into the capsule and cause volumetric expansion in a single capsule. An alternative approach can employ an ion channel in the capsule shell that can transport an ion and/or a molecule by *facilitated diffusion* and result in volumetric expansion of the spherical capsule. Volume change in a single capsule can be augmented using an arrangement as shown in Figure 1.14 to result in bending deformation and shape change of a structure. The applicability of the two concepts relies on the technology to extract the protein transporter, engineer the transporter in a membrane and drive ion transport and associated water transport to generate deformation in the structure. A hardened liposome shell with a protein transporter assembled in functional configuration is essential to form an actuator design using an active transporter or a cotransporter.

Spherical capsules formed from phospholipids were first discovered in 1962 by Bangham [4] and are known liposomes. In 1974, Bangham et. al [5] also demonstrated the

Click here

Figure 1.13: Demonstration of volumetric expansion of a synthetic capsule formed from lipid membranes with ion transporters expending ATP

similarity of the membrane shell of liposome to the cell membrane. Due to the similarity, the liposome served as a tool to analyze protein activity. Since their discovery, researchers have contributed to the knowledge base and have improved on the techniques to produce liposomes and to analyze their properties. Dobereiner[22], Needham[68], Mukherjee[64], Heimburg[36] and many more have unraveled the desirable properties of lipid membranes that form the shell of the liposomes. The desirable properties of liposomes reported in the articles cited above can be summarized as follows:

- Mean shape of a capsule formed from lipid membrane whose and area, volume of the lipids forming the shell remains a constant at a given temperature and osmotic conditions
- Volume of the vesicle adjusts itself to equilibrate for internal and external osmotic pressures
- Semi-permeable to water with high permeability rates for osmotically driven flow
- Excellent candidate to mimic cell membranes and to infuse protein transporters for

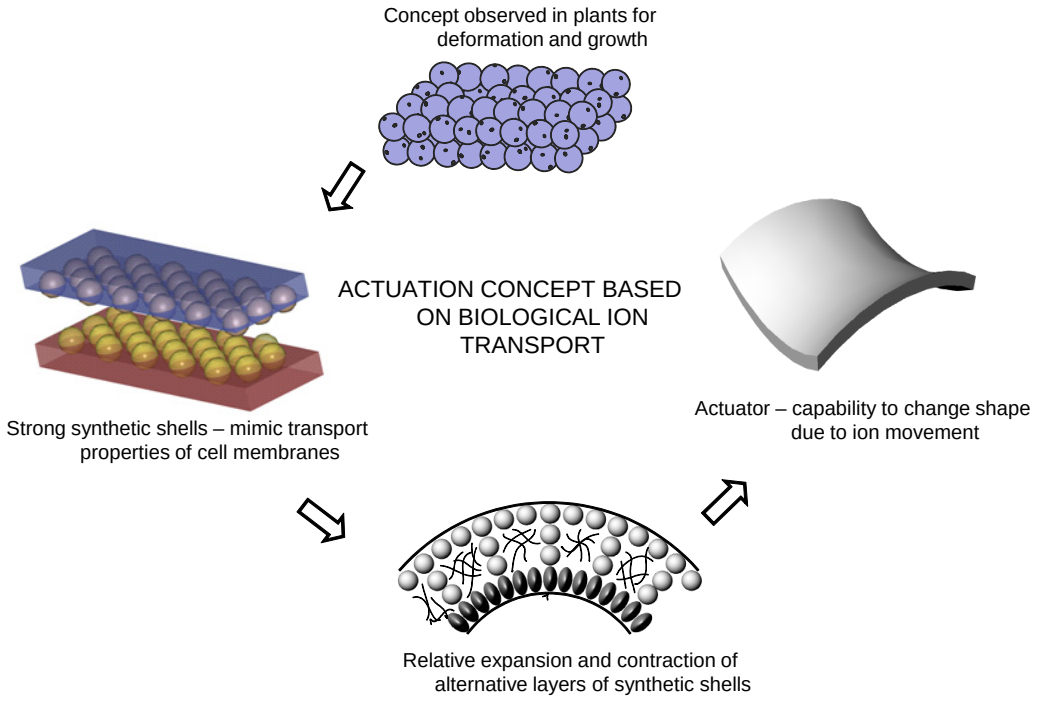

Figure 1.14: Arrangement of spherical capsules in a structure to result in shape change

functional analysis

The fundamental unit of the chemomechanical actuator can be fabricated from liposomes with proteins transporters embedded in the membrane shell as shown in Figure 1.13. The protein can be activated by using the aqueous medium that will apply the chemical stimulus across the membrane shell.

1.5 Chemoelectrical energy conversion

In recent years there has been significant interest in the development of novel power sources for smart material systems. Much of this work has been driven by the development of low-power devices for remote sensing and wireless data transmission. It is possible to build a sensing device with wireless transmission with a total power requirement on the order of 10 mW or less[73]. The availability of low-power devices has led to renewed interest in energy scavenging devices such as piezoelectric and thermal energy harvesters. Piezoelectric energy harvesting devices transform ambient vibration energy into stored electrical energy. Recent work on this topic has shown that continuous power levels on the order of mW are

possible[87]. Similar advances in thermal energy harvesters have also been made due to improvements in materials such as thermoelectrics. The chemoelectric energy conversion developed in this work targets devices with a power consumption envelope of a few microwatts or milliwatts. The power source utilizes a biochemical reaction starting from ATP occurring in an active transporter protein embedded in a plant cell membrane.

In plants cells, plasma membrane H^+-ATPase plays a vital role in nutrient absorption at the cell wall consuming ATP energy[88]. In animal cells, the equivalent enzyme to plasma membrane H^+-ATPase found in plants is the Na^+/K^+-ATPase. The H^+-ATPase and the Na^+/K^+-ATPase belong to a category of transmembrane proteins called P-type ATPase, which uses the energy available in ATP through a phosphorylated intermediate[11]. In addition to the P-type ATPase, the V-type ATPase found in plant and animal cells use ATP to maintain pH and ion concentration within the cell. The V-type pumps commonly found in the vacuolar membranes consume ATP in the cell cytoplasm, establishing a pH gradient across the vacuolar membrane. The established electrochemical H^+-potential is used for symport and antiport of species through channels and channel mediated systems[10]. These ATP-powered molecular machines embedded in the cell membrane convert the chemical energy in ATP into electrochemical gradients through a biochemical pathway.

The V-type ATPase and its location in a plant cell is shown in Figure 1.15. The V-ATPase is a molecular motor that has two major components as shown - a membrane peripheral domain containing the nucleotide binding sites(V_1) and a membrane spanning portion which has the proton channel(V_0). An ATP molecule binds to the V_1 site in the pump and move protons through the membrane spanning proton channel. This energy conversion concept is based on converting the electrochemical potential established by the ATP-driven pump and differs from other biological transporter based energy conversion devices that use the photochemical pathway in *Halobacterium halobium* [45, 54, 59, 8, 39]. The prototype device that does chemoelectric energy conversion concept is referred to as 'BioCell' in this document. The electrogenic properties have been reported by Drachev et. al[23] to verify the electrical potential generated by proton transport through mitochondrial ATPase. This work uses vacuolar ATPase and the intent of this work is fabricate an energy conversion device that can use ATP as the source.

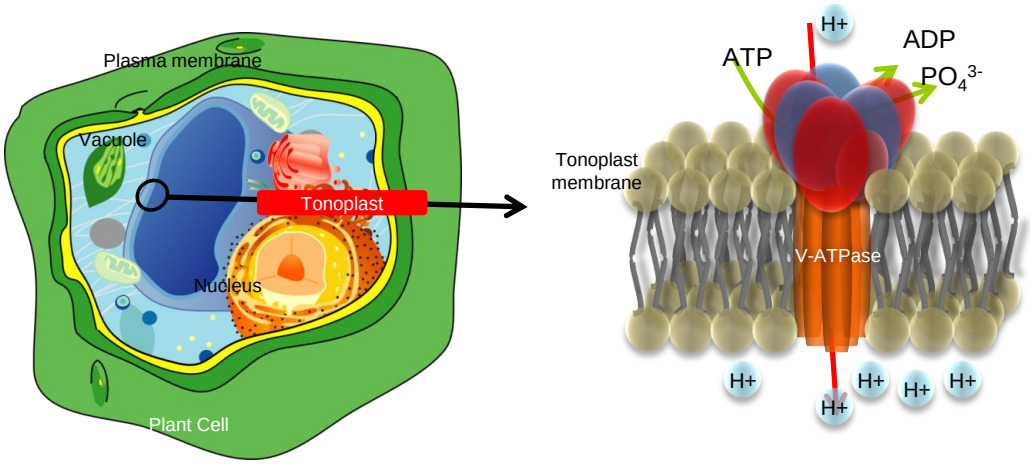

Figure 1.15: V-type ATPase in the tonoplast membrane of a plant cell and its application in a BioCell. The proton pumping enzyme is shown with the membrane peripheral(V_0) and membrane integral(V_1) units. The protein develops an electrochemical proton gradient from chemical energy stored in ATP.

1.6 Contributions

The significant contributions from the work reported in this document is provided in the list below:

- Fluid transport properties of a membrane assembly with SUT4 due to sucrose cotransport has been characterized. The transport experiments in a membrane assembly for different sucrose concentrations provided the characterization curves for fluid transport through the membrane assembly.

- A prototype actuator that uses SUT4 as the gating device for chemomechanical energy conversion has been fabricated. The deformation experiments using the membrane assembly with SUT4 showed that the deformation produced in the actuator can be controlled by changing the sucrose concentration in the system.

- Characterizing fluid transport through a membrane assembly powered by ATP hydrolysis reaction with the intent for using it in an actuator is a third major contribution. This demonstrates the use of H^+-ATPase protein to energize a cotransporter in the membrane assembly of an actuator using a biological fuel.

- Chemoelectrical energy conversion using a protein to generate electrical power starting from ATP as an alternative power source is proposed. The single cell has a measurable

cell voltage and current at a power density of 2 μW/cm^2. Multiple single cells can be stacked in series and parallel to generate higher currents and voltage. This breaks a new ground in using the chemical energy available in living cells to generate electrical power.

1.7 Document overview

This introductory chapter provided the motivation for using biological mechanism for fabricating the actuator. The introduction to cell membranes and proteins formed the foundation for the bio-inspired chemomechanical and chemoelectrical energy conversion concepts presented in this work. The work presented here involves design, fabrication and experimental evaluation of prototypes that use ion transporters to perform mechanical and electrical work. The document is organized into six chapters and chapters two and three discuss fluid transport through the membrane with protein transporter. Chapter two analyzes possible candidate materials for implementing the chemomechanical energy conversion concept, presents a thermodynamic analysis for cotransport and outlines the kinetic rate model for characterizing fluid transport through the membrane assembly. Chapter three presents two major contributions from this work. The first part discusses the experimental work done to characterize fluid transport driven by concentration gradient and the second part presents a novel concept to use ATP as a fuel to trigger fluid transport through the membrane. The ATP powered fluid transport can form the foundation for building an actuator using ATP as the fuel. Chapter four discusses the fabricated prototype actuator that uses a concentration gradient to generate mechanical deformation. The discussion builds upon the concentration gradient driven transport experiments and presents the actuation experiments conducted on a prototype actuator. The fifth chapter in this dissertation introduces the chemoelectrical energy conversion concept that demonstrates our capability to generate electrical power from ATP hydrolysis reaction. The last chapter presents a summary of the work done, conclusions and future directions for this work.

Chapter 2

Chemomechanical Energy Conversion

Chapter 1 discussed different types of ion transporters, transport processes and the significance of lipid membranes in a living cell. The chemomechanical and chemoelectrical energy conversion concepts based on transporter proteins were outlined. This chapter builds upon the chemomechanical energy conversion concept introduced in Section 1.4.2 to develop and design a protein based actuator. Thermodynamics of facilitated solute cotransport through the membrane is used to estimate the operating gradients for cotransport in the actuator. The kinetic rate model for solute cotransport developed by Lieb and coworkers [90] is discussed and modified for the protein based actuator to predict the equilibrium constants and transport rates for fluid flux through the membrane of the actuator..

The chemomechanical energy conversion concept presented in Section 1.4 discussed a possible method to convert chemical energy in ATP into expansion work using protein transporters. The protein transporters in this concept are reconstituted in the shell of a fluid filled capsule. The fundamental unit of actuation is the capsule with a bilayer lipid membrane(BLM) shell carrying the protein transporter. The microcapsule of the actuator described in Figure 1.14 should posses the following properties:

1. The membrane shell of the microcapsule should accommodate biosynthetic components and have higher tensile strength than values reported for liposomes [68]

2. The shape of the capsule should be influenced only by fluid transport through the protein transporter in the membrane shell

3. The capsule shape should be insensitive to solutes that has no effect on the controlled gateway in the membrane shell

4. The turgor pressure generated by each microcapsule should be transmitted to the structure with minimal losses

5. The protein transporter should be inserted into the capsule shell in the desired polarity for transport

The capsule is structurally similar to a liposome and its shape is highly influenced by solute concentrations on both sides of the membrane. Fabricating a microcapsule that meets all of the above requirements and arranging them in an array to demonstrate extensional, bending and morphing properties poses numerous technical challenges. In this effect, the capsule based chemomechanical energy conversion was modified into a design that used a planar membrane assembly as the functional membrane. The actuator is modified to demonstrate extensional actuation using protein transporters formed in a planar BLM. This design that uses a protein transporter extracted from plants for chemomechanical energy conversion is called the protein based actuator or actuator.

2.1 Planar BLM supported on porous substrates

A planar BLM supported on a porous substrate exposes both the sides of the BLM. A protein transporter reconstituted in the planar membrane can be subjected to the desired chemical or electrochemical stimulus by changing the aqueous medium. This convenience has led to use of planar BLMs in electrochemical biosensors that analyze protein function and in immunology[102].

Forming a planar BLM across small pores has been studied since the 1960s and was first demonstrated by Mueller et al [63] in 1962. Their experimental confirmation of forming a BLM by spreading phospholipids across a pore drew in three centuries of observation as reported by Tien and Ottava[100]. Mueller and coworkers showed the self-sealing properties of the planar membrane and also demonstrated electrical excitability using EIM (excitability-inducing molecule). The procedure to form a planar BLM using Mueller's method and various techniques to analyze a BLM is documented in by Tien[99] in his review article. The procedure involves using a teflon sheet with a pore as a partition

between two aqueous chambers. The lipids dissolved in a solvent is spread across the pore and allowed to dry before bringing it on contact with water. On coming into contact with water from both sides, the lipids self-assemble into a pore as shown in Figure 2.1. This method is called the painting technique and relies on the self-assembly. Since the first demonstration to form a BLM by Mueller and coworkers, many other methods have been developed to form a supported BLM. The substrates that can accommodate a BLM have been improved since Tien's first experiment with contributions from Wagner et al[104], Cheng et al [16], Saccani et al[77], Sackmann[78], Yang et al[111], Fujiwara et al[29] and Ide and Ichikawa[43]. A survey on the different techniques is presented here to identify the available techniques for BLM formation on porous solid support. The mechanism of lipid molecule self-assembly is discussed with the methods to form a BLM.

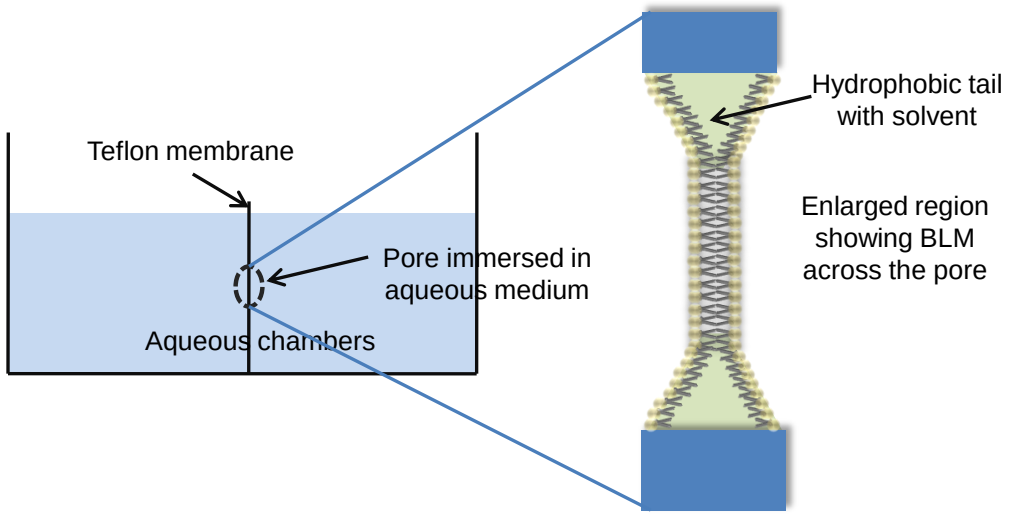

Figure 2.1: Mueller Rudin method of forming a planar BLM

A broad classification on the techniques available for the formation of a planar BLM will fall into the following categories:

1. Lipid self-assembly - Painting technique
2. Liposome fusion
3. Langmuir-Blodgett technique
4. Chemical methods

2.1.1 Lipid self-assembly - Painting technique

The painting technique was the first method to form a BLM on a porous substrate[99]. The self-assembly of lipids in to planar BLM relies on the amphiphilic nature of the lipid molecule. This method is similar to the spreading of a thin film of oil on the surface of water. Such a film is only a molecule thick and the molecules held together by van der Waals forces of interaction. Similar energy interactions arise when a phospholipid molecule is completely submerged in a polar solvent. The lipid molecule aligns itself into bilayer and forms the liposome shell when completely surrounded by the molecules of the polar solvent. The liposome thus formed traps the solvent molecules inside to minimize the hydrophobic and hydrophilic interface interaction. The lipid molecules self-assemble into a planar BLM when coated on a hydrophilic surface and introduced into an aqueous solution. On a hydrophobic surface, the lipids form into a monolayer with the hydrophobic tails attached to the surface. When the lipid molecules are added to a hydrophilic substrate with pores smaller than 0.25 mm, the lipids spread across and seal the pore. The resulting bilayer resembles a planar BLM formed on the surface of a hydrophilic solid substrate. The hydrophilic ends at the periphery of the membrane disc are anchored to the walls of the pore in the solid substrate. The amount of lipids required to form a planar membrane is larger than the lipids that form into a BLM. Painting technique or spreading are the other names used to refer his method. The adhesion of the lipid membrane to the substrate can be varied by selecting a substrate that will maximize interactions.

2.1.2 Liposome fusion

This method is based on the naturally observed phenomenon of cell fusion where the cell membranes of two or more cells merge and form a single cell. A BLM is formed from phospholipids in a two step procedure and was reported for the first time by Cohen and Zimmerberg[17, 115]. The first step in this procedure is liposome formation. To form a liposome, the lipids are dissolved in an organic solvent and introduced into an aqueous medium. The phospholipids self-assemble into a liposome over time and the process is accelerated by mechanical agitation of the solution or by the application of an an alternating electrical signal. Recently preparation of liposomes using inkjet printers have been reported to produce uniform size distribution of the prepared liposomes. In the second step, the

liposome shell is spread on the substrate to form a BLM. Atomic Force Microscopy (AFM) images of liposome fusion by Jass et. al [46] provide an excellent time-lapse information of BLM formation. Since this method relies on self-assembly, the selectivity of the phospholipid to the substrate plays a significant role to form a stable BLM. Other factors like surface roughness, the size of the pore and presence of specific cations in the aqueous medium are reported to control adsorption, rupture and spreading of the BLM during its formation.

Liposome fusion is best suited to introduce purified proteins into a planar BLM formed across a pore to analyze protein activity. A protein extracted from plant or animal cell contains BLM from the host cell membrane. The proteins with the cell membranes form into a liposome on storing them in a neutral solution. During protein reconstitution into a planar BLM, the liposomes with proteins are added to an planar BLM. The lipids from the host cell membranes fuse with the already formed BLM and insert the ion channel across them membrane.

2.1.3 Langmuir-Blodgett method

The Langmuir-Blodgett method is a layer deposition technique multiple layers are built one layer at a time[33]. A layer of lipids is spread on the surface of an aqueous solution in a trough and the substrate is dipped into the solution to adsorb the spread lipids on its surface. Computer controlled equipments are commercially available to form a lipid bilayer on different substrates. The monolayer of lipid molecules scattered on the surface are compacted to form a closely packed monolayer. The substrate on which the lipid bilayer needs to be formed is dipped into the monolayer. As the lipid molecules are adsorbed onto the surface of the substrate, a feedback system maintains a constant surface pressure to provide uniform deposition on the surface. The procedure is repeated to form multiple layers. The polarity of the phospholipid molecule should be accounted to form multiple layers.

From the different methods available for forming a planar BLM discussed, the lipid coating/spreading technique is selected to form a BLM. The method is very simple and relies on the natural affinity of the lipid molecules to spread into a BLM across the pores.

2.1.4 Chemical methods

This method involves preparing the surface on which a BLM is formed to improve adhesion, mechanical stability and mobility of lipid molecules in the BLM[78]. Sackmann[78] discusses three different techniques to chemically bind a BLM to the surface for fabricating biosensors. The first method is to bind the monolayer by a covalent bond or an ion bridge with the substrate as demonstrated by Tamm and McConnell[95]. The second method is to use a polymer bed to tether the BLM to the surface. The third method is to use a BLM resting on a hydrated polymer film. Tamm and Wagner[104] demonstrate poly-ethylene glycol as the tether group that anchors the BLM to the substrate. Cheng et. al [16] demonstrates forming discrete membrane arrays by using a gold layer on the porous substrate and using a lipid molecule that can covalently bind to the substrate, thus securing the BLM on the surface. The chemical methods presented here are examples of different methods available to form a BLM on the surface. Photo polymerization[71] of a lipid film has been recently demonstrated to form a poly methyl methacrylate (PMMA) cross-linked BLM that holds the lipid membrane together in a glass microfiber substrate.

The method for forming a planar BLM on a porous substrate is understood well enough to use it in actuator fabrication. The sophisticated chemical methods can be adopted to form a synthetic lipid membrane with embedded transporters as demonstrated by Nikolelis et al [71] to improve the design. Thus using a planar BLM is a logical step to build the first chemomechanical energy conversion device.

2.2 Protein based actuator

A schematic of the actuator developed in this work is shown in Figure 2.2. A porous substrate supports a planar bilayer lipid membrane with transporter proteins across its pores. The BLM with the proteins are henceforth referred to as the membrane assembly. The membrane assembly is formed between two chambers filled with aqueous solutions that subject the protein transporter to a chemical stimulus. The two chambers are analogous to the interior and exterior of the spherical capsule based concept shown in the movie in Figure 1.13. The top chamber is a cavity in the actuator plate and has a deformable coverplate on top. Ion selective transporters in the planar BLM convert an applied chemical potential into fluid flux through the membrane assembly into the top chamber. The additional volume of

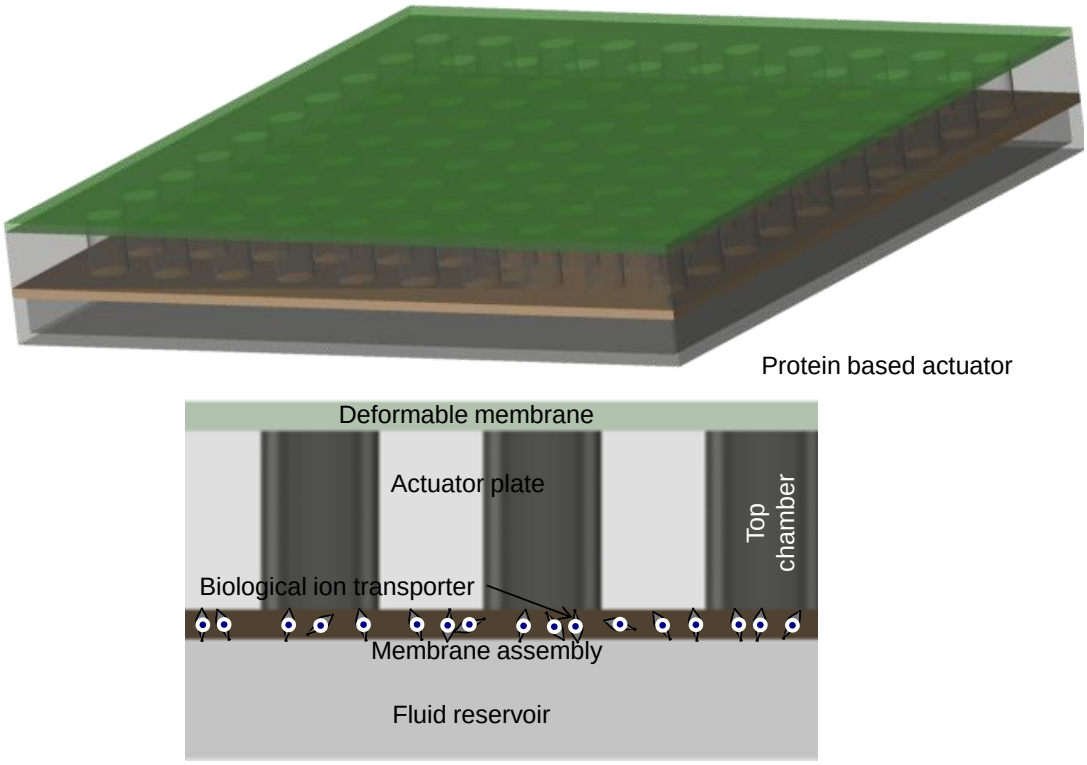

Figure 2.2: The protein based actuator

fluid in the top chamber due to combined ion and fluid transport deforms the top coverplate.

Ion transport and associated fluid transport can be generated using protein transporters across the membrane assembly via one of the three methods:

1. An active transporter that expends ATP and moves an ion with water molecules into the top chamber

2. A secondary active transporter subjected to a concentration gradient of a selective specie that moves a selective specie and water molecules

3. A combination of active transporter and a secondary active transporters in which the active transporter protein sets up the stimulus for the secondary active transporter to result in fluid transport

The three methods to generate ion and fluid transport listed above require extracting a specific transporter from a plant cell membrane. The method in option 1 requires ATP

supplied to the system in the reservoir or the top chamber. The second method generates ion and fluid transport by combining a facilitating signal (chemical or electrical) with concentration gradient of a specie across the membrane assembly. The third method combines the work done by an active and a secondary active transporter to generate fluid flux and deformation in the actuator. This requires ATP fuel and a concentration gradient of species across the membrane assembly.

Fabricating an actuator using any of the three options demands the technology to extract proteins from cell membranes at high levels of purity. The collaboration with Prof. John Cuppoletti's group in the University of Cincinnati gave access to exclusive protein samples for designing the actuator. The first generation of actuator developed in this work uses a secondary active transporter to generate fluid flux and to exhibit volumetric strain. The protein selected for the actuator is a cotransporter. The energy required for the protein to generate fluid flux is the electrochemical gradient of protons across the membrane. The balancing concentration of solute for the applied gradient is obtained from thermodynamics of cotransport.

2.3 Thermodynamics of facilitated cotransport

Thermodynamic analysis of ion transport across a membrane subjected to an ion concentration gradient was developed by Kedem and Curran[49, 47]. The phenomenological equations in their model was based on Onsager's model of solute transport and the process is assumed to be irreversible[72]. Flux through a membrane is related to the forces by phenomenological coefficients. The forces acting in a selectively permeable membrane for driving coupled ion transport are

- Chemical potentials due to difference in concentration of non-electrolytes
- Charge gradient due to difference in concentration of charged species
- Osmotic pressure resulting from electrochemical and osmotic gradients

The flux of different species that balance their chemical potentials across membrane is given by reciprocal equations and the coupling between the flux of non-electrolytes and charged species is expressed as a ratio of phenomenological coefficients.

Thermodynamics of ion transport from Kedem and Curran's work was later applied to different transporter systems[12, 80, 37, 105]. The equations available for a cotransporter system available from the literature cited above is applied to the actuator membrane assembly. In voltage-gated facilitated diffusion, a gradient of positively charged ions provide the driving force for transport. The solute is accumulated on one side of the membrane due to the electrochemical gradient. Non-equilibrium condition in the reciprocal equation gives the flux of species until the system reaches equilibrium. The concentration of the cation and the solute at equilibrium is derived by assuming zero flux in the reciprocal equation. The ratio of fluxes give the stoichiometry of the cation and solute through the cotransporter. The reciprocal equations applicable for solute cotransport is discussed due to its relevance with the actuator membrane assembly. The commonly observed cation in plant cotransporter proteins is a proton and hence the reciprocal equations use the concentration gradient of proton as the driving force for solute transport. The schematic in Figure 2.3 represents

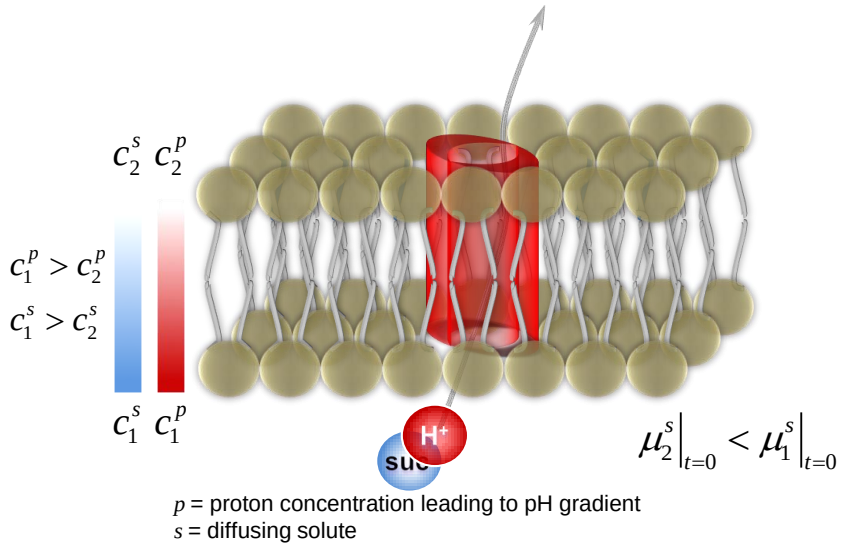

Figure 2.3: Thermodynamic variables to model facilitated cotransport driven by electrochemical gradients

cotransport of a solute s through the protein transporter driven by concentration gradient of protons p across the membrane. The concentration of proton on both sides of the membrane, represented by c_1^p, c_2^p, results in an electrochemical gradient $\Delta\mu^p$. The concentration gradient of solute s across the membrane represented by c_1^s, c_2^s has a chemical potential represented by $\Delta\mu^s$. The gradient of proton (p) and the solute (s) are along the same direction

and they travel together through the transporter from side 1 to side 2 of the membrane as shown in Figure 2.3. It is assumed that as solute travels through the transporter, water molecules travel together to balance the localized osmotic gradient established across the membrane.

Under a non-equilibrium condition, the chemical potentials result in flux ϕ_s and ϕ_p through the protein transporter. The flux through the transporter[92] due to gradients $\Delta\mu_p, \Delta\mu_s$ are related to the chemical potential by the relation[30]

$$\begin{aligned} \phi_s &= L_{s,s}\Delta\mu_s + L_{s,p}\Delta\mu_p \\ \phi_p &= L_{p,s}\Delta\mu_s + L_{p,p}\Delta\mu_p \end{aligned} \tag{2.1}$$

The driving forces that contribute to the flux are[32]

$$\Delta\mu_s = RT \ln\left(\frac{\gamma_s c_1^s}{\gamma_s c_2^s}\right) \tag{2.2}$$

$$\Delta\mu_p = RT \ln\left(\frac{\gamma_p c_1^p}{\gamma_p c_2^p}\right) \tag{2.3}$$

The terms γ_p and γ_s represent the activity coefficients of protons and sucrose and should be accounted for non unity activity. For smaller concentrations the value of $\gamma_p = \gamma_s = 1$. In the presence of an additional transmembrane voltage $\Delta\Psi$ imposed on the system externally, the driving potential is augmented by $zF\Delta\Psi$, where F is Faraday's constant and z is the charge on the specie that moves through the membrane to balance the electrical gradient. The coefficients in the flux equation 2.2 and 2.3 represent the coupling between the ion and solute transport through the membrane. The coefficient $L_{s,s}$ represents the coupling between the solute chemical potential and the solute flux. The coefficient $L_{s,p}$ is the cross coefficient that relates sucrose flux to the proton electrochemical potential and likewise, $L_{p,s}$ relates the proton flux to the solute chemical potential. The cross coefficients $L_{s,p}, L_{p,s}$ are assumed equal due to the Onsager symmetry relationship[72],

$$L_{s,p} = L_{p,s} \tag{2.4}$$

It is assumed that ϕ_s is only related to the proton electrochemical potential and the proton flux ϕ_p is only related to the solute chemical potential as discussed in Gerencser and Stevens [30]. Mathematically, this is represented as

$$|\Delta\mu_p L_{s,p}| > \Delta\mu_s L_{s,s}$$

Using this assumption for fluid transport through the membrane assembly in the actuator, the flux equations are

$$\begin{aligned} \phi_s &\approx L_{s,p}\Delta\mu_p \\ \phi_p &\approx L_{p,s}\Delta\mu_s \end{aligned} \tag{2.5}$$

This assumption can be applied to represent the stoichiometry of proton-solute cotransport through the protein by the expression:

$$\eta_{s,p} = {}^{\phi_p}/_{\phi_s} \tag{2.6}$$

The reciprocal equations and equilibrium condition for cotransport through the membrane is applied to the membrane assembly in the actuator. The two sides of the membrane - bottom chamber and top chamber as shown in Figure 2.2 are referred to as side 1 and side 2 of the membrane assembly. The concentration terms are represented as c_x^y, where x denotes the side of the membrane and y denotes the species of interest. Similar nomenclature is applied for other thermodynamic variables for the solute. Using the notation used in this document, the concentration of protons, solute on side 1 and side 2 of the membrane are c_1^p, c_1^s and c_2^p, c_2^s respectively. The solute concentration on side 2 changes from an initial concentration of $c_2^s|_{t=0}$ to $c_2^s|_{eq}$. The equilibrium concentration of the solute is obtained from the reciprocal equations shown in 2.1. Due the transport of protons with the solute from side 1 to side 2 of the membrane, the concentration of protons decreases on side 1, lowering electrochemical gradient with time. A higher quantity of the solute can be accumulated on side 2 by maintaining a constant driving force across the membrane. To apply a constant electrochemical gradient to the membrane assembly, hydrogen ion buffers are added to both the sides of the membrane. Additionally, the cotransported solute is added to the side 1 of the membrane at the start of the process to achieve fluid transport into chamber 2. At equilibrium, the fluxes, $\phi_s = \phi_p$, are equal to zero. This can be applied to the equations in 2.5 to obtain the final concentration of sucrose. Assuming a stoichiometry of one for cotransport through the channel, a force balance at equilibrium is given by

$$RT\ln\left(\frac{c_1^s}{c_2^s}\right) + RT\ln\left(\frac{c_1^p}{c_2^p}\right) + zF\Delta\Psi = 0 \tag{2.7}$$

In the absence of additional electrical field across the membrane and assuming that the concentration of the solute remains constant on side 1, the equilibrium concentration of the solute on side 2 can be obtained from the relation

$$c_2^s = c_1^s 10^{\Delta pH} \tag{2.8}$$

where $\Delta pH = pH_2 - pH_1$ In the presence of an transmembrane electrical potential($\Delta\Psi$) along the direction of the imposed pH gradient, the equilibrium concentration of the solute on side 2 of the membrane is given by the relation:

$$c_2^s = c_1^s 10^{(\Delta pH + \frac{\Delta\Psi}{RT})} \tag{2.9}$$

In a membrane with zero initial concentration of the solute on side 2 and limited amount of solute on side 1, the equilibrium concentration on both the sides of the membrane is derived by mass balance and the thermodynamic expressions for equilibrium. A limited amount of solute on side 1 of the membrane can be equated to the amount of solute particles on both the sides of the membrane. The number of moles of the solute s on side 1 and side 2 at equilibrium condition be denoted by $n_1^s|_{eq}$ and $n_2^s|_{eq}$. The volume of the chamber on side 1 and side 2 of the membrane be denoted by V_1 and V_2, and the resulting volume ratios defined by $V_r = V_1/V_2$.. At equilibrium condition the number of moles in the system is constrained by

$$n_1^s|_{eq} + n_2^s|_{eq} = V_1 c_1^s \tag{2.10}$$

The equilibrium concentration on side 2 of the membrane is given by the expression in Equation 2.8. Rewriting the equation in terms of the number of moles of the solute on both the sides of the membrane,

$$n_2^s|_{eq} = \frac{n_1^s}{V_r} 10^{\Delta pH} \tag{2.11}$$

Substituting the Equation 2.11 in 2.10, the concentration on side 1 at equilibrium condition is obtained in terms of the initial solute concentration on side 1 of the membrane. Similarly, the concentration of the solute at equilibrium on side 2 of the membrane is obtained. For a cotransporter based system with a constant electrochemical gradient and finite amount of solute on side 1 of the membrane, the expression for the equilibrium concentrations on both sides of the membrane is related to the volumetric ratio $V_r = V_1/V_2$ of the two chambers and the initial concentration c_1^s on side 1 of the membrane by the relations

$$c_1^s|_{eq} = \frac{V_r c_1^s}{V_r + 10^{\Delta pH}} \tag{2.12}$$

$$c_2^s|_{eq} = \frac{10^{\Delta pH} V_r c_1^s}{V_r + 10^{\Delta pH}} \tag{2.13}$$

The resulting concentration gradients of solute can be used to estimate the osmotic potential and evaluate the additional fluid that needs to be on side 2 of the membrane to maintain

osmotic equilibrium. The osmotic pressure can be combined with the mechanics of the coverplate to estimate deformation at the center of the coverplate.

2.4 Kinetic model for facilitated ion transport

The thermodynamic model predicts the bulk properties of the medium on both the sides of the membrane as the reaction proceeds to equilibrium. The model presents very little information on the mechanism of solute transport through the membrane. To overcome this limitation, Lieb and coworkers[90] hypothesized a mechanism for solute transport by facilitated diffusion through an ion channel. The kinetic model based on the this mechanism uses reaction rates to characterize solute transport through the protein. The model presented for fluid transport through the membrane assembly of the actuator is directly based on the four state model first proposed by Lieb[90] and is modified to quantify the fluid flux through the membrane assembly of the actuator.

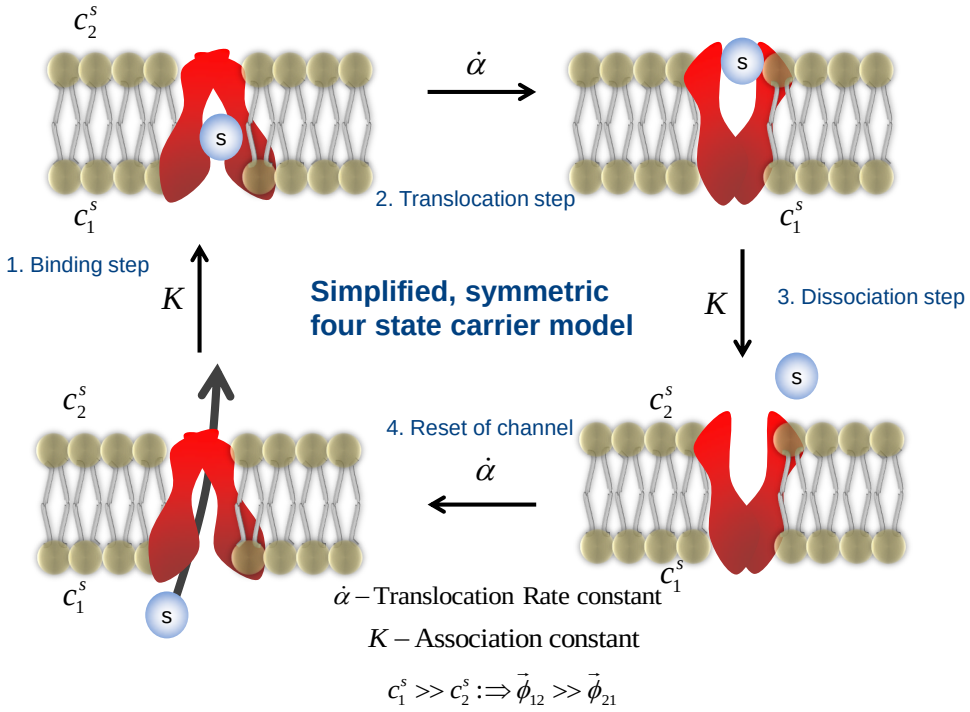

Figure 2.4: Four state carrier model with one diffusing solute

A schematic of the simplified, symmetric, four-state carrier model for the protein transporter is shown in Figure 2.4. The BLM with the cotransporter separate is subjected

to a concentration gradient of the transported solute represented by c_1^s, c_2^s on side 1 and side 2 of the membrane assembly. A constant electrochemical proton gradient is applied across the membrane. The side 1 of the membrane has a higher concentration of protons and hence has a lower pH than side 2. The pH gradient activates the protein channel for cotransport from side 1 to side 2. Transport of the solute through the channel is assumed to occur in four discrete steps[90]

1. Binding step
2. Translocation
3. Dissociation
4. Reset step

The reaction steps are characterized by equilibrium constant K and translation rate $\dot{\alpha}$. The concentration gradient of the solute s across the membrane assembly is directed from side 1 to side 2 of the membrane and the flux due to reaction steps in the reverse direction is considered negligibly small.

Binding step: The transporter protein in the membrane assembly is activated by the transmembrane pH gradient and binds with a sucrose molecule in the aqueous medium on side 1. This step can be written as a first-order chemical reaction with a equilibrium constant K. An unbound transporter T combines with a solute s to become a bound transporter sT on side 1 of the membrane assembly. The chemical reaction for this reaction step is written as:

$$T_1 + s_1 \underset{\leftharpoondown}{\overset{K}{\rightharpoonup}} sT_1 \tag{2.14}$$

The mass of unbound transporters per unit area on side 1 is represented by m_1^T and number of solute bound transporters is represented by m_1^{sT}. The equilibrium constant K for the binding reaction due to the solute concentration c_1^s is given by:

$$\frac{c_1^T c_1^s}{c_1^{sT}} = K \Rightarrow \frac{m_1^T c_1^s}{m_1^{sT}} = K \tag{2.15}$$

Translocation: Depending upon the concentration of solute on side 1 of the membrane assembly, a finite mass fraction of the transporters will not be bound to a solute. Independent of the bound state, it is assumed that the protein switches its state from side 1 to side 2 given by a translation rate $\dot{\alpha}$. The bound transporter on side 1 of the membrane assembly

changes its confirmation in this step to expose the solute to side 2 of the membrane assembly. The flux rate of the solute s through the membrane is dependent on $\dot{\alpha}$ and the flux of the protein through the membrane is zero as it remains bound to the membrane. This can be mathematically represented as

$$\dot{\phi}_T = \dot{\alpha}\left(m_1^T - m_2^T\right) \tag{2.16}$$

$$\dot{\phi}_{sT} = \dot{\alpha}\left(m_1^{sT} - m_2^{sT}\right) \tag{2.17}$$

Dissociation: The bound transporter on side 2 of the membrane dissociates to release a solute molecule and becomes an unbound transporter. The dissociation reaction on side 2 can be written as:

$$ST_2 \overset{K}{\rightleftharpoons} T_2 + S_2 \tag{2.18}$$

The dissociation reaction equilibrium constant K is assumed equal to the association equilibrium constant. The mass of proteins with bound and unbound solutes on side 2 is given by m_2^{sT} and m_2^T respectively.

$$\frac{c_2^T c_2^s}{c_2^{ST}} = K \Rightarrow \frac{m_2^T c_2^s}{m_2^{sT}} = K \tag{2.19}$$

Reset step: The final step of the hypothetical mechanism resets the unbound transporter on side 2 of the membrane to become an unbound transporter on side 1 of the membrane. The reset is assumed to occur at the same switching rate $\dot{\alpha}$ as the forward translocation step. At the end of this step, the transporter molecule is ready for its next cycle of operation to move another solute from one side 1 to side 2 of the membrane. This step is insignificant due to the symmetric transition frequencies assumed in the model.

2.5 Sensitivity of the membrane assembly to solute concentration

The reaction kinetics based model for facilitated transport identified the different steps of a hypothetical mechanism for solute transport through the protein transporter. The equilibrium constant and the translocation rate for the protein can be used to derive the fluid flux through the membrane assembly of the actuator. The initial steps in the procedure listed below is similar to the model proposed by Lieb[90]. Assumptions for the protein

based actuator are introduced in the derivation and an expression for fluid flux through the membrane assembly of the actuator is obtained.

Conservation of the transporter: The mass of the protein in the different states of the the four state model is equal to the total mass of protein reconstituted in the membrane. Representing the mass of proteins in different states by m_{T1}, m_{T2}, m_{sT1}, m_{sT2}, the conservation law can be written as

$$m_1^T + m_1^{sT} + m_2^{sT} + m_2^T = M \tag{2.20}$$

where M is the total amount of proteins reconstituted in the membrane.

Transporter molecule displacement: This step is an outcome of the translocation constrain placed on the transporter protein. It was stated that the flux of the solute through the membrane is given by the translocation rate of the transporter and the flux rate of the transporter across the membrane is zero. This condition can be mathematically written as

$$\dot{\phi}_T + \dot{\phi}_{sT} = 0 \Rightarrow$$

$$\dot{\alpha}\left(m_1^T - m_2^T + m_1^{ST} - m_2^{ST}\right) = 0 \tag{2.21}$$

where $\dot{\alpha}$ is the transition frequency of the transporter molecule in the bilayer.

Flux rate of the solute: The flux rate of the solute, $\dot{\phi}$ is proportional to the translocation rate of the transporter molecule. The flux of the solute passing through the transporter is given by

$$\dot{\phi}_S = \dot{\alpha}\left(m_1^{sT} - m_2^{sT}\right) \tag{2.22}$$

Transport of the solute through the membrane accumulates the solute on side 2 of the membrane. The increase in concentration of the solute s on side 2 produces an osmotic gradient from side 1 to side 2. The osmotic gradient resulting from the solute transport is balanced by diffusion of water from side 1 of the BLM to side 2. The thickness of the BLM is few nanometers and hence the diffusion of water to balance the osmotic gradient over this thickness can be assumed to occur instantaneously. Hence, for every solute molecule that is transported through the protein, water molecules pass through the membrane and balance the osmotic gradient. Since the actuation concept relies of fluid transport through the membrane, the number of water molecules that travel across the membrane is obtained from the flux of solute given in Equation 2.22. The flux rate of the solute through the protein

is multiplied with a constant to obtain flux of the aqueous medium through the membrane. Thus the parameter $\dot{\alpha}$ that represents the translocation rate of solute is modified with the number of water molecules to obtain $\dot{\alpha}_w$. The expression for flux rate of the fluid is given by

$$\dot{\phi}_s = \dot{\alpha}_w \left(m_1^{sT} - m_2^{sT} \right) \tag{2.23}$$

where $\dot{\alpha}_w = n_w \dot{\alpha}$. Combining equations 2.15, 2.19, 2.20, 2.21 and 2.22, the flux rate for fluid transport can be represented as:

$$\dot{\phi}_s = \left(\dot{\phi}_s \right)_{\max} \left(\frac{c_1^s}{K + c_1^s} - \frac{c_2^s}{K + c_2^s} \right) \tag{2.24}$$

where the maximum flux rate for fluid transport is given by

$$\left(\dot{\phi}_s \right)_{\max} = \frac{n_w \dot{\alpha} M}{2} \tag{2.25}$$

The rate parameters can be integrated to obtain the maximum flux attained by the cotransporter system when the solute concentration on side 2 of the membrane is zero and all the transporter sites on side 1 is saturated with the solute.

$$(\phi_s)_{\max} = \frac{\alpha_w M}{2} \tag{2.26}$$

From the maximum flux observed for a transporter system, the the number of cycles the protein will have to operate to reach equilibrium can be computed from experimental data. The flux rate equation,

$$\dot{\phi}_s = (\dot{\phi}_s)_{\max} \left(\frac{c_1^s}{K + c_1^s} - \frac{c_2^s}{K + c_2^s} \right)$$

can again be written as a vector sums of solute flux rates: outward flux rate due to the concentration gradient of solute from inside and inward flux due to the concentration gradient of solute from outside.

$$\dot{\phi}_s = \left(\overrightarrow{\phi_{12}} - \overleftarrow{\phi_{21}} \right) \tag{2.27}$$

Thus, the inward flux rate can be assumed to be negligible when the concentration gradient from side 1 is much larger than the driving force in the opposite direction. In experiments the back flux is not measured and is assumed to be zero. The resulting equation that will quantify flux rate experiments can be written as:

$$\dot{\phi}_s = \left[\dot{\phi}_s \right]_{\max} \left(\frac{c_1^s}{K + c_1^s} \right) \tag{2.28}$$

The rate equation can plotted in reciprocal coordinates to find the equilibrium constant and maximum flux through the membrane assembly.

$$\frac{1}{\overrightarrow{\phi}_s} = \frac{1}{(\phi_s)_{\max}}\left(1 + \frac{K}{c_1^s}\right) \tag{2.29}$$

Hence, by plotting $1/\overrightarrow{\dot{\phi}_s}$ vs. $1/c_1^s$ and calculating the slope and intercept, $(\phi_s)_{\max}$ and K are obtained. The integrated form of the expression in Equation 2.29 from time, zero to time to equilibrium t_{eq} is represented by

$$\phi_s = [\phi_s]_{\max}\left(\frac{c_1^s}{K + c_1^s}\right) \tag{2.30}$$

The maximum flux rate obtained from the reciprocal plot is used to represent the relation between the steady-state flux and solute concentration. The plot resulting from this expression is similar to Michaelis-Menton plot. The dependent variable for this plot is the solute concentration c_1^s on side 1 of the membrane. The change in steady state fluid flux through the membrane for a change in the input stimulus can be obtained from this plot. The hyperbolic plot has a linear region for which the flux through the membrane is linearly related to the solute concentration. The experiments required to characterize the binding step equilibrium constant and the translocation rate will quantify fluid flux through the membrane assembly for different initial solute concentration on side 1 of the membrane. The experimental data when represented on a reciprocal plot can be used to compute $(\phi_s)|_{\max}$ and K. These values can be used to quantify the change in flux through the membrane due to a change in solute concentration on side 1 of the membrane. This quantity is also closely related to the flux rate through the membrane and can be extended to predict real-time flux through the membrane.

2.6 Chapter summary

A prototype protein based actuator has been designed to implement the chemomechanical energy conversion concept. The membrane assembly of the prototype actuator uses cotransporter proteins extracted from plant cell membranes as gating devices for fluid transport. The electrochemical proton gradient across the membrane assembly provides the energy for the protein transporter to remain conductive. The fluid flux through the membrane assembly can be influenced by changing the proton gradient and the concentration of the the

diffusing solute in the actuator. Thermodynamics of cotransport was discussed to identify the magnitude of the required gradient for cotransport through the membrane. The last section in the chapter discussed the simple, symmetric four state carrier model for solute cotransport. The expression for solute flux in the four state model was modified to obtain an expression for fluid flux through the membrane assembly. The derived expression was used to find the equilibrium constant and the maximum steady state flux through the membrane. to quantify the flux through the actuator membrane assembly as a function of the applied solute concentration. The kinetic rate based model will be applied to the transport results in chapter 3 and deformation results in chapter 4 to characterize the membrane assembly.

Chapter 3

Transport Experiments

The configuration of the protein based actuator was discussed in Chapter 2. The protein based actuator has a planar membrane with cotransporter proteins supported on a porous substrate. The cotransporter protein is triggered by an electrochemical gradient of protons. The balancing solute concentration for the applied electrochemical gradient was derived for the actuator configuration from thermodynamics of solute cotransport. The simplified, symmetric four state carrier model was modified to predict the fluid flux through the cotransporter in the membrane assembly. A procedure was outlined for experimentally determining the equilibrium constant and the flux rate through the membrane assembly. This chapter builds upon the models discussed for cotransport to design the membrane assembly. The discussion in this chapter begins with the selection of cotransporter protein, lipids and supporting substrates for the actuator. This is followed by the fabrication and characterization of the membrane assembly for fluid transport. The results from transport experiments are used to compute material parameters for the membrane assembly. The chapter concludes with an experimental demonstration of ATP driven transport through SUT4 using a proton pump. In this demonstration, the pH gradient required for SUT4 is replaced by the ATPase proton pump that can develop a pH gradient using ATP.

3.1 Component selection for the actuator

3.1.1 Protein: SUT4 proton-sucrose cotransporter

The actuator configuration discussed in Section 2.2 uses cell membrane proteins as the gating device for fluid transport. Selection of protein transporter for the actuator depends on the transport properties, availability and technology to isolate and purify the transporter from plant cell membranes. According to Muench's hypothesis, solute transport through plant cell membranes drives water transport and generates hydrostatic pressure[24] in plant cells. Since sucrose is a widely transported molecule in plant cell[103], transport of sucrose is considered to be the driving solute for water transport through sieve element[89, 15]. Additionally, sucrose transport from the leaves to the cells where they are broken down to release energy is vital for plant growth and life [20]. Due to the significance of sucrose transport in plants, molecular biologists have attempted and have been successful to extract and characterize different sucrose transporters from plant cell membranes. Articles by Williams et. al[108], Kuhn[53], Shakya and Sturm[85], Schulze et. al[81] are few of the many reviews on the different sucrose transporter proteins discovered in plant cell membranes. From the reviews available, it is observed that sucrose carriers are present throughout the plants and vary in their carrying capacity. From among the list of known sucrose transporters, a protein with high throughput of sucrose is desirable for the actuator. Such a sucrose transporter will rapidly create a sucrose gradient required for osmotic flow through the membrane assembly and generate volumetric strain in the actuator. This served as the motivation to use a sucrose transporter in the membrane assembly of the actuator.

A sucrose cotransporter - SUT4 common to Arabidopsis, potato and tomato was isolated by Frommer and coworkers[106] in 2000. The sucrose uptake through the transporter is reported to be 10 fold greater than other sucrose transporters known to exist in plants. The functioning of SUT4 protein in a plant cell membrane is depicted in the schematic shown in Figure 3.1. The SUT4 proteins, like other sucrose transporting proteins, coexist with active transporters in the cell membrane of plants[103]. The proton pumps in plant cell membrane function as active transporters for sucrose transport by establishing a proton gradient across the membrane[14]. The SUT4 protein uses the proton gradient established by proton pumps to generate sucrose flux through the membrane. In an *in vitro* environ-

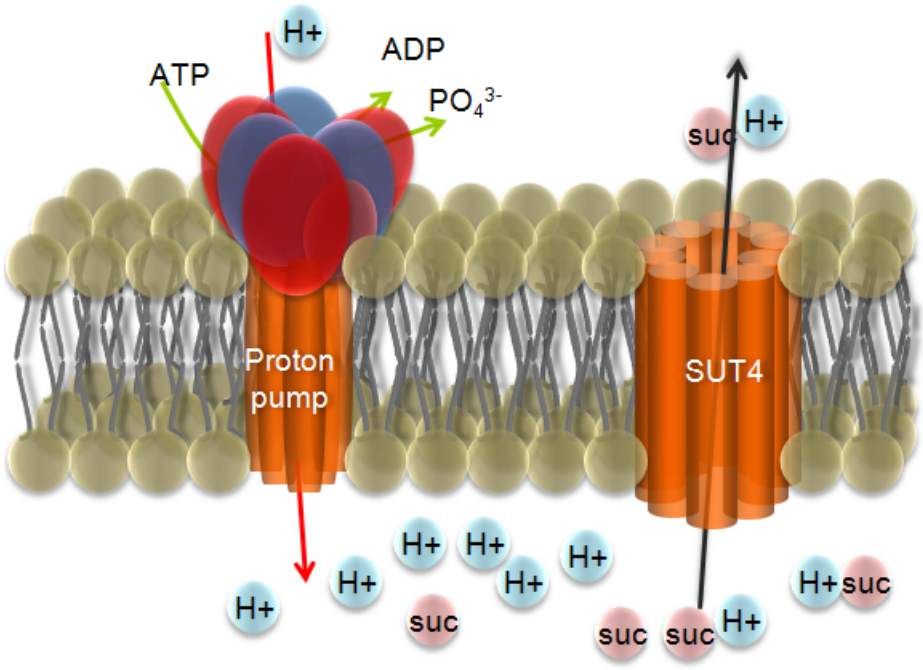

Figure 3.1: SUT4 protein exists in plant cell membrane with other proteins. The gradient established by active transporters is used by SUT4 for sucrose transport.

ment, SUT4 can be triggered by an artificially imposed pH gradient to transport sucrose as shown in Figure 3.2(a). The data table shown in Figure 3.2(b) shows the experimentally observed relation between sucrose flux rate and external pH through SUT4 expressed in yeast cell membranes (Weise et al[106]). The experiments done at 1 mM sucrose indicates that the throughput of sucrose increases till pH4.0 and then begins to decrease. From the known properties of SUT4, the membrane assembly of the actuator with this protein can be subjected to a pH gradient to produce sucrose flux. The sucrose flux through the membrane assembly will induce water transport and generate deformation in the actuator. Finally, the technology to manufacture SUT4 at Prof. Cuppoletti's facility led to its selection as the gating device for the actuator.

The SUT4 proteins required for the fabrication of the actuator were supplied by Prof. John Cuppoletti in the University of Cincinnati. The following received as a personal communication is a brief outline of the preparation procedure of SUT4 used in the project - *"The sucrose carrier, atSUT4 cDNA from Arabidopsis, in the yeast expression vector pDR196 was the kind gift from Wolf B. Frommer, Carnegie Institution, Stanford,*

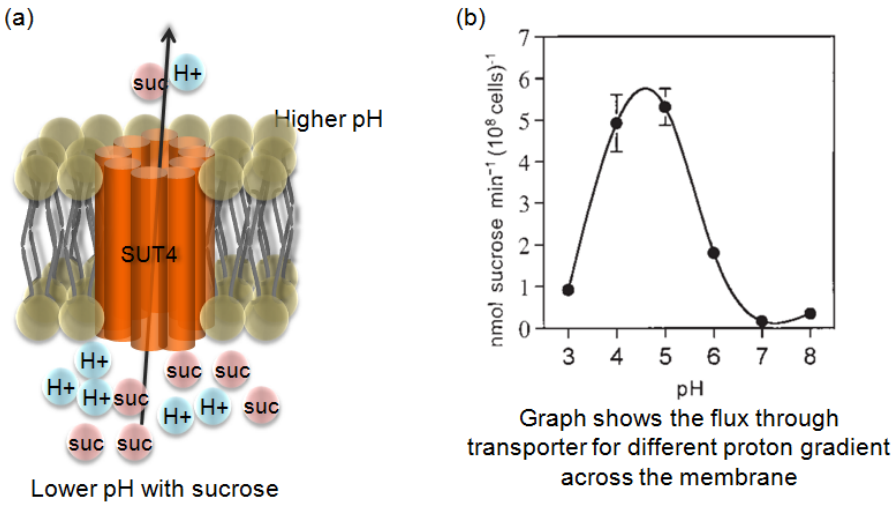

Figure 3.2: Mechanism of sucrose transport through SUT4 protein. (a) Flux of sucrose molecules through SUT4 due to an imposed pH and sucrose gradient. (b) Mean sucrose flux for different pH imposed in the extracellular medium published by Weise et. al [106] shows the dependence of flux on imposed pH gradient

CA to John Cuppoletti, University of Cincinnati. Yeast expressing atSUT4 was grown as described by Weise et al [106]. Yeast plasma membranes were prepared essentially as described by Huang et al[42]. An estimate of the percentage of SUT4 content in the membrane preparation based on SDS-PAGE was about 0.1Further purification of SUT4 was not carried out." Assuming pH7.0 as the intracellular concentration in the reported experimental data in Figure 3.1(b), the applied pH gradient across the cell membrane equals a thousand fold proton gradient. A higher sucrose flux observed through SUT4 for a 1000 fold pH gradient obtained from the data reported in Figure 3.2(b) led to the selection of pH4.0 vs. pH7.0 gradient as the driving force for the actuator. Since the applied pH gradient is balanced by a sucrose gradient, the equilibrium concentration of sucrose across the membrane assembly can be estimated from thermodynamics of cotransport discussed in Section 2.3. The formulae that gives the equilibrium concentration of sucrose for an applied pH gradient in the actuator are

$$c_1^s|_{eq} = \frac{V_r c_1^s}{V_r + 10^{\Delta \mathrm{pH}}}$$

$$c_2^s|_{eq} = \frac{10^{\Delta \mathrm{pH}} V_r c_1^s}{V_r + 10^{\Delta \mathrm{pH}}}$$

The equilibrium concentration in the two chambers computed for different volume

Table 3.1: Equilibrium concentration of sucrose in the two chambers of the actuator for pH4 vs. pH7 applied across the membrane assembly

c_1^s	1 mM	5 mM	10 mM	15 mM	20 mM	25 mM	30 mM
$V_r = 100$							
$c_1^s\|_{eq}$	0.09 mM	0.45 mM	0.90 mM	1.36 mM	1.81 mM	2.27 mM	2.72 mM
$c_1^s\|_{eq}$	0.090M	0.454M	0.90M	1.36M	1.81M	2.27M	2.72M
$V_r = 75$							
$c_1^s\|_{eq}$	0.06 mM	0.34 mM	0.69 mM	1.04 mM	1.39 mM	1.74 mM	2.09 mM
$c_1^s\|_{eq}$	0.069M	0.34M	0.697M	1.04M	1.39M	1.74M	2.09M

ratios $V_r = 75,\ 100\ (= V_1/V_2)$ is given in Table 3.1. From the table, different sucrose gradients are established across the membrane for different initial sucrose concentration on one side of the membrane. Thus by varying the sucrose concentration on one side of the membrane assembly, the equilibrating osmotic pressure can be varied to produce different amounts of deformation in the actuator. This led to the selection of sucrose concentration gradient as the control variable for controlling the strain developed by the actuator.

3.1.2 Lipids and Substrates

The SUT4 protein transporters extracted from plants are supplied as inclusions in the liposome membrane shell. The purification process during the manufacture of proteins concentrates the amount of SUT4 in liposome. To assist the spreading of purified SUT4 into a planar BLM, phospholipids are added to the porous substrate. A common combination of lipids[114, 21] for ion channel reconstitution in a bilayer lipid membrane is a mixture of 1-Palmitoyl-2-Oleoyl- sn- Glycero-3- [Phospho-L-Serine] (Sodium Salt) (POPS) and 1-Palmitoyl-2-Oleoyl- sn- Glycero-3- Phosphoethanolamine (POPE) lipids. The POPS and POPE lipids (Figure 3.3) mixed in the ratio 3:1(w/w) and dissolved in n-decane (40 mg/ml) is added to the porous substrate with the transporter proteins to form the membrane assembly of the actuator.

A porous substrate with a hydrophilic surface can support planar BLM across its pores[93]. Two contrasting candidates - track-etched polycarbonate substrate and lead silicate glass plates are chosen as the supporting substrates for the membrane assembly. Micrographs of the PCTE membranes and lead silicate glass plate are shown in Figure 3.4. The track-etched polycarbonate (PCTE) membranes are available with different pore sizes

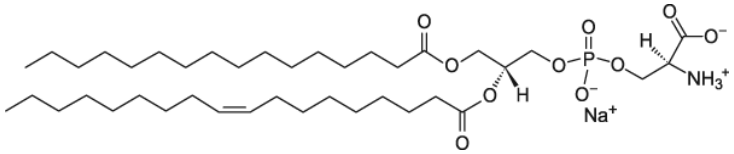

1-Palmitoyl-2-Oleoyl-*sn*-Glycero-3-[Phospho-L-Serine] (Sodium Salt) (POPS)

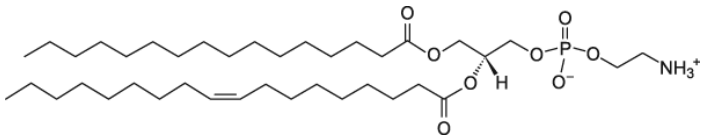

1-Palmitoyl-2-Oleoyl-*sn*-Glycero-3-Phosphoethanolamine (POPE)

Figure 3.3: Phospholipids - POPS and POPE used for BLM self-assembly and protein reconstitution

with an effective porosity of 5-20%. The naturally hydrophobic surface is coated with PVP (poly-vinyl pyrolidine) that makes it hydrophilic. From the micrographs shown in Figure 3.4, it is observed that the pores in the polycarbonate substrate are not truly cylinderical. The pore dimeter specified is found to be an average number computed over a unit area. The PCTE membranes are available at pore sizes as small as few tens of nanometer. In spite of some of the shortcomings, the availability of very small pore sizes and more importantly - a hydrophilic surface makes PCTE a suitable candidate for supporting a planar BLM. The porous lead silicate glass plates are naturally hydrophilic and have an organized array of pores with 50% porosity. The choices for pore size on commercially available substrates are limited, but the pores are perfectly cylindrical for all the sizes available . Higher porosity and organized pore structure makes the lead silicate glass plates a desirable candidate for the supporting substrate of the actuator. Thus, track-etched polycarbonate membrane (PCTE) and lead silicate glass plates are chosen as the supporting substrates for the first actuator prototypes .

3.2 Membrane assembly fabrication

The actuation concept relies on fluid transport through the membrane assembly and hence it is required to characterize fluid transport through the membrane. The following sections in the chapters discusses the fabrication of the membrane assembly and fluid transport characterization through membrane assembly formed on different substrates. The complete list of materials required for fabricating and characterizing the membrane assembly is provided

below:

- Transport assay multi-well cups with polycarbonate membrane, supplied by Millipore Corporation
- Porous lead silicate glass plate (2μm and 50μm pores with 50% porosity), supplied by Collimated Holes, CA
- SUT4 protein cloned from *Arabidopsis thaliana* in yeast, extracted and purified, suspended in pH7.0 medium (20.2 mg/ml), supplied by Prof. Cuppoletti's lab, University of Cincinnati, OH
- 1-Palmitoyl-2-Oleoyl- sn- Glycero-3- [Phospho-L-Serine] (Sodium Salt) (POPS) mixed with 1-Palmitoyl-2-Oleoyl- sn- Glycero-3- Phosphoethanolamine (POPE) in the ratio 3:1 (w:w) and dissolved in n-decane(40 mg/ml). Lipids were purchased from Avanti Lipids, AL, USA and n-decane from Sigma-Aldrich, USA
- Silver-Silver Chloride half-cell reference electrode, purchased from World Precision Instruments, Sarasotta, FL, USA
- Platinum electrode wire - 0.8 mm diameter, supplied by SurePure Chemetals, NJ, USA
- Socorex micropipetor with pipet tips

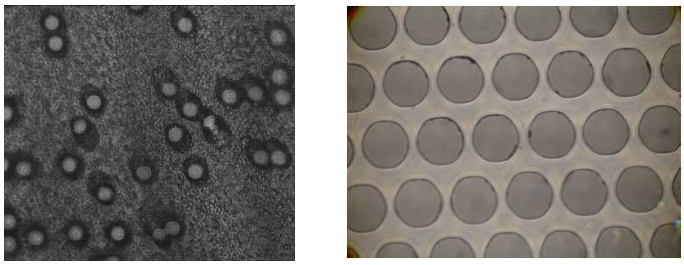

Figure 3.4: Porous polycarbonate membrane and Lead silicate glass plate used as supporting substrates for the membrane assembly

3.2.1 Self-assembly of the bilayer lipid membrane

The procedure for forming the membrane assembly on the two substrates differ and are presented separately.

Polycarbonate membrane

The first step in fabricating the membrane assembly is to form the bilayer membrane. Lipids form into a planar BLM by self-assembly due to the unique properties of the phospholipid molecule discussed in Chapter 1. A stock solution of POPS and POPE lipids in n-decane is mixed as per the composition in the materials list. The lipid mixture is added to a new polycarbonate substrate using a micropipet and spread uniformly on the surface using a brush. The excess in the stock solution is stored in the freezer at -20^{o}C. The coated substrate is allowed to stand in air for 10 minutes for the solvent to evaporate from the surface. At the end of ten minutes, the substrate is immersed in the aqueous medium and the lipid molecules in the pores self-assemble [63, 99, 100, 112] into a lipid bilayer on coming into contact with polar water molecules.

Lead silicate glass

The lead silicate glass plate used for supporting a BLM with SUT4 is shown in Figure 3.4(b). The micrograph shows an organized array of pores as seen under a microscope [Carl Zeiss Axiovert 40] at 100X magnification. A special fixture is built to hold the glass plate between two chambers. The lipid stock solution prepared for polycarbonate membranes is also used on the glass substrates. It is observed that spreading lipid solution over a large area is inconsistent and hence all but a small circular port of diameter 0.45 cm is masked using an adhesive backed neoprene tape. Prior to masking, the glass plate is cleaned in aqua regia to remove any organic residue from handling and storage. The plates are thoroughly rinsed in deionized water to remove traces of acid in the pores. The masked plate is clamped between two custom made pieces of plexi glass that serve as the top and bottom chamber. The exposed circular area forms the backbone for supporting the membrane assembly. The glass plate after masking is thoroughly washed with 50% iso-propyl alcohol (50% IPA) and de-ionized water. Filtered compressed air at 150 kPa is used to blow away the remaining water in the pores. Between trials, the glass plate in the fixture is cleaned with IPA and

compressed air. This fixture is also designed for fluid transport characterization through the membrane assembly. The maximum capacity of the bottom chamber is 150 ml and that of the top chamber is 1.5 ml. The chambers carry 120 ml and 1.25 ml of fluid during trials.

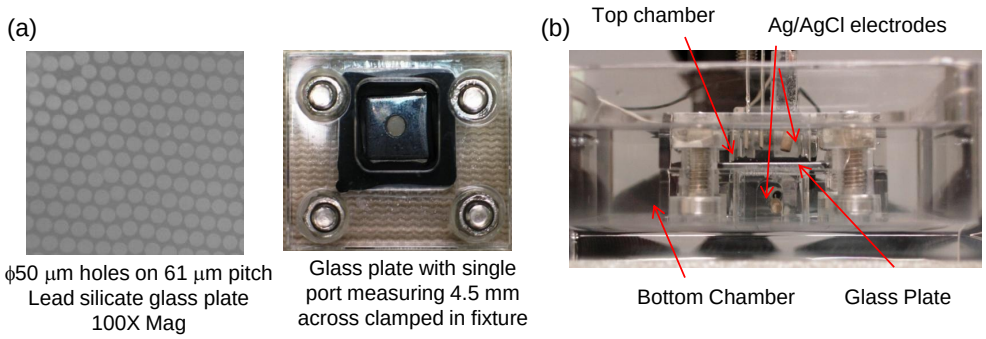

Figure 3.5: Porous lead silicate glass plate shown with the exposed circular port and clamped in the fixture

Impedance spectroscopy is used to detect the presence of the membrane assembly. Two silver-silver chloride electrodes kept immersed in the aqueous solutions on both sides of the membrane are used to measure the complex impedance of the BLM. Impedance is measured over a frequency range of 5 Hz to 1 MHz at 50 mV oscillator level. The planar BLM formed across the pores of the membrane is modeled as a capacitor and conductor in series and the electrolyte between the electrodes and the BLM is modeled as a resistor. The equivalent 2-resistor 1-capacitor model for the BLM with transporters is shown in Figure 3.6. An equivalent network model is developed to compute the capacitance and conductance of the membrane. The HP 4192A Impedance analyzer is used to calculate the capacitance of the self-assembled BLM. The stability of the measured impedance value over time is used as a qualitative measure to detect the stability of the BLM. Similar methods have been reported by other researchers[61, 66, 91, 76] to detect the presence of a BLM formed on a porous substrate.

3.2.2 Self-assembly of SUT4 in bilayer lipid membrane

The SUT4 proteins in the liposome shell mix and spread into a BLM by a process similar to liposome fusion discussed in Section 2.1.2. The thawed proteins (10 μl) are added using a micropipet to the lipid coat on the porous substrate. The coated substrate is allowed to

stand in air for 15 minutes to allow the liposomes carrying the proteins to mix with the lipid molecules on the substrate. The lipid and the proteins spread on the pores self-assembly into a BLM on introducing the porous substrate into an aqueous medium. The protein in the liposome shell is thus delivered into the planar BLM formed across the pores. A schematic of the BLM with incorporated SUT4 is shown in Figure 3.6. The impedance measured across the membrane assembly with and without the proteins serves as a qualitative measure to detect the presence of SUT4 in the membrane. The presence of SUT4 in the membrane assembly can be tested and analyzed by measuring transport through the membrane with and without the transporter for pH and sucrose concentration gradients. The transport experiments in the presence of SUT4 proteins is presented in Section 3.1.1 to characterize the transport properties of the membrane assembly.

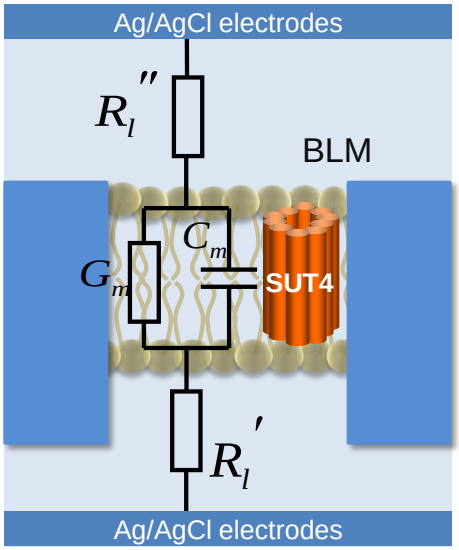

Figure 3.6: Planar BLM in the porous substrate modeled as a RC in parallel. The access electrolyte is modeled as a resistor and the measured value represents a 2R-1C network model

3.2.3 Electrical model of the bilayer lipid membrane

The electrical properties of the BLM can be obtained from the measured impedance. The BLM is approximated as a parallel resistor-capacitor and the electrolyte is considered to be a resistor in series as shown in Figure 3.6. The circuit has a unique time constant τ_m which is directly related to the parallel capacitance (C_m) and parallel admittance (G_m) of the membrane. The series resistor does not impact the characteristic frequency of the

circuit. The measured admittance of the 2-resistor, 1-capacitor series circuit represented as a complex-valued function of frequency is

$$\mathbf{Z} = R + jX \tag{3.1}$$

where R and X are the real and imaginary parts of impedance. The complex admittance of the membrane is a frequency dependent function represented by the membrane admittance (G_m) and capacitance (C_m),

$$Y = G_m + j\omega C_m \tag{3.2}$$

The total impedance of the 2 resistor-1 capacitor in Equation 3.1 can be represented in terms of the system components as

$$\mathbf{Z} = R + jX = R_l + \frac{G_m - j\omega C_m}{G_m^2 + \omega^2 C_m^2} \tag{3.3}$$

The time constant of the parallel admittance, capacitor circuit is given by

$$\tau_m = (C_m/G_m) \tag{3.4}$$

The characteristic frequency of a 2-resistor 1-capacitor network is defined as the apex frequency for the network on the Z-plot [31] and is related to the time constant by

$$f_c = \frac{1}{2\pi\tau_m} \tag{3.5}$$

Equation 3.3 can be rearranged to result in a combined equation for complex impedance.

$$R + jX = \left\{ R_l + \frac{1}{G_m^2 + \omega^2\tau_m^2} \right\} - j \left\{ \frac{\omega\tau_m}{G_m\left(1 + \omega^2\tau_m^2\right)} \right\} \tag{3.6}$$

The corresponding phase is given by

$$\Phi = \tan^{-1}\left[\frac{\omega C_m}{G_m\left(1 + R_l G_m\right) + \omega R_l C_m^2} \right] \tag{3.7}$$

The measured data can be represented on a Nyquist plot and compared with the modeled data. The characteristic frequency is the frequency corresponding to the peak of the inverted parabola and is used to compute the time constant of the parallel circuit. The equations with the component variables for real and imaginary parts of the modeled complex impedance is used to estimate the values of equivalent circuit components.

3.3 pH gradient driven transport

The membrane is subjected to the chemical potential discussed in Section 3.1.1 by assembling it in the transport experiment fixture. The pH gradient is applied across the membrane assembly using pH4.0 and pH7.0 buffer. Sucrose gradient is applied by dissolving sucrose in pH4.0 buffer on one side of the membrane. The volume ratio of the bottom chamber to top chamber is approximately 100 in the transport experiments. The experimental setup and characterization experiments for the membrane formed in polycarbonate and lead silicate glass plate are presented separately.

3.3.1 Porous polycarbonate membranes

The experimental setup for characterizing fluid transport through membrane assembly supported on polycarbonate is shown in Figure 3.7. The fixture has a cup holder that sits in a chamber (referred as bottom chamber). The cup with the membrane forms the top chamber. The bottom chamber is filled with pH4.0 buffer and sucrose (concentration as required) and pH7.0 is added to the top chamber. The buffer solutions apply the required electrochemical gradient.

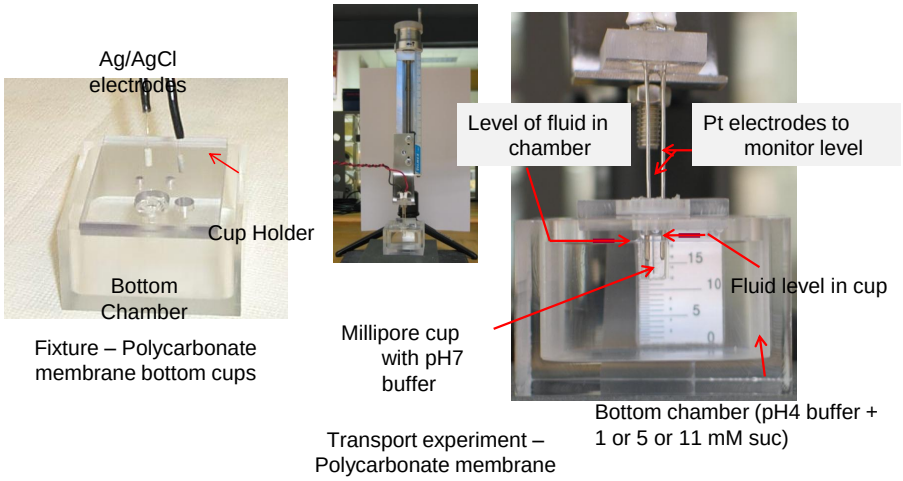

Figure 3.7: Fixture to characterize the membrane assembly on polycarbonate substrate

The porous polycarbonate(PC) membrane in the cup bottom provides the framework for the planar BLM with SUT4. The PC membrane is similar to the PCTE membrane selected for the actuator as discussed in Section 3.1.2. A planar BLM is allowed to self-

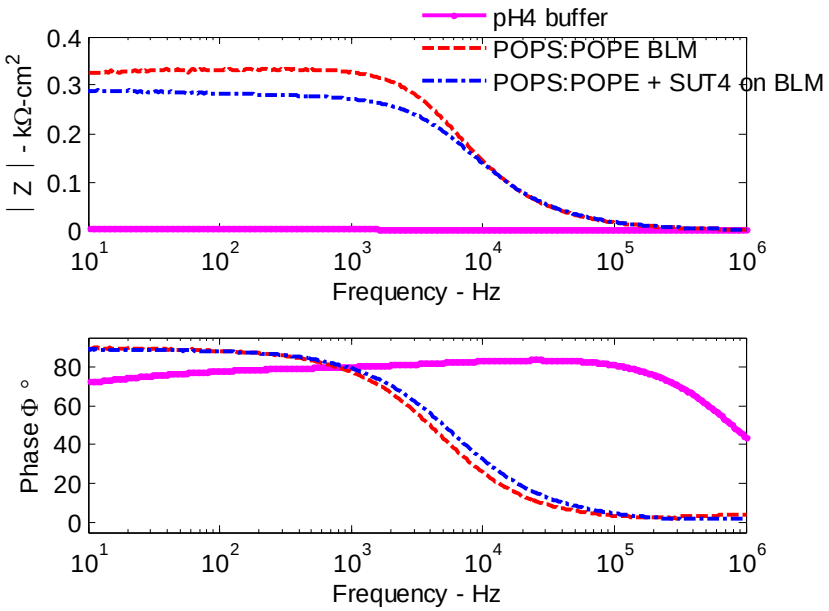

Figure 3.8: Measured impedance on the PC membrane assembly from 5 Hz to 1 MHz

assemble in the PC membrane using the procedure in Section 3.2. At the start of the experiment, impedance across the membrane without lipids is measured as a baseline. The lipid stock solution(10 μl) is added to the membrane and self-assembly of the BLM is detected by electrical impedance measurements across the PC membrane. It is observed that an impedance of few hundred ohms in the absence of lipids on the membrane increases by 2 to 3 orders of magnitude in the presence of lipids on PC membrane. A self-assembled BLM will restrict the mobility of ions between the electrodes kept on either sides of the membrane and will result in a higher impedance. A stable impedance value higher than the baseline is indicative of a self-assembled BLM in the pores [63]. The impedance measured across the PC membrane for different test conditions is shown in Figure 3.8. The complex impedance is plotted on a Nyquist plot as shown in Figure 3.9 to obtain the equivalent electrical parameters for the membrane. The electrolyte resistance(R_l), capacitance and conductance(R_m,G_m) of the modeled membrane are computed to be R_l = 2k Ω, G_m = 180 μS/cm^2, C_m = 6.5 nF/cm^2.

The next step in forming the membrane assembly is to reconstitute the protein transporter(SUT4) following the procedure described in Section 3.2. The SUT4 proteins

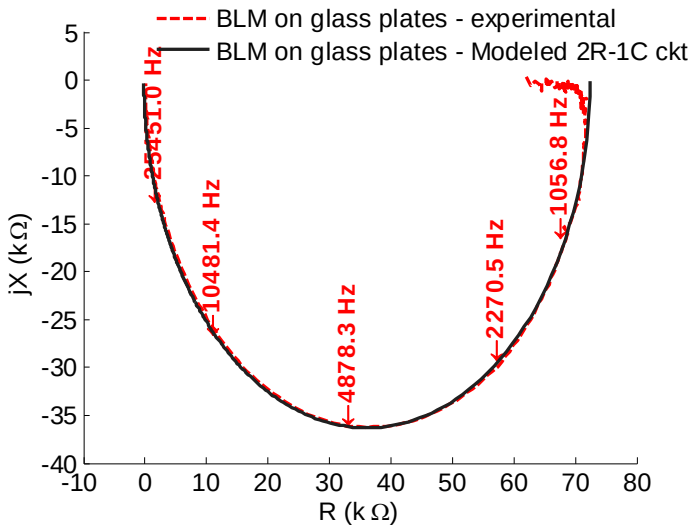

Figure 3.9: Z-plot for the measured impedance data for the BLM. From the 2R-1C model, the capacitance and conductance of the BLM in the pores are 6.008 nF/cm^2 and 173.212 μS/cm^2 respectively

available in the liposome membranes self-assemble into the planar BLM. Since there is no visual indicator of SUT4 self-assembly into the membrane, impedance spectroscopy is used. Measured impedance is used in a qualitative manner to detect the presence of the transmembrane protein in the membrane. The impedance data measured across BLM without SUT4 is compared with the data from the BLM with SUT4. A candidate result from an experiment is shown in Figure 3.8. It is observed that the impedance drops by 10% for BLM in SUT4 supported on PC membranes in the assay cup. This drop in impedance is attributed to the leakage current through the transporter in the membrane. The impedance measured across BLM with SUT4 is observed to vary between trials. A more quantitative method to detect the presence of SUT4 is to test for transport function of the protein in the membrane. This test is performed not only to detect the presence of SUT4, but also to characterize the membrane assembly for fluid transport. The SUT4 proteins are sucrose carriers driven by an electrochemical gradient of protons. The selectivity of SUT4 to pH gradient and sucrose concentration gradient across the membrane will result in a volumetric flux from the side with lower pH and sucrose to the side with higher pH. Based on the discussion presented in Section 3.1.1, changing the initial concentration of sucrose on the lower pH side will change the flux rate and steady state flux through the membrane. In the

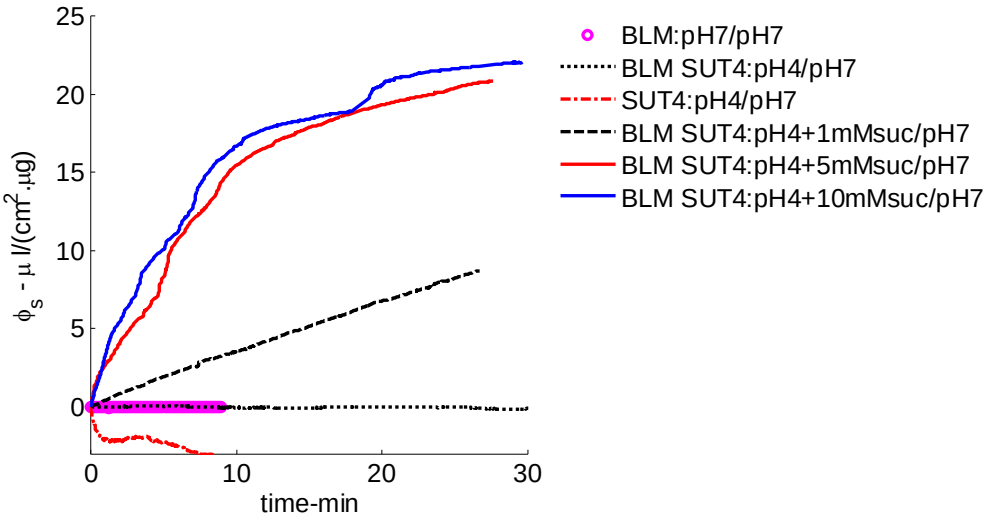

Figure 3.10: Normalized flux through membrane assembly on PC.

transport characterization experiment the membrane assembly is subjected to pH4.0/pH7.0 gradient selected from the discussion in Section 3.1.1. The baseline transport tests are performed with (1) the plain lipid membrane subjected to pH and sucrose gradient; (2) the plain lipid membrane and SUT4 subjected to pH gradient and (3) SUT4 spread across the porous substrate and subjected to pH and sucrose gradient. The baseline tests show that there is no fluid transport through the membrane in the absence of pH gradient and sucrose gradient applied to the membrane. Also, there is no observable fluid flux without SUT4 in the membrane. Thus concentration gradients and SUT4 are essential for fluid flux through the membrane. In the absence of lipids, the contents in the top chamber flow down into the bottom chamber through the pores in the substrate indicating that the lipids from the liposome shell are not sufficient to spread across the pores and support SUT4. The results from functional analysis on the membrane assembly supported on polycarbonate membrane is shown in Figure 3.10.

In the next set of experiments, the membrane assembly is subjected to sucrose and pH gradient, and the initial concentration of sucrose in the bottom chamber is varied from one trial to another. With sucrose present in the bottom chamber, there is a measurable flux through the membrane assembly into the top chamber. Increasing the concentration from 1 mM and 5 mM results in higher measurable flux through the membrane. It is observed from many trials that increasing the concentration of sucrose to 10 mM and above does not result in a proportional increase in flux through the membrane. The amount of

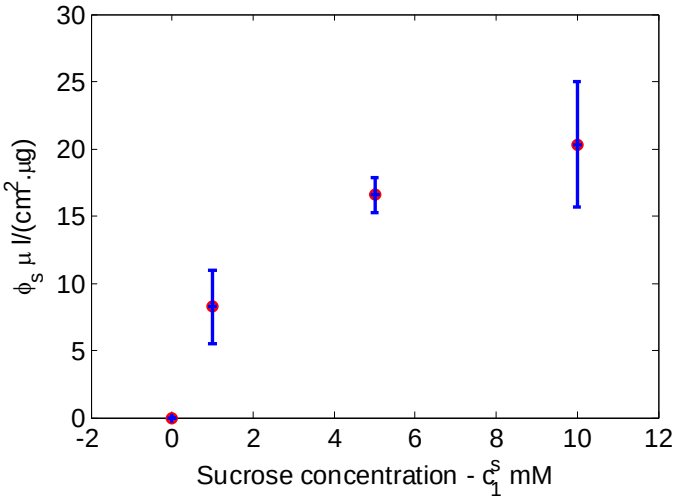

Figure 3.11: Normalized flux through the membrane on PC for different sucrose concentration

fluid transported through the membrane saturates between 5 and 10 mM concentration of sucrose in the bottom chamber as shown in Figure 3.11. The error bars represent 95% confidence interval for flux through the membrane calculated from Student-'t' distribution applied to the steady state flux through the membrane from 5 trials. It is observed that there is no flux through the membrane in the absence of sucrose in the bottom chamber.

The dependence of flux and flux rate on sucrose concentration in the presence of SUT4 and saturation of flux through the membrane at a higher concentration of sucrose indicate that fluid transport occurs through finite number of conductive pathways in the membrane assembly. The porosity of the PC membrane in the assay cup is 3% and hence the effective membrane area for fluid transport is small and correspondingly a smaller flux is observed through the membrane. In order to generate a higher flux through the membrane a larger BLM with SUT4 is required. A higher BLM area is achieved by increasing the porosity of the supporting substrate. The lead silicate glass plates with 50% porosity and 50 μm pores are used as the supporting substrate for demonstrating fluid transport for an applied chemical potential.

3.3.2 Lead silicate glass plates

Experimental analysis of BLM formation in glass plates

Forming a BLM on the pores of lead silicate glass plate is the first step in characterizing fluid transport through the membrane assembly. The quantity of lipids required to form BLM on 50 μm pores is determined iteratively.

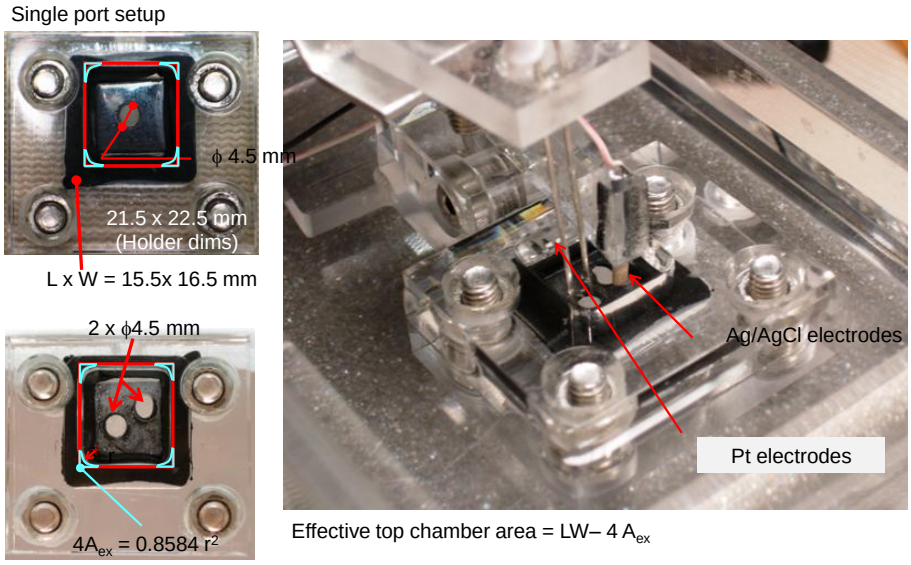

Figure 3.12: Experimental setup - Lead silicate glass supported membrane assembly

A series of experiments are performed where the quantity of lipids spread on the lead silicate glass substrate is varied and impedance is measured. Student-'t' distrubution is appled to the experimental data for statistical analysis on the impedance measured for different amount of lipids.

The lipid membrane in a pore is reported to have a thick annular region where it is attached to the walls of the substrate with solvent molecules filling the space between the hydrophobic tails . The solvent spreads into a 'microlens' between the hydrophobic tails in the center of the BLM[35]. It is reported that the amount of solvent in the BLM has an effect on the mechanical properties[35], electrical conductivity[67] and rupture characteristics. To test the effect of n-decane solvent on the BLM impedance measured, trials are performed where the substrate is allowed to stand in air for a longer duration (15 minutes) and dried

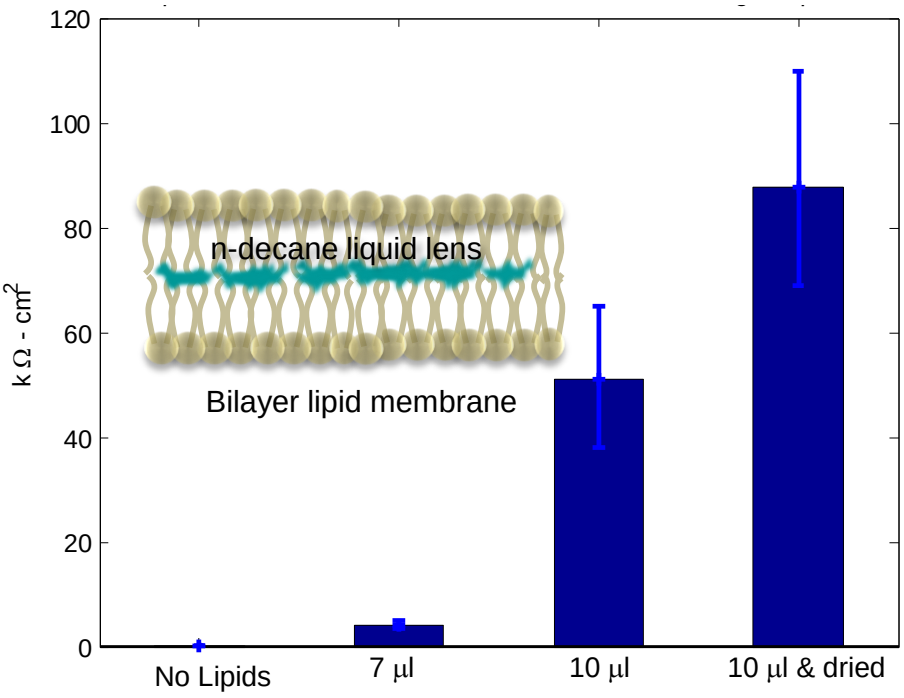

Figure 3.13: Amount of lipids added vs. Measured impedance (n-decane microlens fills in the region between the hydrophobic tails is shown in the inset)

under nitrogen gas before introducing it in the aqueous medium. The longer duration in air is considered to vaporize a higher portion of n-decane solvent spread on the substrate. The results from the experiments are compared to formulate the procedure required for forming a 'good' BLM in the pores of the substrate. A minimum of 7 trials for each test case are performed. To be consistent between trials, impedance is measured across the substrate with lipids fifteen minutes after introducing the substrate in aqueous medium. The measured impedance from different trials is shown the histogram in Figure 3.13. The results show that a minimum of 10μl of lipid solution is required for an area of 0.079 cm^2 which corresponds to 125 μl/cm^2 of porous area. The initial impedance for quantities smaller than 10 μl was observed to be comparable with 10μl, but the value steadily dropped within 15 minutes to reported values. Using the equivalent electrical network model, the capacitances of the membranes are computed to be around 6.5 nF/cm^2 for all the successful trials. The composition of the BLM being the same across substrates, this value compares well with the 7 nF/cm^2 capacitance observed across membrane on PC substrate. It should be noted that the impedances observed across the BLM's is **significantly** smaller than usually reported values in literature for a 'good seal'. The numbers reported in literature usually consider the

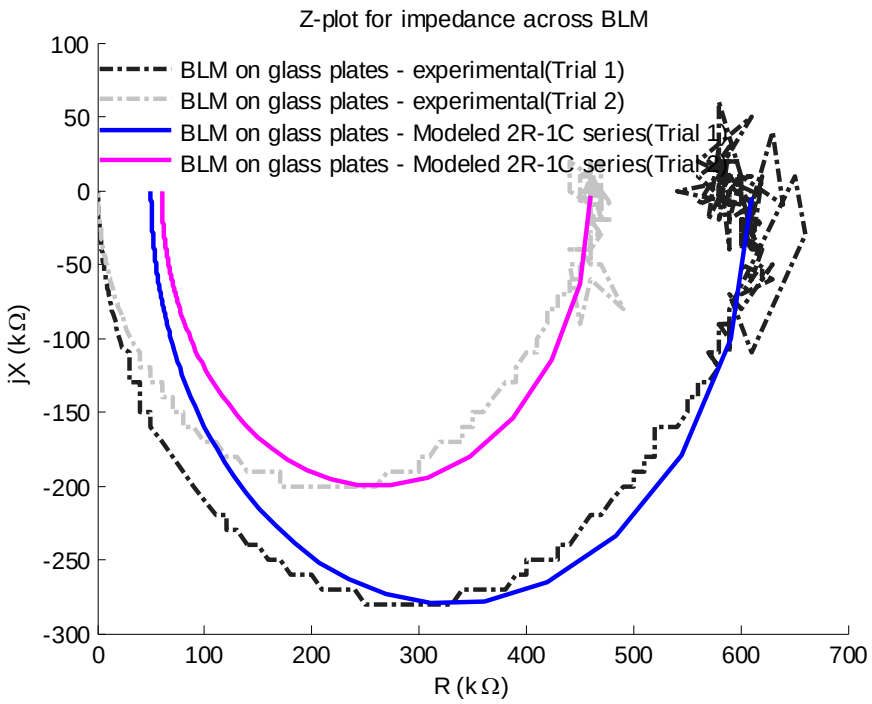

Figure 3.14: Nyquist plot of two of the trials reported for 10 μl lipids on the substrate.

impedance measured over a single pore, while the numbers reported in this work is on an array of pores. The resistances corresponding to the BLM in each pore are all connected in parallel in the equivalent circuit. From electrical network theory, the impedance measured across a resistor-capacitor network in parallel is scaled down approximately by the number of elements. Thus the impedance of the BLM in one pore will numerically scale by the number of pores in the substrate. For the porous lead silicate glass plate, it is found that there are at least 5000 pores in the substrate. The impedance of a pore will equal few hundred megaohms which is comparable to the reported high value for similar phospholipid combination by Dhoke et. al[21].

After determining the amount of lipids required for forming a BLM on the pores of the substrate, SUT4 is reconstituted with the lipids in the BLM. The insertion of SUT4 in the BLM is detected by comparing the impedance measured with and without the protein. The impedance data shown in Figure 3.15 shows the measured impedance across the substrate with and without SUT4 added to the substrate. As observed in the polycarbonate membranes, the impedance decreases in the presence of SUT4. The impedance measured at lower frequencies is 50% smaller when SUT4 is added to the pores when compared with

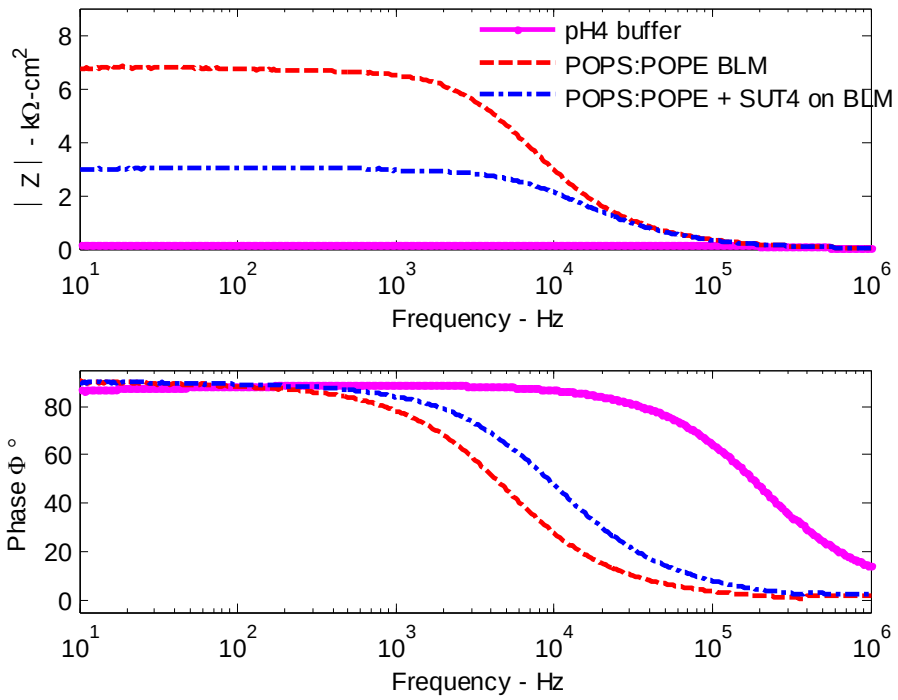

Figure 3.15: Measured impedance with and without SUT4 in BLM on lead silicate glass substrate with 50 μm pores. Computed capacitance and conductance of the BLM are 6.5 nF/cm^2 and 150 μS/cm^2

the 10% drop observed in polycarbonate substrate. The increased drop is attributed to the higher porosity and larger pores in the lead silicate glass substrate.

Transport experiments

The next step in characterizing the membrane assembly is to test the membrane for fluid transport. The SUT4 protein is reconstituted in the BLM by adding 10μl of lipids on the substrate coated with lipids. The glass plate with the contents is allowed to stand for 10-15 minutes and introduced in the transport fixture with pH4.0 buffer solution and sucrose. The top chamber is filled with pH7.0 buffer solution. The membrane assembly in the transport experiment fixture is ready for data analysis analysis. The experimental setup for transport experiments on the porous lead silicate glass plates is shown in Figure 3.12. The experimental setup shows the Pt electrodes that function as the sensing element in the top chamber for the capacitance meter, which is used to measure the amount of fluid transported through the membrane assembly. The capacitance meter used in the experiment is described in Appendix A. The concentration of sucrose in the bottom chamber is varied

based on the experimental condition.

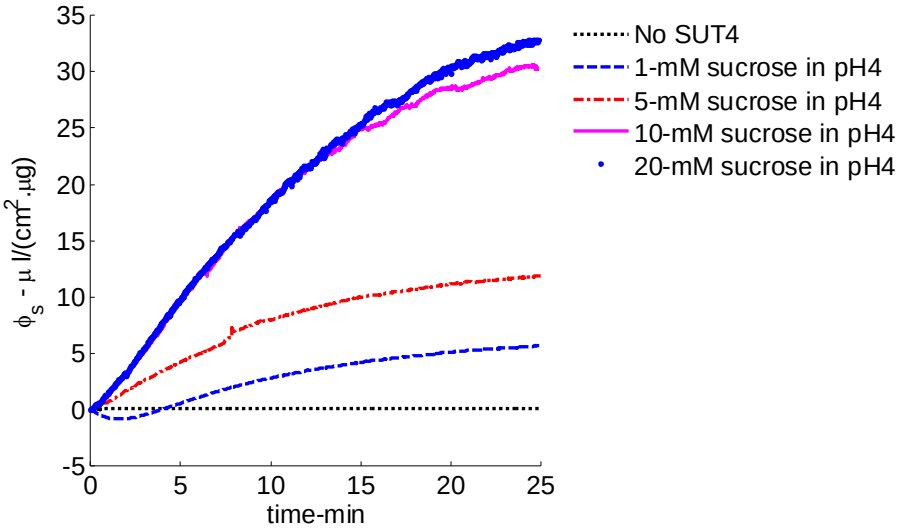

Figure 3.16: Normalized flux through membrane assembly - time response(Lead silicate glass with 50μm pores)

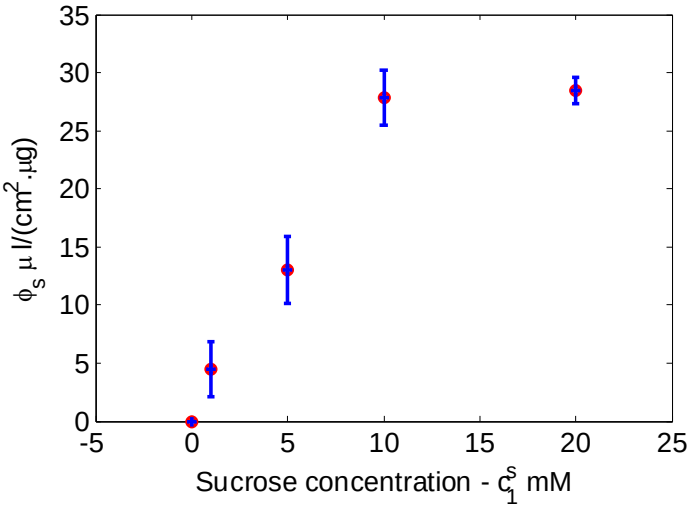

Figure 3.17: Normalized flux through the membrane for different sucrose concentration (Lead silicate glass with 50μm pores)

A baseline with no SUT4 in the membrane assembly and no sucrose in the bottom chamber is performed. In the absence of SUT4 or sucrose in the experimental setup, there is no observable fluid flux through the membrane assembly. Measurable flux through SUT4 in the membrane is observed in the presence of sucrose in the bottom chamber. The observed flux and flux rate through the membrane increases with increasing concentration and begins

to saturate at higher concentrations. The fluid flux through lead silicate glass plates with 50 μm pores for the baseline and different initial sucrose concentration is shown in Figure 3.16. This is similar to the earlier observation in polycarbonate membrane shown in Figure 3.10. The concentration above which the flux through the glass plate membrane assembly saturates is slightly higher than the experimentally observed value for polycarbonate membrane and occurs between 10 and 20 mM of sucrose in the bottom chamber. The variation of fluid flux through the membrane for different sucrose concentration is shown in Figure 3.17. The error bars represent 95% confidence interval for flux through the membrane calculated from Student-'t' distribution applied to the steady state flux through the membrane from 3 trials.

The transport experiments discussed so far demonstrate the role played by SUT4 in fluid transport through the membrane. The maximum average steady state flux is slightly higher than 100 μl for 150 μg of proteins in the BLM of area 0.079 cm^2 and is dependent on the concentration of sucrose in the bottom chamber. The experiments have also quantified the amount of fluid flux through the membrane assembly by changing the concentration of sucrose in the bottom chamber. To design a membrane assembly that can move larger quantities of fluid, the amount of proteins in the membrane assembly should be increased to allow the system to reach equilibrium faster. This should produce a larger volume change as more transporters are operating in the membrane to equilibrate the two chambers. The dual port membrane assembly is designed to experimentally validate the capability to generate larger flux through the membrane. The glass plate substrate is prepared using the procedure described in Section 3.2.1 to have dual port as shown in Figure 3.12. The membrane is placed under a pH4.0/pH7.0 gradient and 10 mM sucrose concentration gradient. The parameters varied in this study are the amount of transporters in the membrane and the membrane area. The amount of proteins in the membrane assembly is assumed to be at 100% for 150 μg reconstituted in 0.079 cm^2 of BLM area. Fluid flux through the membrane assembly for 100%, 150% and 200% proteins is measured and the the results are shown in Figure 3.18. It can be observed from the plot that the flux rate is proportional to the amount of transporters and a higher steady state flux results with more transporters in the membrane assembly. This preliminary study only demonstrates the feasibility to generate a larger flux through the membrane and a detailed investigation is warranted.

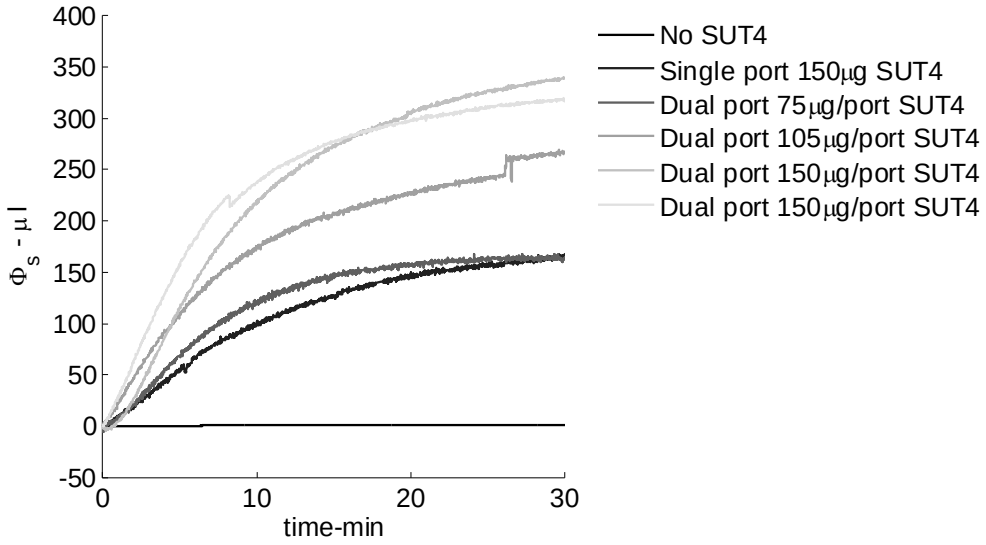

Figure 3.18: Effect of protein density and BLM area on fluid transport

The pore size of 50 μm is considered to be at the higher end of the spectrum for BLM self-assembly. Recent studies by Hopkinson and Leo[41] have demonstrated that the self-assembled BLM on smaller pores can endure higher pressure before failing than than their counterparts formed on larger pores. Designing the membrane assembly that can withstand higher pressure is much desired for the actuator. In order to characterize the membrane assembly formed on a substrate with a smaller pore, the transport experiments were repeated on a lead silicate glass plate with 2 μm pores. The glass plate with 2 μm pores is prepared using the same procedure described for the plates with 50μm pores and a single port substrate is prepared. The port area and the effective membrane area are maintained the same on this substrate. A minimum of three functional trials were performed for each concentration and typical flux data is shown in the plot in Figure 3.19. The normalized flux measured through the smaller pores compares with the flux through membranes supported on PC substrate and on lead silicate glass with 50 μm pores. The flux for different sucrose concentrations on one side of the membrane is shown in Figure 3.20. The error bars represent 95% confidence interval for flux through the membrane calculated from Student-'t' distribution applied to the steady state flux through the membrane from 3 trials. The steady state flux increases by increasing the concentration of sucrose. A larger scatter is observed for higher sucrose concentrations. This is attributed to the non-repeatability of protein transporter insertion in the BLM. At smaller sucrose concentration, only a smaller number of transporters are required and is available for transport. At higher

concentration, a larger number of proteins are needed for repeatability. A consistent higher number of proteins is not available and hence a larger scatter is observed in the measured fluid flux.

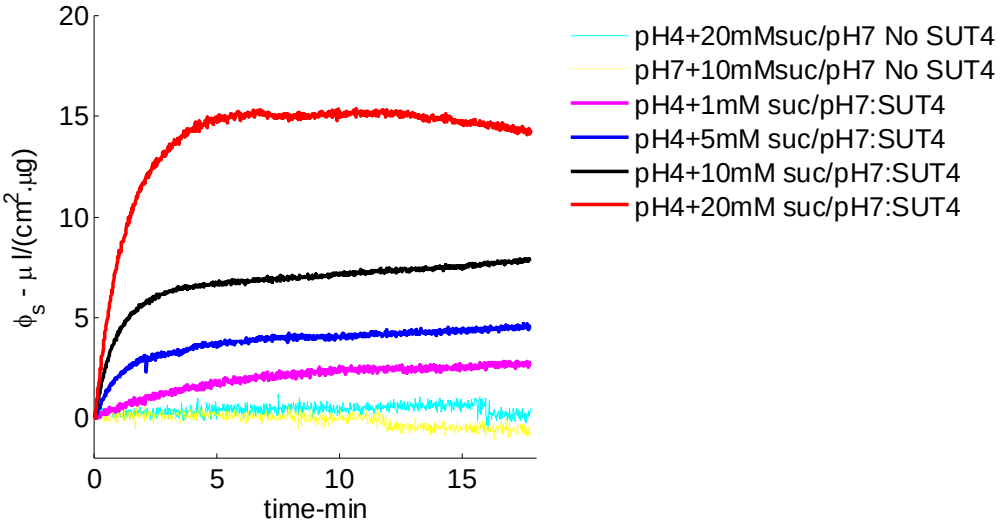

Figure 3.19: Normalized flux through membrane assembly - time response(Lead silicate glass with 2μm pores)

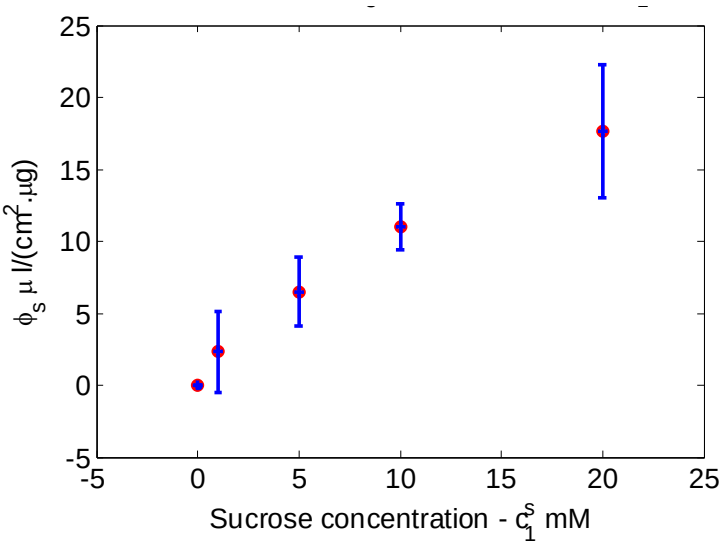

Figure 3.20: Normalized flux through the membrane on 2 μm pores for different sucrose concentration

3.3.3 Rate constants for fluid flux

The transport experiments have quantified the amount of fluid transported through the membrane assembly for an applied pH gradient and concentration gradient of sucrose. The four state carrier model discussed in Chapter 2 is applied to the flux data from the experiments to find relevant material constants of the membrane assembly formed on different substrates. The simple, four-state symmetric model relates the maximum flux rate($\dot{\phi}_{\max}$) through the membrane to the affinity of the diffusing solute to the protein(K) and the concentration of the solute(c_1^s) driving fluid transport by the relation

$$\dot{\phi_s} = (\dot{\phi_s})_{\max} \left(\frac{c_1^s}{c_1^s + K} \right) \tag{3.8}$$

The units for the flux rate terms $\dot{\phi}_s$, $\dot{\phi}_{\max}$ is μl/μg.cm^2.min and the concentration terms c_1^s, K is mM. The flux rate ($\dot{\phi}_s$) through the membrane for the time of interest gives the numerical value of volume change in the top chamber. Likewise, the maximum flux rate $(\dot{\phi}_s)_{\max}$ gives the maximum steady state volume change in the top chamber. The numerical value of the maximum volume change obtained from this expression is significant for actuation as it quantifies the maximum steady state deformation that can be developed by the actuator.

The maximum steady state flux($(\phi_s)_{\max}$) is obtained from the maximum flux rate($(\dot{\phi}_s)_{\max}$) in equation 3.8. The procedure for obtaining maximum flux rate ($(\dot{\phi}_s)_{\max}$) from experimental data is as follows: The flux data at different concentration are used to draw the reciprocal plots shown in Figure 3.21. The intercept on the negative x-axis is the reciprocal of the association constant in the model and the intercept on the positive y-axis gives the reciprocal of the maximum flux rate through the membrane. The values obtained from the plot are shown in Table 3.2. The maximum flux rate $(\dot{\phi}_s)_{\max}$ is a rate parameter and is

Table 3.2: Flux rate through membrane assembly for different substrates

c_1^s	1mM	5mM	10mM	20mM	K mM	$\dot{\phi}_{s\max}$
$\dot{\phi}_s$(PC)	0.34	0.76	0.84		2.02 $\pm$0.3	1.04 $\pm$0.15
$\dot{\phi}_s$(50μm)*	0.2	0.61	0.72	1.25		
$\dot{\phi}_s$(2μm)	0.28	0.56	1.42	1.55	5.35 $\pm$0.9	1.26$\pm$0.46

All flux rate terms are in μl/(μg.min)

$*$ The data is not a fit for the reciprocal relation

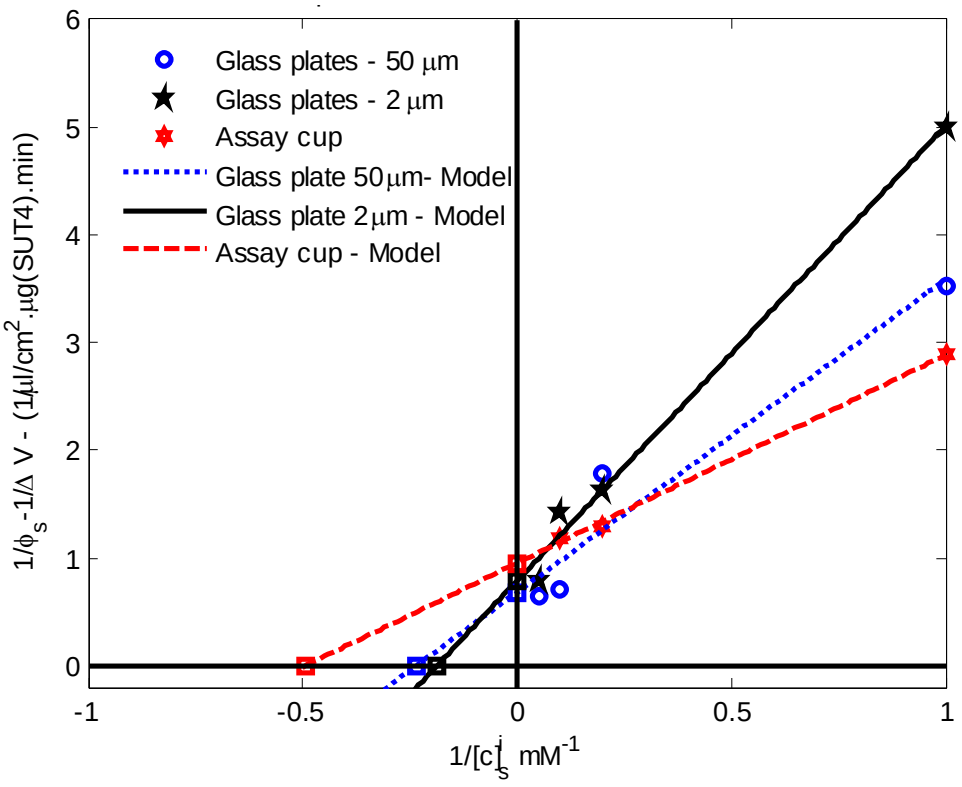

Figure 3.21: Reciprocal plots from experimental data for the membrane assembly with SUT4 formed on PC membranes & lead silicate glass

converted back to flux assuming linear rate for the time of interest. This gives the maximum volume change in the top chamber for the time of interest. With the numerical values of K and $(\phi_s)_{\max}$ the steady state flux through the membrane for different concentrations can be obtained. The steady state flux from experiments and the model as a function of sucrose concentration for different membrane assemblies are shown in the plots in Figure 3.22. This curve is an analogue of the sensitivity of an actuator to the input stimulus. The sensitivity of the membrane to different concentrations of sucrose is fairly linear at lower concentrations of sucrose in the bottom chamber. A change in deformation can be expected in the actuator as the concentration of sucrose is varied upto 6 mM sucrose for glass plate substrate and 3 mM for the polycarbonate substrate. Above these numerical values of sucrose concentration, the model estimates that there will not be an appreciable change in volume within the time of interest by increasing the sucrose concentration.

The numerical value of the translocation rate through the membrane is computed using the equation 2.25. The expression $\dot{\phi}_{s\max} = \frac{\dot{\alpha}_w M}{2}$ can be rearranged to compute $\dot{\alpha}_w$

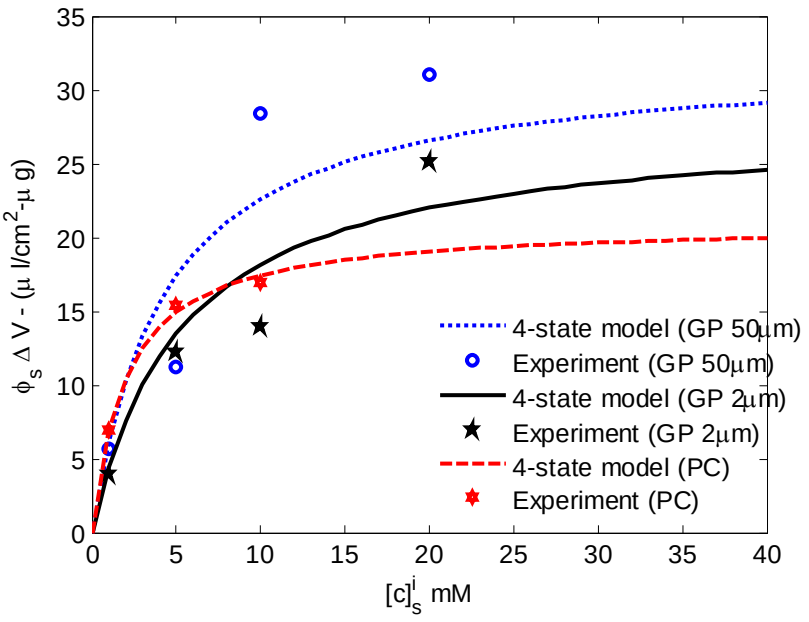

Figure 3.22: Sensitivity of the membrane formed on different substrates to concentration gradient of sucrose

Table 3.3: Translocation rate through different membrane assemblies

Substrate	$\dot{\alpha}_w$ μl/μg.min
Polycarbonate	2.08
Lead silicate glass (2 μ m)	2.52 $\pm$0.46

as:

$$\dot{\alpha}_w = \frac{2(\dot{\phi}_s)_{\max}}{M} \tag{3.9}$$

The parameter $\dot{\alpha}_w$ has the units μl/(μg $-$ min.cm^2) which is the rate at which fluid is transported across the membrane per μg of protein assembled into the membrane. The translocation rate through the membrane assembly with SUT4 is experimentally determined to be 2.5$\pm$0.46 μl/μg.cm^2.min. The flux variables are normalized with respect to the amount of transporters added to the membrane and hence the translocation rate was not taken up for discussion. The discussion on saturation flux and sensitivity of flux to sucrose concentration can be presented in terms of the translocation rate through the membrane. The integrated value of translocation rate through the membrane gives an estimate of the number of cycles of operation for the transporter to transport sucrose and consequently water molecules through the membrane.

3.4 ATP driven transport for actuation

The transport experiments discussed so far in this chapter uses a proton gradient as the driving force to transport a solute and water molecules across the membrane assembly formed in the pores of different substrates. In a plant cell membrane, a pH gradient is generated by a biochemical reaction consuming ATP as shown in the Figure 3.1. The energy producing reaction in the plant cell membrane is referred to as the hydrolysis reaction. The proteins that can catalyze hydrolysis of ATP in a cell membrane are called ATPases. The transmembrane ATPases are membrane integral proteins that use the energy from hydrolysis to move solutes across the cell membrane. The transmembrane ATPases can be broadly classified into three types: the plasma membrane ATPase (PM ATPase), vacuolar ATPase (V-ATPase) and F-ATPase. The PM ATPase uses ATP energy to transport a proton across the plasma membrane of the cell and few other cellular organelles. The PM-ATPase forms a phosphorylated intermediate with ATP to move a proton across the cell membrane. The F-ATPase pump is found in inner mitochondrial membranes and in chloroplast thylakoid membranes. Apart from hydrolyzing ATP, the F-ATPase can also synthesize ATP from an electrochemical gradient. A V-type ATPase is restricted to the vacuolar membrane of the plant cell and is also referred by the names V-ATPase and H^+ V-ATPase. In a V-type ATPase, the ATP molecule binds to the nucleotide biding site on the protein, hydrolyzes and provides the energy for proton transport through the membrane. The transport of protons establishes an electrochemical proton gradient. Thus, in a proton cotransporter based system for fluid transport, the gradient of protons required for solute and water transport can be generated *in situ* by using a proton transporter. This chapter is a concept demonstration of using the energy from a primary active transporter like V-type ATPase to generate the desired proton gradient and use it in a cotransporter based system for fluid transport.

3.4.1 Mechanism of ATP driven transport

The mechanism for demonstrating fluid transport using the energy available from ATP hydrolysis in a engineered device is shown in Figure 3.23. The V-ATPase enzyme is shown reconstituted in the phospholipid BLM formed across the pores of the supporting substrate. The ATPase enzyme hydrolyzes ATP on one side of the membrane and transport

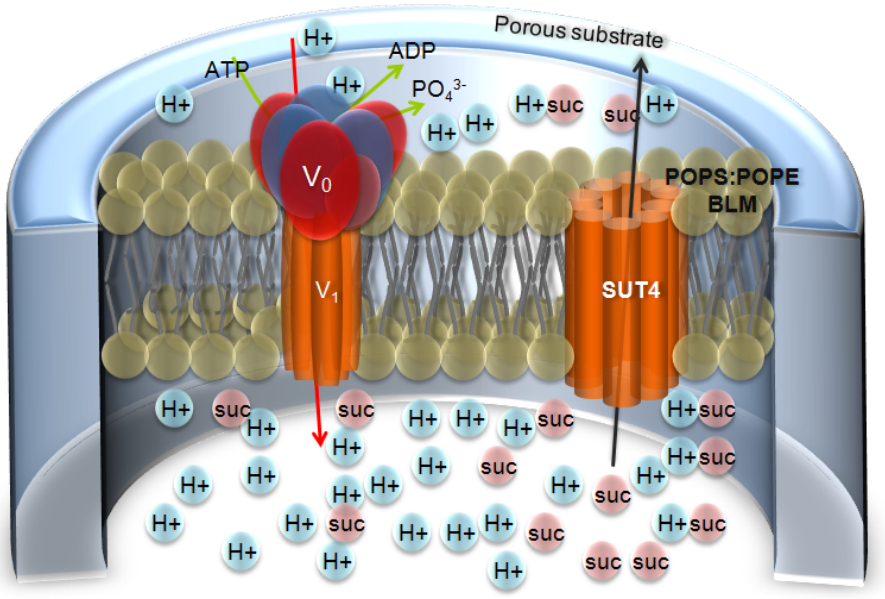

Figure 3.23: Principle of ATP-hydrolysis powered fluid transport

protons through the conductive channel in the pump. The stoichiometry of proton transport is dependent on the transmembrane electrochemical gradient. The accumulation of the translocated proton on the other side of the membrane results in a proton gradient across the membrane. In the presence of a cotransporter like SUT4 and a sucrose gradient along the established electrochemical gradient, a proton and sucrose molecule is transported back through SUT4. It is expected that water molecules travel with sucrose due to the osmotic gradient resulting from sucrose transport according to Muench's hypothesis[24, 89]. The schematic shows that ATP hydrolysis reaction in an phospholipid BLM formed across the pores of a synthetic substrate can generate solute and fluid transport. The fluid transport resulting from ATP hydrolysis can be used for actuation. An actuator built using a combination of primary active and secondary transport processes will generate deformation from an energy producing biochemical reaction.

The SUT4 protein used for demonstrating pH gradient driven transport is an ideal candidate for coupling the electrochemical gradient available from ATP in the presence of ATPase enzyme into fluid transport through the membrane. The discovery and demonstration of this process in plant cell membranes dates back to 1989 with the first demonstration reported about the same time by Lemoine[55] and Bush[14] using sugar beet leaves. Their work involved smaller concentrations of enzymes and cotransporters in the surrogate cell to demonstrate the idea. This demonstration attempts to implement the idea to gener-

ate fluid transport for bio-inspired actuation. The proton sucrose cotransporter - SUT4 - characterized in the previous sections for pH gradient driven fluid transport is used with ATPase to demonstrate ATP driven fluid transport. The ATPase proteins required for the demonstration is provided by Prof. John Cuppoletti. The following received as a personal communication is a brief outline of ATPase preparation procedure used in the project. "Beet plasma membrane H+-ATPase was prepared and purified from beets essentially as described by Lino et al [57]. Activity of 6 different preparations varied from about 411 enzymeU/ml to 2816 enzymeU/ml as measured by the method of Yoda and Hokin[113]".

3.4.2 Materials used

The demonstration of ATP-hydrolysis powered fluid transport uses V-ATPase enzyme extracted from red beet tonoplast membranes. The enzyme is reconstituted in a planar bilayer membrane supported on a porous substrate. The substrates used for reconstituting the enzyme is identical to the porous substrates used for transport experiments described in Section 3.3. The hydrolysis reaction in the enzyme requires a medium with hydrogen ion concentration comparable to living cells. A pH7.0 medium, conducive for the reaction is used on both sides of the bilayer membrane reconstituted with the enzyme. The ATP fuel required for the reaction is dissolved in the buffer medium on one side of the membrane. The V-type ATPase enzyme converts energy in ATP into an electrochemical gradient. The SUT4 cotransporter that uses the electrochemical gradient is reconstituted in the membrane together with the enzyme. The sucrose required for the cotransporter to generate fluid flux is dissolved in pH7.0 buffer on the side of the membrane opposite to ATP. The glass substrate required for this experiment is prepared similar to the procedure outlined in Section 3.2.1. A complete list of materials used for the experimental demonstration is provided below:

- Porous lead silicate glass plate 50μm pores and 50% porosity, supplied by SRI International
- SUT4 protein cultured from *Arabidopsis thaliana*, cloned in yeast, extracted and purified, suspended in pH7.0 medium (20.2 mg/ml), Red beet ATPase, supplied by Prof. Cuppoletti's lab

- 1-Palmitoyl-2-Oleoyl- sn- Glycero-3- [Phospho-L-Serine] (Sodium Salt) (POPS) [4] mixed with 1-Palmitoyl-2-Oleoyl- sn- Glycero-3- Phosphoethanolamine (POPE) in the ratio 3:1 (w:w) and dissolved in n-decane, purchased from Sigma-Aldrich Inc.,
- Platinum electrode wire - 0.8 mm diameter
- Silver-silver chloride electrodes (EP2) obtained from WPI Inc.

3.4.3 Experimental setup

The experimental setup with the transport fixture is shown in Figure 3.24. The micrograph of a cleaned substrate is shown in Figure (a) and BLM with the proteins are reconstituted in the 50μm pores in the substrate. Figure (b) shows the prepared substrate with a port 4.5 mm in diameter on to which the lipids, enzyme and transporters are added. The experimental setup in Figure (c) shows the prepared substrate with lipids and proteins in a bottom chamber filled with pH7.0 buffer carrying 10 mM sucrose. The top chamber is filled with pH7.0 buffer and 5 mM Mg-ATP salt. The volume ratio between the two chambers is approximately 120. The platinum electrodes used as the sensor element for capacitance meter (Appendix A) are inserted into the top chamber to a depth of 5 mm. The operating frequency of the capacitance meter is increased to 125 kHz from 100 kHz used for pH gradient driven transport. It is observed that the steady level capacitance drifts in the presence of ATP in the top chamber. The drift was marginal on increasing the frequency to 125 kHz. Due to this change, the resolution of the level meter decreases, but remains within measurable limits and permits data acquisition to monitor the flux rate due to transport.

The vials containing the liposomes with SUT4 and ATPase are thawed during substrate preparation. The lipid mixture is added to the substrate followed by SUT4 and ATP-ase enzyme. The porous substrate in the fixture with lipids and proteins is allowed to stand in air for 10-15 minutes and placed in the aqueous medium. On coming in to contact with polar water molecules, the lipids self-assemble into the pores and form a planar lipid membrane with SUT4 and ATPase enzyme reconstituted in the membrane. The self-assembly is tested using impedance analysis. The measured impedance on the membrane assembly with lipids and additional proteins (ATPase and SUT4) is shown in Figure 3.25.

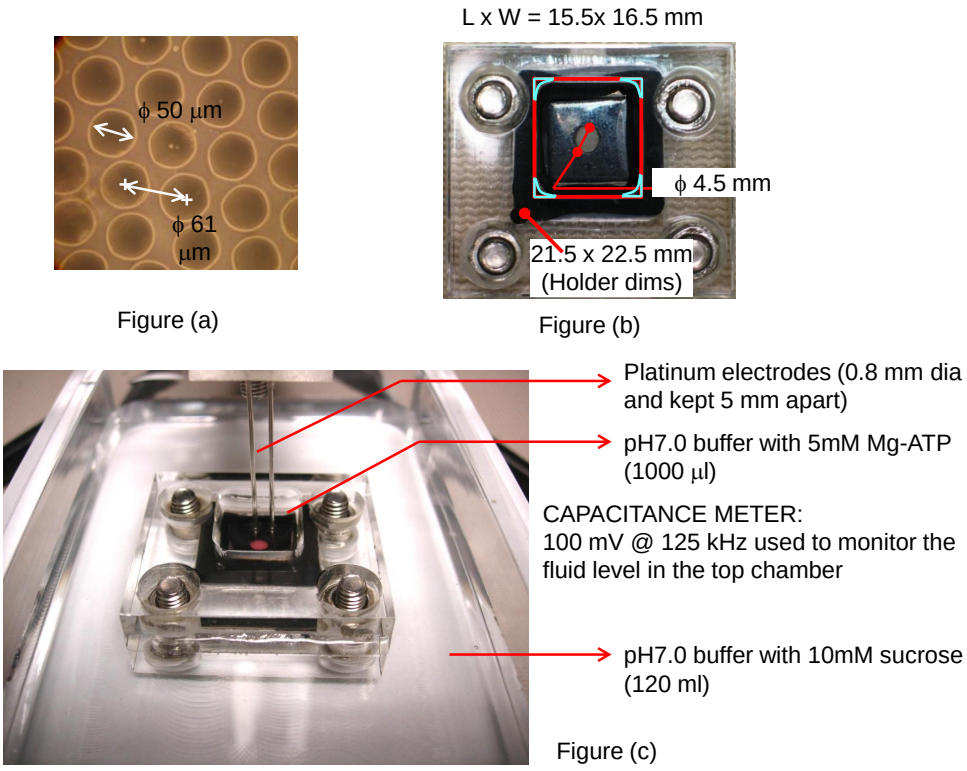

Figure 3.24: Experimental setup for measuring ATP hydrolysis driven transport through the membrane assembly

The impedance measured across a plain BLM in the pores is the highest. In the presence of additional proteins, the measured impedance decreases. It is generally observed to decrease by 50% for the membrane assemblies formed on porous lead silicate glass plate substrates used in this work. The membrane assembly shown in the impedance plots are formed in separate trials and the data presented shows the observed trend.

3.4.4 Results - ATP powered transport

The objective for this experiment is to measure fluid transport through a membrane assembly using ATP hydrolysis reaction as the stimulus. The biological components required for transport, ATPase enzyme and SUT4 protein are reconstituted in the membrane assembly. The required pH7.0 buffer with dissolved ATP and sucrose are available on opposite sides of the membrane. The control study to test the feasibility to influence fluid transport should leave out the fuel required for the reaction or not have the molecular pump that can stimulate the cotransporter. In accordance, the baseline tests are performed leaving out ATPase

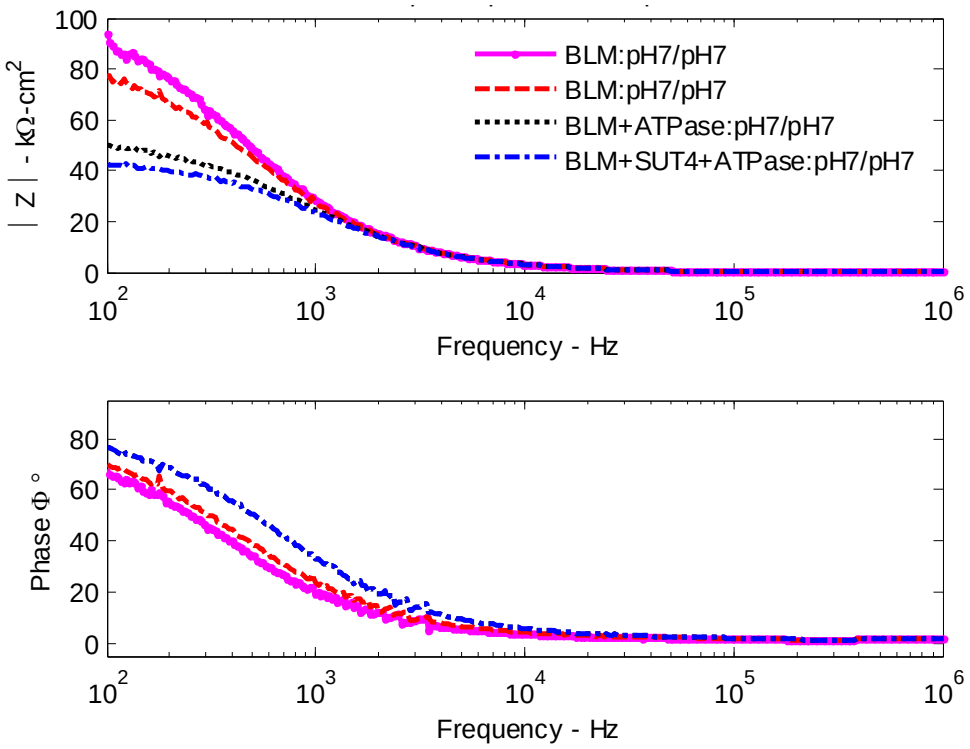

Figure 3.25: Measured impedance on the substrate for different membrane assemblies

in the membrane assembly or ATP in the medium. In both the cases, it is observed that there is no significant quantity of fluid transported through the membrane. The results for the control study are shown in Figure 3.26. The effect of the ATP present in the medium is seen in the fluctuations observed in the capacitance meter, while a similar noise is notably absent in the data for the case without ATP. The baselines indicate that the SUT4 proteins and ATPase enzyme are required for transport through the membrane. Also it is observed that a constant level is maintained in the top chamber with ATPase and SUT4 in the membrane assembly. This shows that the proteins are impervious to the contents in the top chamber without the required stimulus. The quantity of ATPase and ATP added to the BLM is varied to study the effect of the amount of pumps on fluid transport.

The experimental parameters in the membrane assembly and the chambers were kept a constant to study the effect of the amount of ATPase on fluid flux through the membrane assembly. Relevant parameters for each component in the experiment is listed in Table 3.4.3. The plots in Figure 3.27 shows a typical response for the flux observed through

Table 3.4: System parameters for ATPase experiments

ATP driven fluid transport Experimental conditions	
Amount of SUT4	150 μg
Initial sucrose concentration (c_1^s)	10 mM
Volume of liquid in top chamber (V_2)	900-1000 μl
BLM area	0.079 cm^2
Volume of liquid in bottom chamber(V_1)	120 ml

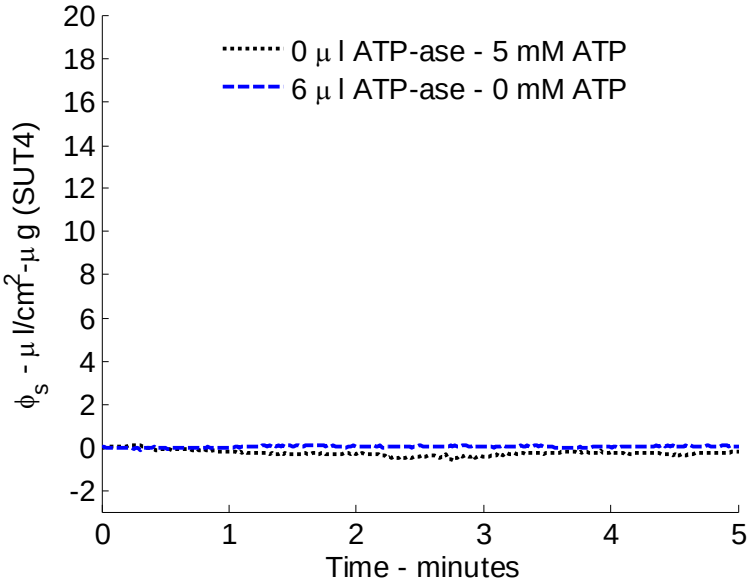

Figure 3.26: Fluid flux through the membrane assembly in ATPase driven transport experiments - Baseline trials

the membrane for different amounts of ATPase reconstituted in the membrane. The results in Figure 3.28 shows 95% confidence interval from Student t-test for the steady state flux observed through the membrane at difference amounts of ATPase in the membrane. The flux observed for the smallest concentration of ATPase enzyme in the BLM (3 μl corresponding to 38 μl/cm^2 of ATPase) has a smaller interval at 95% confidence. This suggests that the flux through the membrane is not expected to vary between trials. It is safe to conclude that the flux through the membrane is repeatable. Increasing the concentration of enzyme by a factor of two, the flux observed through the membrane increases and the 95% confidence interval for the flux widens. Further doubling the enzyme concentration, it is observed that the mean flux through the membrane increases and the confidence interval to predict the flux through the membrane increases by a factor of two. From the average flux from 5 trials

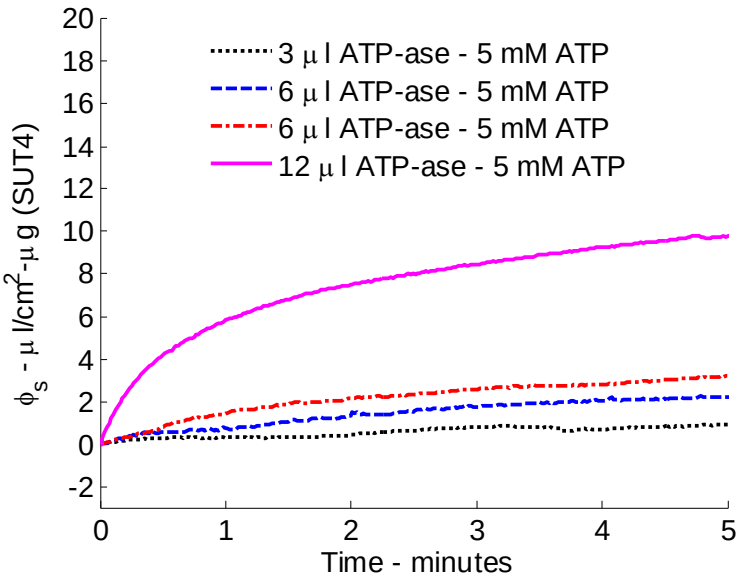

Figure 3.27: Fluid flux through the membrane assembly in ATPase driven transport experiments

at 3 different enzyme concentration in the membrane, an increasing trend is observed. It is concluded that the amount of fluid transported through the membrane increases with the amount of enzyme in the membrane assembly. A higher density of pumps in the BLM producing a greater electrochemical proton gradient across the membrane with SUT4 could explain the observed increasing trend.

The spread in data between trials with different amounts of enzyme in the membrane could point to a poor repeatability of one of the steps in membrane fabrication or the energy conversion process. The membrane is formed by self-assembly of enzymes, protein and BLM in the pores of the substrate. There is no visual method of interrogating the presence of different components in the membrane assembly and care is not taken in the fabrication procedure to maintain a uniform distribution of enzyme and cotransporter. The ATPase proton pump used in this work has a directional preference for proton transport through the membrane. During self-assembly in the membrane, there is very little done to get all ATPase pumps have their V_o subunits face the side of the membrane with ATP. Furthermore, the pore size of 50 μm used for forming the membrane assembly is considered higher for BLM formation. In spite of all these deficiencies in the system, the results of this first implementation of the novel concept for an engineering application shows the system in favorable light for actuation. Since the flux rate through the membrane assembly is

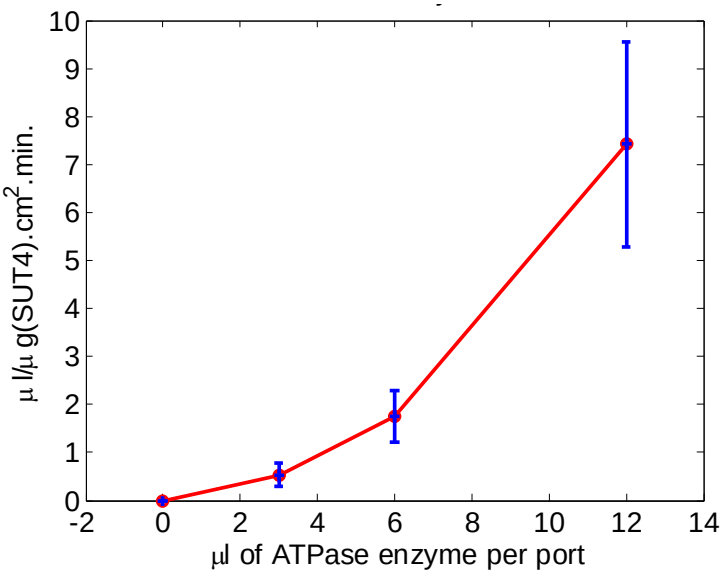

Figure 3.28: Flux rate through the membrane as a function of the amount of ATPase reconstituted in the membrane

repeatable for smaller concentration of enzyme and otherwise at higher amounts, it can be concluded that the membrane fabrication process could be modified to address some of the issues discussed here to get a higher and repeatable flux through the membrane assembly.

3.5 Chapter summary

The chapter demonstrates fluid transport through a membrane assembly that uses biological proteins as the functional components. Fluid transport through the membrane is triggered by a pH gradient or by using a biochemical reaction starting from ATP. The pH gradient driven transport discussed here forms the basis for designing the chemomechanical actuator. This chapter discussed the component selection, fabrication and transport characterization of the actuator membrane assembly. The SUT4 protein in the membrane assembly formed across the pores of polycarbonate and glass plate substrate generates a maximum of 25 μl/μg.cm^2 flux through the membrane that corresponds to a the maximum flux rate of 1.25 μl/μg.cm^2.min. The fluid flux data obtained from different experiments were applied to the kinetic rate model developed in Chapter 2 to compute rate constants for fluid transport through the membrane. The half-maximum velocity concentration that corresponds to the binding rate for the solute to the transporters from different substrates is found to be 5.24$\pm$1.3 mM. The maximum translocation rate is found to be 1.25$\pm$0.35

μl/μg.cm^2.min. This discussion on membrane assembly provides the relevant information required to demonstrate chemomechanical actuation in the protein based actuator.

The last section in the chapter discussed fluid transport using ATP hydrolysis reaction. A V-type ATPase enzyme that can hydrolyze ATP replaces the pH gradient required for fluid transport through the cotransporter. The results from ATP powered transport experiments demonstrate that the transport through the membrane assembly is due to the presence of ATPase enzyme and the amount of fluid transported increases with the concentration of the enzyme in the membrane assembly.

Chapter 4

Actuation Experiments

Transport experiments in Chapter 3 demonstrated the technical feasibility to generate fluid flux through a membrane assembly for an applied chemical stimulus using transporter proteins as the active element. The chemical stimulus applied to the membrane is a transmembrane proton gradient. The equilibrium constant for the binding reaction of transported sucrose to the transporter and translocation rate of sucrose and water through the membrane is computed from the experimental data. This chapter presents the work on using the characterized membrane assembly in an actuator to demonstrate chemomechanical energy conversion. Prototype actuators that use porous polycarbonate and porous glass plate as supporting substrates have been fabricated and are discussed separately.

4.1 Polycarbonate membrane as supporting substrate

4.1.1 Actuator configuration

The first prototype actuator that uses a polycarbonate membrane as the supporting substrate is shown in Figure 4.1. The bottom chamber in this design is connected to an external reservoir. The supporting substrate is attached to the bottom of the top chamber. The top chamber with the cover plate is assembled on top of the bottom chamber and the entire assembly is clamped in a fixture. The alignment and design of the carrier plate ensures that there are no air pockets trapped between the PC membrane and the aqueous medium in the bottom chamber.

The components of the actuator are fabricated from photocurable poly-propylene

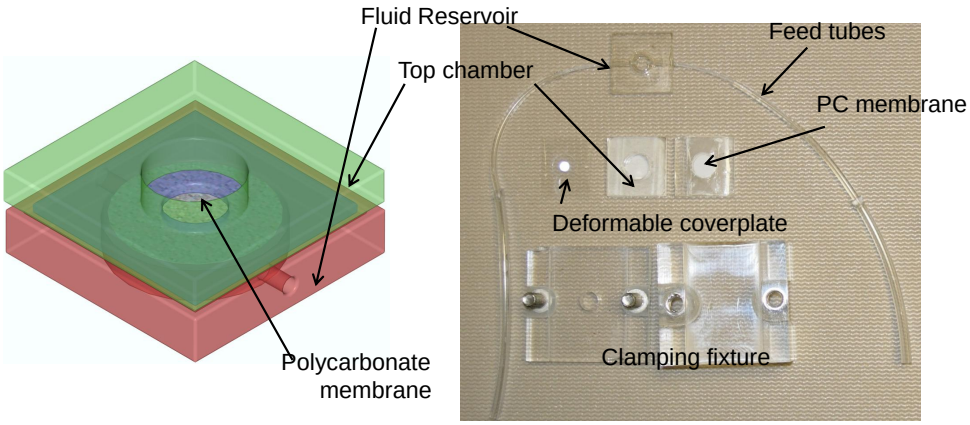

Figure 4.1: Microhydraulic actuator element- schematic & prototype

glycol diachrylate (PPG-DA) by SRI International, Menlo Park, CA. The top chamber and the bottom chamber are identical in dimension and measure ϕ 8mm x 4 mm. The track etched polycarbonate membrane discs in the actuator have an average pore diameter of 1.2 μm and 20% porosity. Tubes attached to the bottom chamber are connected to a reservoir that serve as an additional source of sucrose and pH4.0 buffer. A new PC membrane is used for every trial and the entire actuator is assembled before every trial. A mylar membrane supported on transparent tape forms the deformable membrane of the actuator element. Details of different components of the actuator are listed in Table 4.1.

Table 4.1: Polycarbonate substrate based actuator - dimensions

Top chamber	ϕ8 mm x 4 mm	0.2 ml
Bottom chamber	V_1 (including reservoir)	35 ml
	Volume ratio (V_r)	175
Membrane assembly	Porous polycarbonate	1.2μm pores, 20% porosity
	Port area (diameter=0.8cm)	0.5 cm^2
	Effective BLM area	0.10 cm^2
	Mylar membrane	2.5 μm thick and ϕ4.5 mm

The first step in fabricating the actuator is to coat 15 μl of lipids and 15μl of SUT4 protein on the porous substrate and allowing it to stand in air for 10 minutes. The bottom chamber is filled with pH4.0 buffer and the concentration of dissolved sucrose is varied based on the experiment. The top chamber with the coated PC substrate is assembled above the bottom chamber and pH7.0 buffer is added to it. The mylar membrane cover plate is clamped above the top chamber in the fixture to result in the assembled configuration

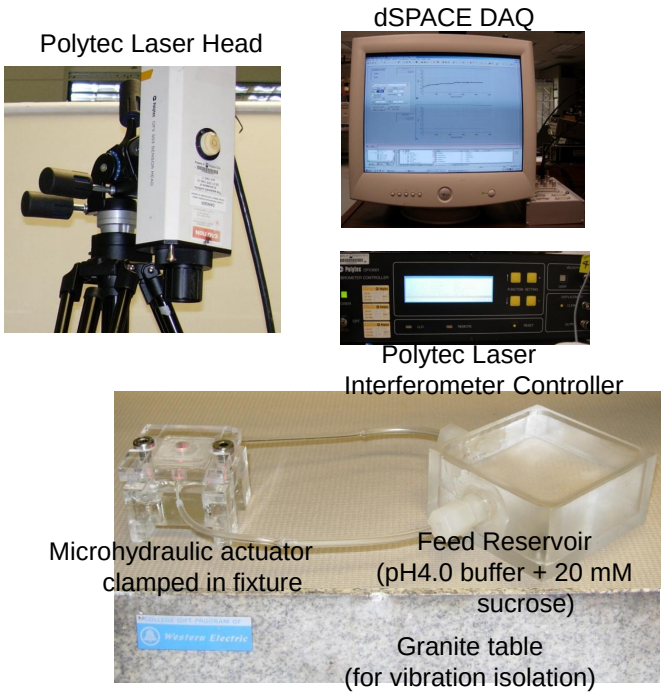

Figure 4.2: Experimental arrangement to measure deformation

shown in Figure 4.2. The fixture is designed to hold the actuator elements in an assembled configuration and to keep the bottom chamber above the level of fluid in the reservoir. This prevents gradient driven flow into the top chamber.

4.1.2 Experimental setup

The data acquisition system for measuring the deformation in the assembled actuator is shown in Figure 4.2. The polytec laser vibrometer measures the deflection of the reflective spot at the center of the mylar membrane. The displacement signal from the vibrometer is fed to a dSpace DAQ system in Windows XP workstation via DS1104 data acquisition system. The actuator assembly is placed on a granite table to prevent structural vibrations from interfering with the highly sensitive instrumentation. Displacement is measured in the actuator element for different chemical stimulus applied to the actuator.

The chemical stimulus required to produce a deformation in the actuator is pH gradient and sucrose concentration gradient across the membrane assembly with SUT4 transporter proteins. Various baseline measurements are performed with one required component in the actuator or stimulus left out. The different baseline conditions tested on the

actuator to demonstrate the concept are

- Bare polycarbonate membrane, without the membrane assembly, with pH gradient
- A plain BLM formed across the pores of the PC substrate with pH gradient
- A BLM with SUT4 across the pores of the PC substrate with pH gradient and without sucrose in bottom chamber
- A plain BLM across the pores of the PC substrate with pH gradient and 10 mM sucrose in the bottom chamber

The test is repeated with SUT4 in the BLM subjected to pH4.0/pH7.0 gradient and different initial sucrose concentrations in the bottom chamber. The results from the baseline and validation experiments are shown in Figure 4.3 and 4.4.

4.1.3 Results and discussion

The actuator in the first baseline test has a porous polycarbonate substrate without any lipids subjected to a pH4.0 vs pH7.0 gradient. The result in Figure 4.3 shows that the cover plate deforms into the top chamber. This is due to the contents in the top chamber draining out through the pores of the PC membrane. This test rules out any inflow into the top chamber due to capillarity. The lipids are added to the PC substrate for the second baseline and a pH gradient is applied. There is no appreciable change in level of the coverplate for the first 4 minutes indicating the presence of a self-assembled lipid membrane across the pores. Failure of the BLM formed on the pores is attributed to the deformation of the cover plate into the top chamber after fourth minute in the reported trial in Figure 4.3. This result shows that there is no observable osmotic flow through the BLM due to the buffer salts in the aqueous medium in the two chambers.

The third baseline test is on an actuator with a BLM and SUT4 added to the substrate and subjected to a pH4.0 vs. pH7.0 gradient. Sucrose is left out in this baseline and it is observed that there is no change in the coverplate position. In this trial, the SUT4 proteins does not have sucrose molecules required for establishing an osmotic gradient to drive fluid flow into the top chamber . The fourth baseline test is on an actuator without any SUT4 in the BLM. The membrane assembly is subjected to a pH gradient and the

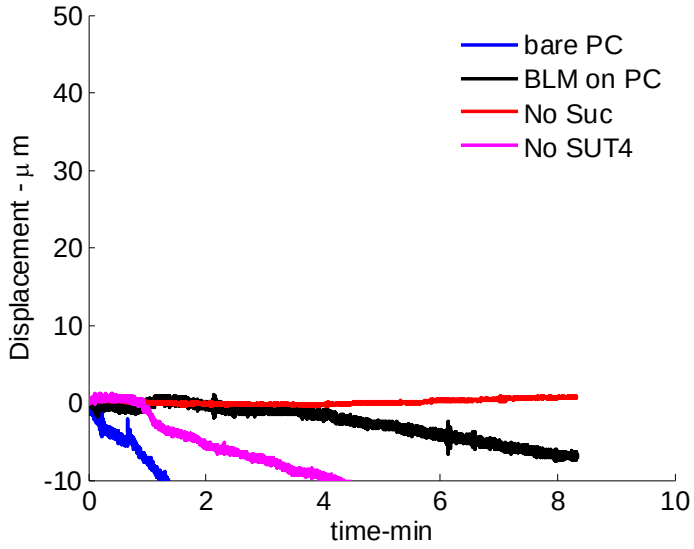

Figure 4.3: Measured deformation in the actuator for different baseline cases

bottom chamber has 10 mM sucrose dissolved in it. The cover plate deforms into the top chamber which could be explained by the movement of water from the top chamber through the BLM driven by osmotic gradient.

All the baseline tests indicate that the coverplate does not deform in the absence of one of the working components in the actuator. The coverplate of the actuator deforms out when the membrane assembly with SUT4 is subjected to a pH and sucrose gradient. The deformation in the actuator is tested for three initial concentrations of sucrose in the bottom chamber and 95% confidence interval for deformation in the coverplate calculated from Student-'t' distribution applied to the data from at least 3 trials is shown in Figure 4.5. The measured deformation in the actuator at 5 mM sucrose concentration is smaller than 20 mM sucrose in the bottom chamber. Due to scatter in the deformation data for initial sucrose concentrations between 5 mM and 20 mM a trend is hard to predict.

In the absence of a trend, one could assume that the deformation increases with an increase in initial sucrose concentration from 5 mM to 20 mM. To test the validity of this assumption, the initial sucrose concentration in the bottom chamber is increased to 30 mM. It can be seen that the steady state deformation in the actuator for an initial 30 mM sucrose is smaller than the deformation for 20 mM. It is possible that the deformation increases between 5 mM and 20 mM initial sucrose concentrations and begins to decrease for higher initial sucrose concentrations. One reason for a smaller displacement at higher

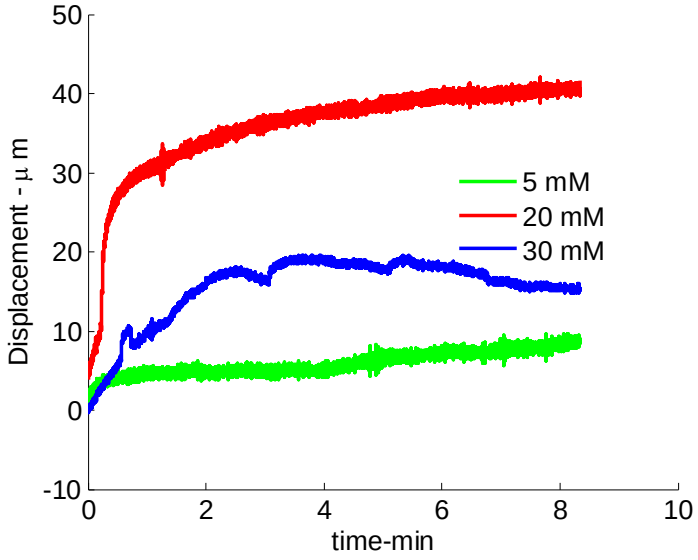

Figure 4.4: Measured deformation in the actuator for different baseline cases

values of initial sucrose concentrations could be that the osmotic gradient acts against the flow of proton-sucrose through the transporter and results in a back flow. The first prototype actuator is found inconsistent in the deformation it produces for the same chemical stimulus applied to the membrane. Detailed results from deformation experiments on this first prototype are shown in Figure 4.12 that shows the non-repeatability in deformation produced in the actuator. In spite of the shortcomings with this initial design, the experiments served its purpose to demonstrate the concept and provided insight into the actuator design. Using inputs from this first design, a second iteration of the actuator is designed that uses lead silicate glass plate as the supporting substrate.

4.2 Lead silicate glass as supporting substrate

4.2.1 Actuator configuration

The second prototype actuator fabricated to demonstrate chemomechanical energy conversion is shown in Figure 4.6. All the components in the actuator are machined out of plexiglass except for the supporting substrate and sealing gaskets. As in the previous design, there is a bottom chamber and a top chamber in the actuator separated by a membrane assembly. The bottom chamber has an integral reservoir that provides additional sucrose and buffer. The top chamber is covered by a mylar coverplate that deforms due to fluid

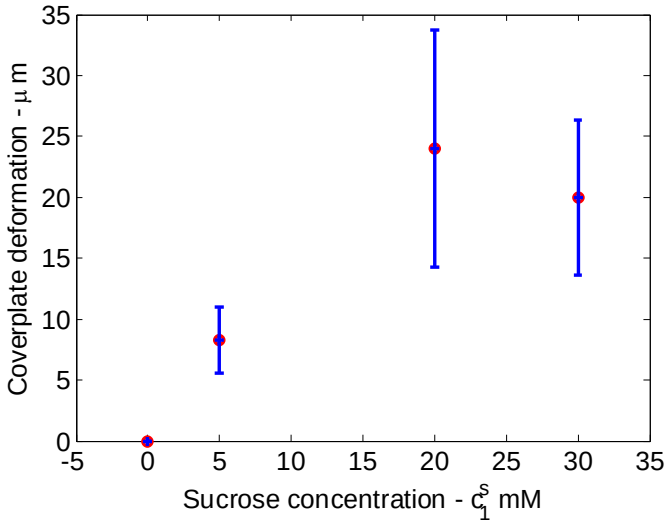

Figure 4.5: Measured deformation for different concentrations of sucrose developed by the actuator with polycarbonate supporting substrate

transport from the bottom chamber. The coverplate is restrained by a holding plate that is attached to the top chamber. The screws that attach the holding plate are designed to lock after specific number of turns to ensure a uniform clamping force. The lead silicate glass substrate is attached to a 20 mil kapton film. Rubber gaskets are provided wherever required to avoid leak in the actuator assembly. The assembled actuator is placed on a viscoelastic pad on a granite table to prevent structural vibration from interfering with measurements. A reflective tape is attached to the center of the mylar membrane to measure the deformation using a laser vibrometer. Table 4.2 lists all the relevant dimensions of the actuator components. The actuator is assembled with a clean porous lead silicate glass plate for every trial using the procedure described below.

Table 4.2: Lead silicate glass plate substrate based actuator - details

Top chamber	ϕ14 mm x 10 mm	0.54 ml
Bottom chamber	V_1 including reservoir)	50 ml
	Volume ratio (V_r)	92
Membrane assembly	Lead silicate glass plate	2μm pores, 50% porosity
	Port area (diameter=0.65cm)	0.33 cm^2
	Effective BLM area	0.165 cm^2
	Mylar membrane	2.5 μm thick and ϕ9.75 mm

The actuator chambers are thoroughly cleaned with methanol and deionized water before assembly. The glass substrate is cleaned with isopropyl alcohol, methanol and

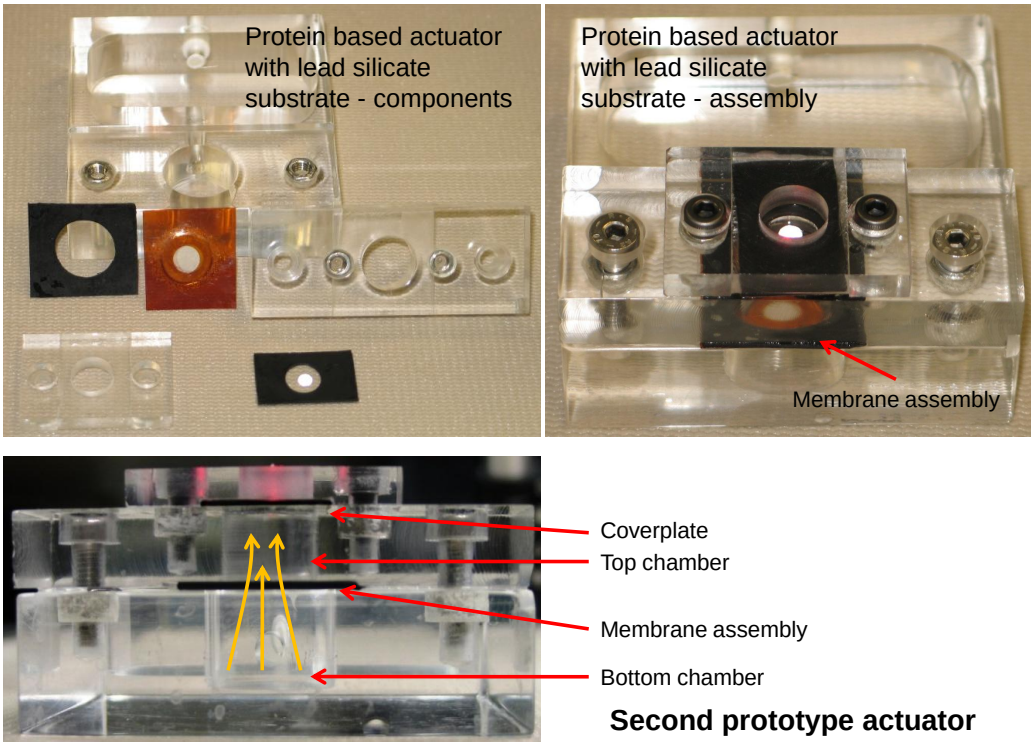

Figure 4.6: Second prototype actuator - components and configuration

deionized water in order and clean compressed air at 1.5 atm is forced through the pores to force out all cleaning agents. The glass plate is held on a separate holder and 10 μl of the prepared lipid solution (POPS:POPE in 3:1 ratio dissolved in n-decane - 40 mg/ml) is painted on the surface. This is followed by adding 10μl of SUT4 transporters available as liposomes in pH7.0 buffer to the porous substrate. The bottom chamber is filled with pH4.0 buffer with a known concentration of sucrose based on the trial. The glass plate with the added contents is placed on the bottom chamber after allowing it to stand in air for 15 minutes. The chambers, glass plates and the mylar membrane are assembled as shown in Figure 4.6 . The assembly is dismantled and repeated if any air is trapped below the cover plate or the supporting glass substrate. The completed assembly is placed under the laser vibrometer in a data acquisition identical to the one shown in Figure 4.2.

4.2.2 Results and discussion

The actuator is fabricated to test the baseline conditions and with different control stimulus. The different baseline tests done on this actuator are

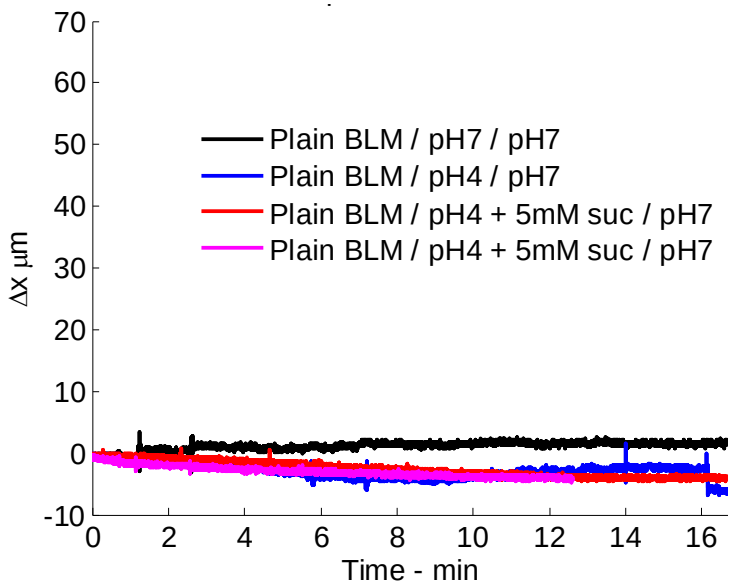

Figure 4.7: Measured deformation in the second prototype actuator for different baseline cases

- BLM with pH7.0 buffer on both sides of the membrane
- BLM with pH4.0/pH7.0 gradient without sucrose dissolved in the bottom chamber
- BLM with pH4.0/pH7.0 gradient with 5 mM sucrose dissolved in the bottom chamber

The results from baseline tests done on the second prototype are shown in Figure 4.7. There is no deformation in the coverplate for the case with pH7.0 buffer on both the sides of the membrane. Similarly, the coverplate does not show an appreciable deformation for a pH gradient applied to the membrane. The third baseline condition where pH4.0 buffer with 5mM dissolved sucrose is added to the bottom chamber, the coverplate deforms into the top chamber. This is similar to the result observed with the first prototype actuator and this is attributed to the migration of water molecules from the top chamber to the bottom chamber driven by the osmotic gradient.

The next set of experiments are performed on an actuator assembled with all of the required components and by varying the input stimulus. The concentration of sucrose in the bottom chamber is varied based on the test condition to quantify the response of the actuator. Different sucrose concentrations tested on the actuator are 1 mM, 10 mM, 20 mM and 30 mM. Representative results from these experiments are shown in Figure 4.8

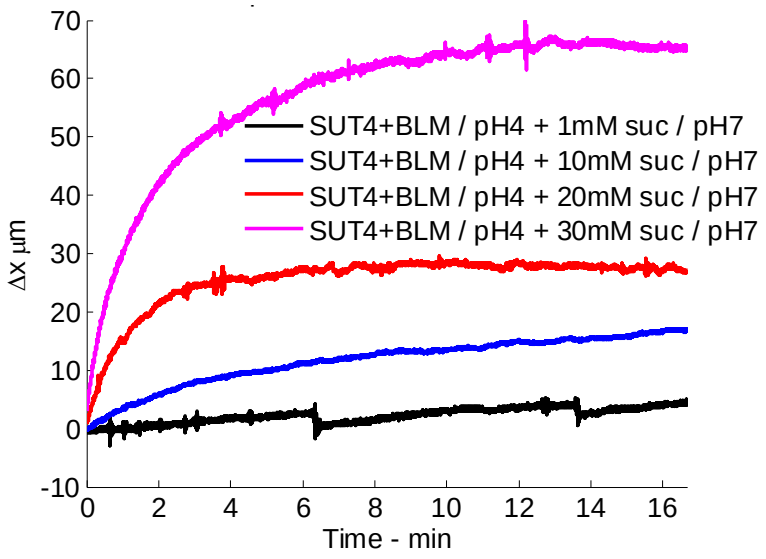

Figure 4.8: Representative deformation time histories measured in the actuator with 2 μm pores in lead silicate glass plates for different test cases

and the dependence of deformation on sucrose concentration is shown in Figure 4.8. The error bars represent 95% confidence interval for deformation in the coverplate calculated from Student-'t' distribution applied to the experimental from from at leat 3 trials. The deformation observed in the coverplate is observed to increase with the initial concentration of sucrose in the bottom chamber. The rate at which the membrane deforms out also increases with the concentration of sucrose. It is observed that for trials on the actuator at 30 mM, the coverplate begins to deform out and abruptly starts to deform back into the top chamber. This behavior is not shown in the Figure 4.8, but is provided toward the end of the chapter in Figure 4.13. A multitude of reasons can be attributed for this behavior with the first guess being BLM stability and adhesion to the supporting substrate. The steady state deformation observed in the actuator for different concentrations of sucrose is shown in Figure 4.9. The minimal scatter in the results indicate the repeatability of the deformation produced by the actuator for smaller initial sucrose concentration. The scatter at 20 mM is expected at 30 mM as well. Some of the trials for 30 mM sucrose were excluded from statistical analysis and hence a closer confidence interval is shown in Figure 4.9. It should be noted that 3 out of 5 trials did not work at 30 mM initial sucrose concentration. The scatter in the coverplate deformation data at higher concentration is attributed to the non-availability of the required number of SUT4 for transport inserted into the BLM. This is similar to the discussion on fluid flux through the membrane from transport experiments

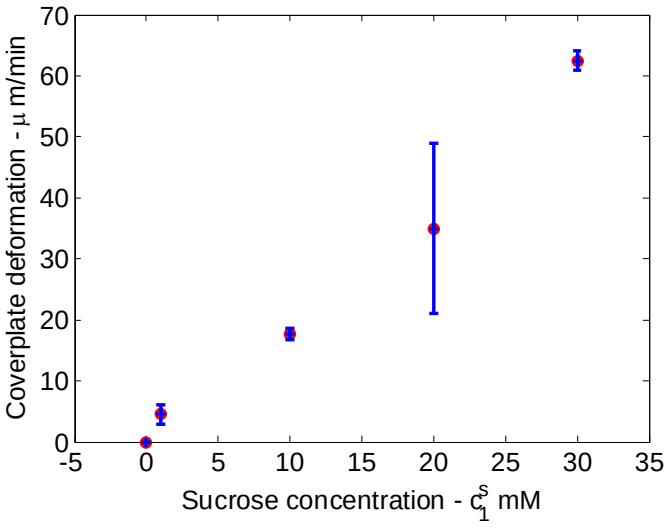

Figure 4.9: Measured deformation in the second prototype actuator for different concentrations of sucrose

on an identical supporting substrate in Section 3.3.2.

4.3 Comparing transport and actuation results

The results from the transport and actuation experiments can be compared by finding the change in volume in the actuation experiments. The change in the volume in the top chamber ϕ_s that results in a deformation Δx at the center of the coverplate can be obtained by integrating the profile of the deformed coverplate. The deformation $\Delta x^{'}$[34] at any radius $r_c^{'}$ due to a uniformly distributed, axisymmetric load ΔP acting on the coverplate of radius r_c is

$$\Delta x^{'}(r_c^{'}) = \frac{\Delta P}{64 G_{\mathrm{m}}} \left\{ 2 {r_c}^2 {r_c^{'}}^2 - {r_c^{'}}^4 \right\} \tag{4.1}$$

where G_{m} is the flexural rigidity of the coverplate material. The change in volume ΔV resulting from the deformation can be estimated from the integral

$$\phi_s = \int_0^{2\pi} \int_0^{r_c} \Delta x^{'}(r_c^{'}, \theta)\ r_c^{'}\ dr_c^{'}\ d\theta \tag{4.2}$$

Due to symmetrical loading, $\Delta x^{'}(r_c^{'}, \theta) = \Delta x^{'}(r_c^{'})$ and the expression for change in volume ΔV becomes

$$\phi_s = 2\pi \int_0^{r_c} \Delta x^{'}(r_c^{'})\ r_c^{'}\ dr_c^{'} = \frac{2}{3}\{\pi\ r_c^2\} \left\{ \frac{\Delta P\ r_c^4}{64\ G_{\mathrm{m}}} \right\} = \frac{2}{3} A_c \Delta x \tag{4.3}$$

The volume of the fluid in the top chamber at $t = 20$ min is chosen to be the steady state volume change in the top chamber. The flux rate through the membrane for actuation experiment is few nanoliters through an area of one cm^2 per microgram of SUT4 in the membrane. The applied chemical energy is spent in deforming the coverplate and hence the amount of fluid expanding against the pressure in the top chamber is much smaller when compared with transport experiments. The computed volume change from experimental data for the second prototype actuator is given in Table 4.3. The fluid transported into the top chamber in the actuator is due to the cotransporter protein and hence the four-state, symmetric, simplified model presented in Chapter 2 can be applied to the flux rate through the membrane in actuation experiments. The rate constants can be obtained from a reciprocal plot of the flux rate through the membrane and applied sucrose concentration

$$\dot{\phi}_s = (\dot{\phi}_s)_{\max} \left(\frac{c_1^s}{c_1^s + K} \right)$$

The flux rate terms $\dot{\phi}$ are represented in μl/(μg.cm^2.min) and the concentration terms are represented in mM. The reciprocal plot for actuation data for the two actuator prototypes are shown in Figure 4.10. The experimental data is available for the polycarbonate substrate

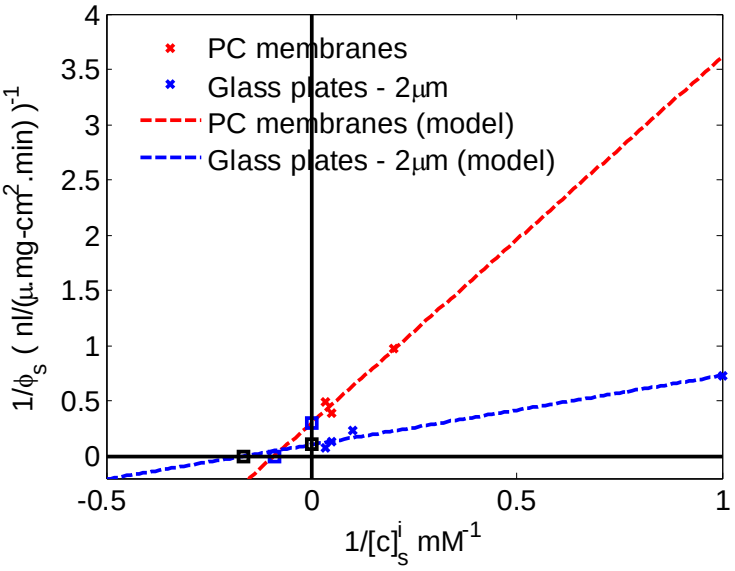

Figure 4.10: Reciprocal plot from concentration and volumetric flux obtained from actuation data

based actuator for only three data points and have a large error margin for those available. The material constants for the membrane are not found for the first prototype and are is

computed only for the second prototype actuator. The volumetric flux from the transport experiments is compared with the flux from deformation data for the glass plate with 2 μm pores and is tabulated in Table 4.3.

Table 4.3: Volume change in the top chamber computed from transport and actuation experiments for glass plate substrate with 2μm pores

c_1^s	Transport experiment		Actuation experiment $\phi_{s\max} = 2/3 A_c \Delta x_{\text{mean}}$		
	$\phi_s\|_{\text{t=20min}}$ μl	Normalized $\dot{\phi}_s$ μl/(μg-cm^2.min)	Δx_{mean} μm	$\phi_s\|_{\text{t=20min}}$ μl	Normalized $\dot{\phi}_s$ μ l/(μg-cm^2.min)
1 mM	10	0.2	6.0	0.31	2.8 x10^{-3}
5 mM	45	0.6			
10 mM	95	0.7	18.6	0.93	4.3 x10^{-3}
20 mM	145	1.25	34.2	1.71	7.9 x10^{-3}
30 mM			62.3	3.10	14.3 x10^{-3}

The computed values of the binding constant (K) is 6.01 mM and the max flux rate through the membrane is 9.61 nl/μg.cm^2.min. It is observed that the average binding rate constant from actuation data is 6.01 mM and compares well with the value of 5.25 mM obtained from transport data. This indicate a similarity in the mechanism of sucrose transport through the membrane.

4.4 Analysis of deformation results

The deformation produced by the two prototypes cannot be compared with one another directly due to the different geometries and different amount of proteins in the membrane assembly. From the results, it is observed that the actuator prototype with glass plate as the supporting substrate is consistent in the deformation generated compared to the polycarbonate substrate based actuator. The data from the second prototype is only used for analysis in this section. Since the deformation in the actuator is due to stretching the mylar membrane, the radial strain in the coverplate accounts for the mechanical work done by the chemical gradient. The change in radius is obtained from trigonometric ratios for the membrane shown in Figure 4.11 is

$$\Delta r_c = \frac{\Delta x_{\max}}{\sin\ \theta} - r_c \tag{4.4}$$

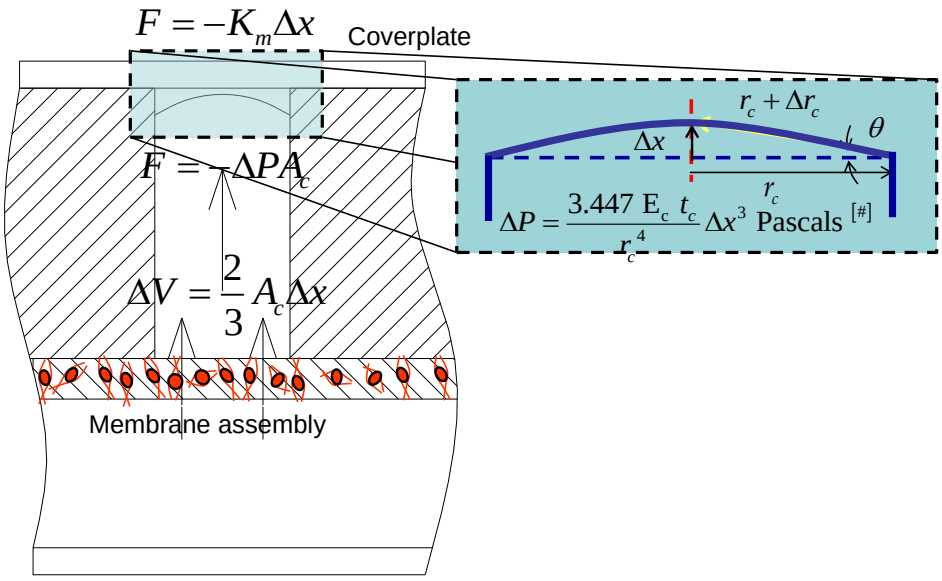

Figure 4.11: Pressure in the top chamber and force exerted by fluid transport

where $\theta = \Delta x_{\max}/r_c$. The force and radial strain for different sucrose concentrations are shown in Table 4.4.

The mechanical work ($W_m = F\Delta x$) done by the membrane assembly in extensional actuation is computed from the force exerted by the expanding fluid on the coverplate as shown in the schematic in Figure 4.11. The force due to the deforming membrane, modeled as a linear spring, is computed from pressure inside the top chamber. The uniform pressure[101] that causes a deformation(Δx) at the center of the cover plate is

$$\Delta P = \frac{3.447\,\mathrm{E_c} t_\mathrm{m}}{r_\mathrm{c}^4} \Delta x_{\max}^3\,\mathrm{Pascals} \tag{4.5}$$

where E_c is the elastic modulus, t_m is the thickness and r_c is the radius of the coverplate membrane and force on the coverplate of area A_c is given by $F = \Delta P\, A_c$. The maximum force developed by the protein based actuator is observed in the second prototype for 30 mM initial sucrose concentration. The magnitude of this force is comparable with other electroactive polymer actuator.

The energy density can be computed from the volume of the membrane assembly or from the volume of the entire top chamber. The energy density computed from using the entire volume of the top chamber will lead to a smaller number and not represent the energy conversion possible by the active ingredient. For the sake of argument, it can also stated that the energy density computed from only the active ingredient does not include

Table 4.4: Analysis of the deformation data from the two prototypes

c_1^s	Deformation Δx μm	Force mN	Radial strain ϵ_r %
1 mM	6.0	-	-
10 mM	18.6	0.02	0.001
20 mM	34.2	0.15	0.002
30 mM	62	0.89	0.008

the fluid in the top chamber required to deform the coverplate. To address both the sides, two values of the actuator energy density if computed and it is left to the audience - the scientific community at large to pick their number of choice. The work done by the actuator actuator membrane assembly on the cover plate is used to computed the energy density. The energy density can be computed from the volume of the membrane assembly or the volume of the entire top chamber. The energy density computed from using the entire volume of the top chamber will lead to a smaller number and not represent the energy conversion possible by the active ingredient. For the sake of argument, it can also stated that the energy density computed from only the active ingredient does not include the fluid in the top chamber required to deform the coverplate. To address both the sides, two values of the actuator energy density if computed and it is left to the audience - the scientific community at large to pick their number of choice. The computed values of energy density from the two volumes are given in Table 4.5. The volume of the membrane assembly is computed from the effective BLM area and the thickness of the BLM (≈7nm).

Table 4.5: Energy density of the second prototype actuator

Deformation $\Delta x_{\max}$ μm	Force F mN	Mechanical Work W Joules	Volume m^3	Energy density kJ/m^3
62	0.89	55.7x10^{-9}J	$V_m = 0.115\text{x}10^{-12}$	480
			$V_2 = 540\text{x}10^{-9}$	1x10^{-4}

The work done by the membrane in extensional actuation is computed to be few nanojoules and is a justifiably so considering the mass and volume of the BLM. Accordingly, the energy density computed from the volume of the actuator is approximately 500 kJ/m^3, comparable to that of the conducting polymer actuators shown in Figure 1.1. Another value of energy density shown in Table 4.5 shows the energy density of the membrane when

engineered into a system. This metric can be referred to as the 'packaged energy density' of the actuator. The value is smaller by a few orders when compared with the energy density of the membrane assembly. Since this value is closely related to the actuator geometry it can be improved by better packaging design and fabrication procedure.

4.5 Chapter summary

The chapter discussed fabrication, testing and characterization of a protein based actuator that works with a transmembrane proton and sucrose concentration gradient. The deformation developed in the actuator can be controlled by varying the pH or sucrose gradient. In this study, only sucrose gradient is demonstrated for controlling the force developed in the fabricated actuator. Two functional prototypes - with porous polycarbonate and lead silicate glass plate as the supporting substrate are tested. The maximum force generated by the membrane assembly on a flexible mylar membrane is computed to be approximately 1 mN. The energy density of the active material in the actuator is computed to be 500 kJ/m^3, which is comparable to that of conducting polymer actuators. Thus the actuator developed in this work can be considered at par with actuator systems that use ion transport as the driving force for actuation. The frequency of operation is limited to the diffusion process through the membrane and is not the focus of this work. This can be improved by fabricating a thin actuator and better design.

4.6 Actuation Experiments - Detailed results

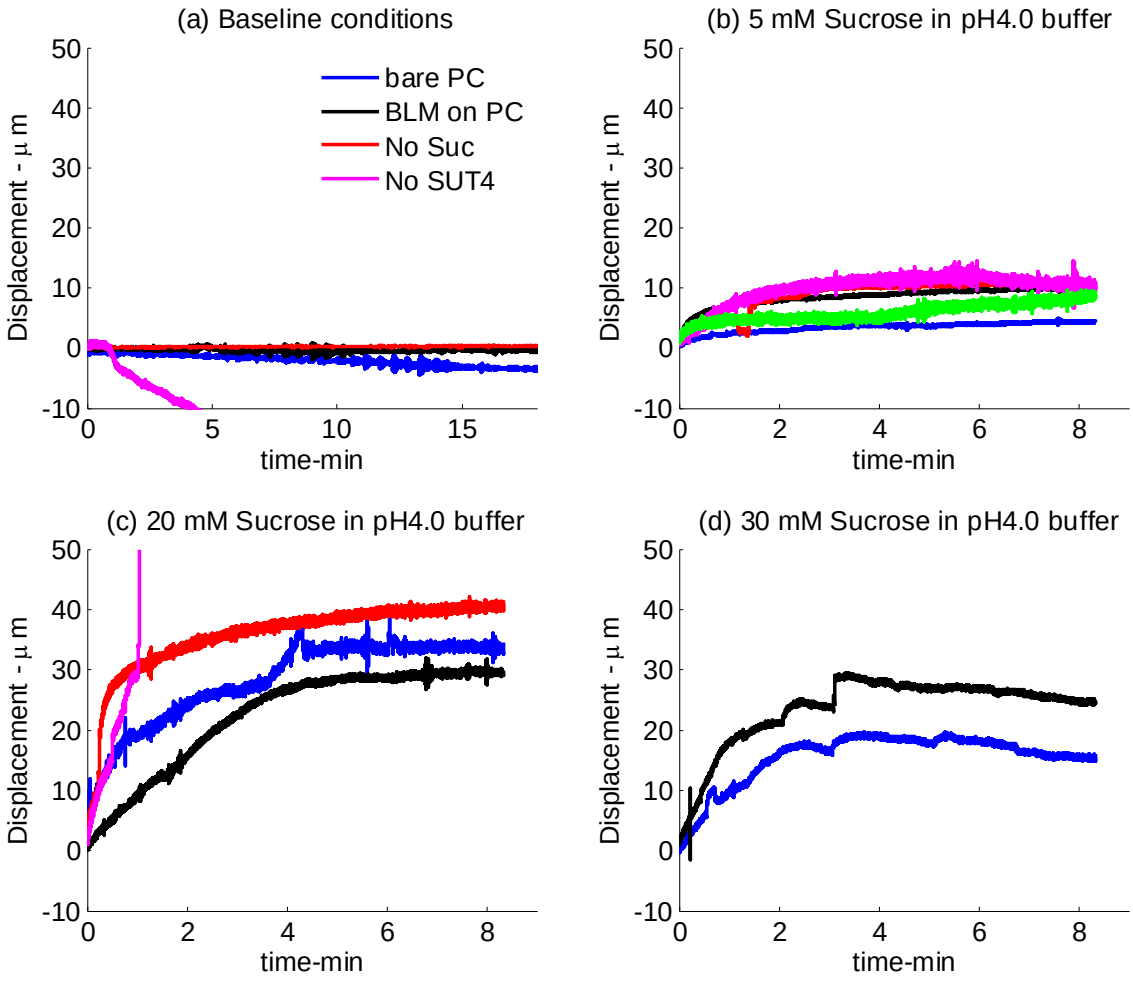

Figure 4.12: Measured deformation in the second prototype actuator for different baseline cases and for different concentrations of sucrose

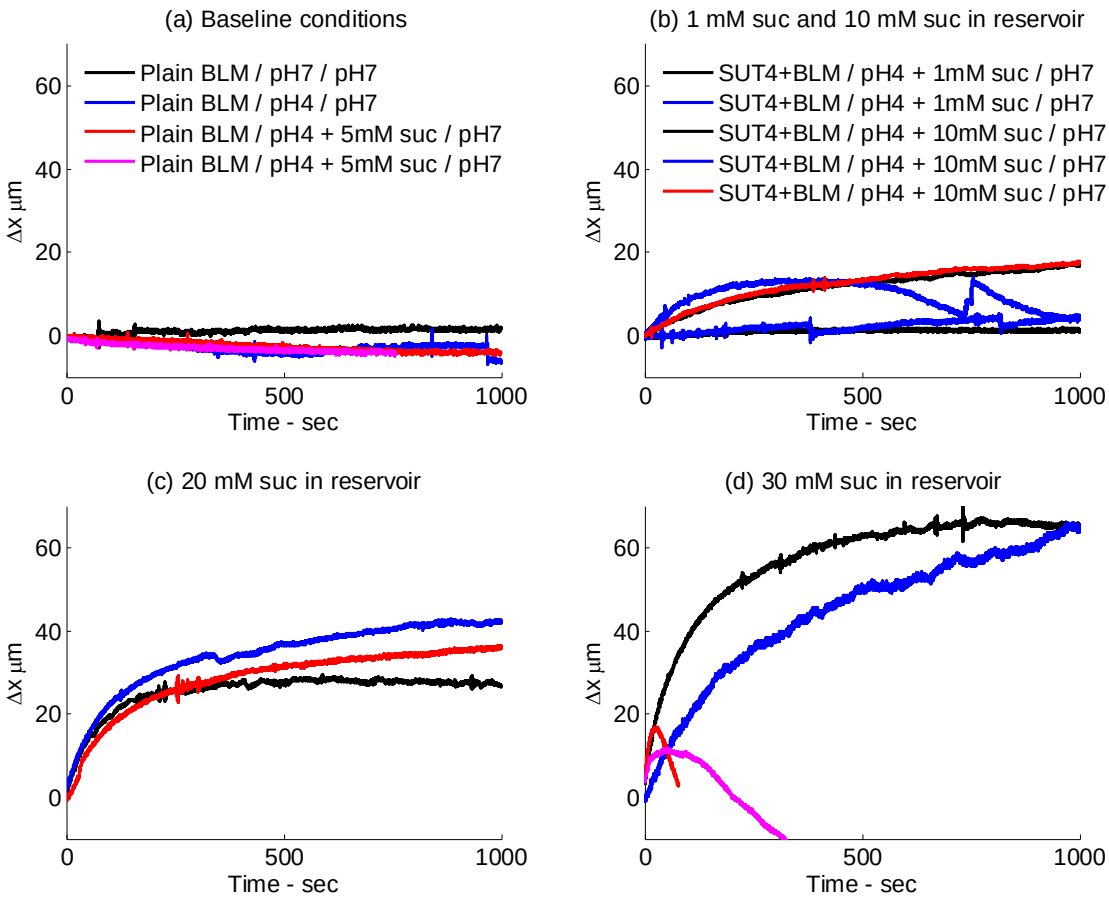

Figure 4.13: Measured deformation in the second prototype actuator for different baseline cases and for different concentrations of sucrose

Chapter 5

Chemoelectrical energy conversion

The abundance of ions in water that permeates the bulk of a living cell has helped in the evolution of plant and animal cells. The living cell has all the required tools confined within the cell membrane to develop pathways for transporting different ions in its environment. Plant and animal tissues use ion transport to transfer and convert the energy available in different sources into a biologically expendable form like sugars and ATP. The energy rich molecules synthesized in the cell are used for membrane ion transport to maintain an electrochemical gradient. This is used by biological processes for metabolism and growth.

The previous chapters focused on using fluid transport resulting from an electrochemical gradient for mechanical actuation. It is theoretically possible to convert the chemical energy available as an electrochemical gradient across a living membrane into electrical power. The work discussed in this chapter measures the power output from transporter proteins incorporated in a BLM. The protein transporter in this study is demonstrated to be a source of electrical power. The transporter used for this initial demonstration is a proton pump in the vacuolar membranes of red beets - H^+ ATPase. The V-ATPase pump is reconstituted in a lipid membrane in a engineered device. The constructional features, experimental methods and analysis of the results are presented here.

5.1 Prototype energy conversion device

The energy conversion device consists of two chambers separated by a membrane assembly (Figure 5.1) and is referred to as the BioCell. The terms used to describe the components of the BioCell are similar to the actuator. The ATPase proteins are reconstituted in a BLM

and supported on porous track-etched polycarbonate(PCTE) substrate. The BLM with ATPase transporters formed on the supporting PCTE substrate is the membrane assembly of the device. A pH7.0 buffer is added on both sides and the ATP fuel is dissolved in pH7.0 buffer in the top chamber. Hydrolysis reaction in the top chamber results in a phosphate ion and adenosine diphosphate(ADP). The energy released from the reaction provides energy for ATPase pump to move protons across the membrane assembly. The phosphate ions from the hydrolysis reaction and protons leaving the top chamber result in the production of a charge gradient across the membrane. Ion selective silver-silver chloride electrodes immersed in the buffer medium on both the sides of the membrane assembly convert the charge gradient into electrical current.

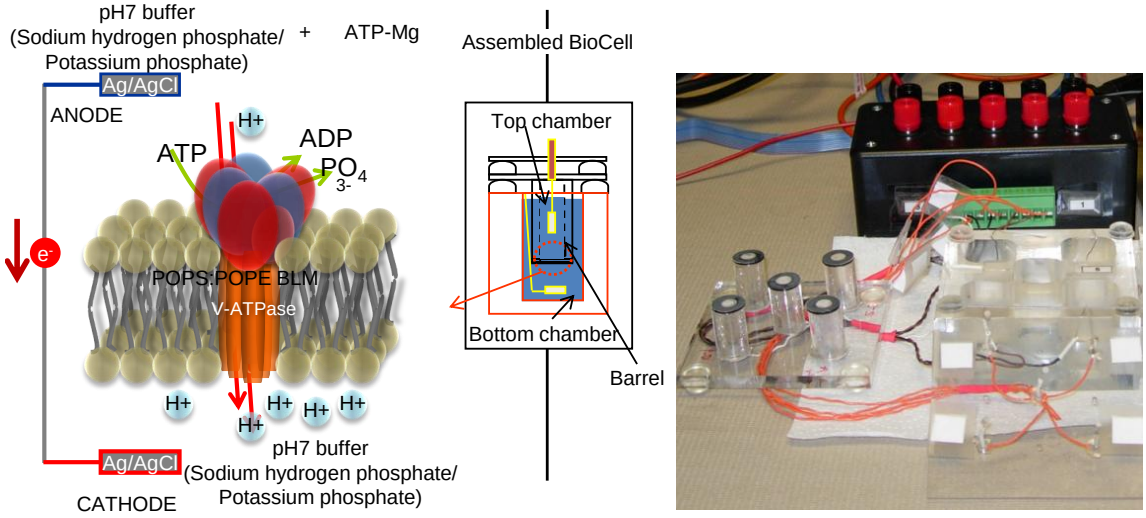

Figure 5.1: Chemoelectrical energy conversion of adenosine triphosphate using ATPase in BioCell shown with the location of the membrane assembly in the cell. The components for the prototype BioCell fabricated is shown alongside. The top chamber in the picture is shown with polycarbonate membrane attached to the bottom.

The following materials are purchased and prepared for the experimental demonstration:

- Track-etched polycarbonate membrane with 200nm pores coated with PVP, 13 mm diameter, 7-22μm thickness and 5-20% porosity. (IsoporeTM Membrane Filter, Millipore Corporation, Part No.: HTTP01300)

- Purified 1-Palmitoyl-2-Oleoyl-sn-Glycero-3-Phosphocholine (POPC) and

1-Palmitoyl-2-Oleoyl-sn-Glycero-3-[Phospho-L-Serine](POPS)
phospholipids (Avanti Polar Lipids., Inc., AL, USA). 50mg/ml of POPC and POPS (6:1 w/w) dissolved in n-decane (Sigma-Aldrich)

- Adenosine triphosphatase(ATP-ase) purified from red beets (specified by activity level, provided by Dr. Cuppoletti's lab)
- 11 mM adenosine 5'-triphosphate (ATP) - magnesium salt ($C_{10}H_{16}N_5O_{13}P_3$) (Sigma-Aldrich) in powder form dissolved in pH7.00 buffer solution (contains sodium and potassium phosphate) (VWR)
- Half-cell silver-silver chloride reference electrodes purchased from WPI Inc.

The ATPase proteins added to the BLM is the molecular pump in the BLM and ATP-magnesium salt dissolved in pH7.0 buffer is the fuel. A cell with ATPase in the BLM and ATP fuel available in the top chamber is considered a *full cell*.

5.2 Fabrication and characterization

The polycarbonate membrane (with hydrophilic PVP coating) is attached to the bottom surface of an acrylic barrel which forms the top chamber(Figure 5.1). Equal amounts (15μl) of the lipids and transporter proteins are deposited successively using a micropipette onto the substrate in the barrel bottom. The porous substrate and the BLM formed across the pores creates a physical barrier between the top and bottom chambers. The bottom chamber is filled with 7 ml of pH7.0 buffer and 0.5 ml of 11 mM ATP in pH7 buffer is added to the top chamber. Half-cell reference electrodes (silver-silver chloride) are placed in each of the two reservoirs to conduct electrical charges resulting from the biochemical reaction.

Electrical impedance measurements on complete and partial BioCell assemblies are performed using an HP 4192A impedance analyzer. The leads of the half-cell reference electrodes are connected to the impedance analyzer and the modified membrane system is excited with a 50mV (AC) signal at frequencies from 5Hz to 1MHz. The real and imaginary components of the impedance data are used to calculate the corresponding magnitude and phase of the impedance measured between the two half-cells. The presence of a BLM on the porous polycarbonate substrate is confirmed by comparing the impedance measured (5 Hz -

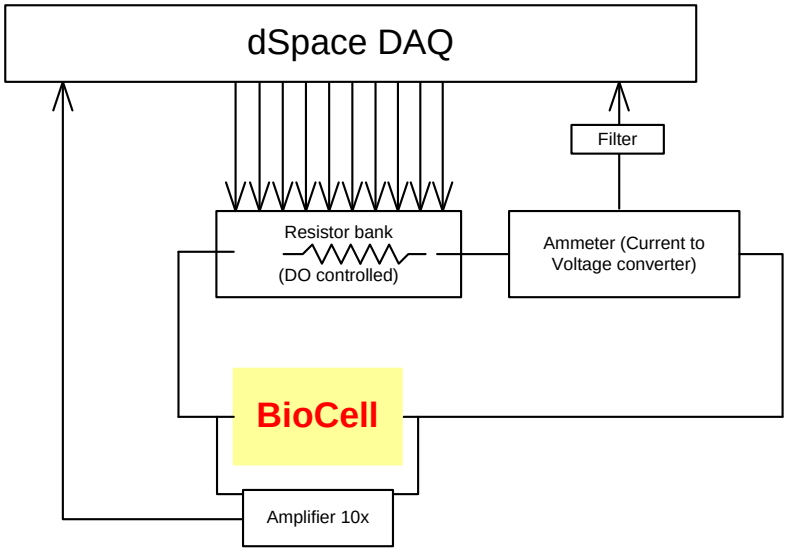

Figure 5.2: Experimental setup - Electrical load analysis of BioCell

1 MHz for a 50 mV test signal) on the porous substrate with and without the phospholipids. The impedance of the porous polycarbonate substrate is found to be 800 - 1000 Ω at 5 Hz without the lipids and with the lipids it is found to be above 100 kΩ. A stable value of around 100 kΩ for impedance measured across the substrate indicated the formation of a BLM in the pores[76, 91].

The power output of the BioCell is characterized by connecting the electrodes to different load resistors in the circuit shown in Figure 5.2. The current through the circuit is measured with a current-sensing op-amp circuit. The cell voltage and the voltage signal, proportional to circuit current from the current-sensing circuit are recorded using an 8-channel dSpace CP1104 controller board. Digital I/O channels on the dSpace board triggered relay switches for turning on (and off) each resistive load. Power characterization loading cycles consisted of alternating 1-minute sourcing intervals and 2-minute open-circuit charging periods.

5.3 Cell configuration

A series of electrical impedance measurements are performed to understand the role of each component of the BioCell. The first series of experiments are performed on an aqueous solution of pH7.0 buffer with two Ag/AgCl electrodes placed in the solution. The electrical

impedance of the buffer solution is shown in Figure 5.3. The impedance exhibits a frequency dependence that is characteristic of a resistor in series with a resistor-capacitor network. The resistance of the solution is placed in series with a parallel resistor-capacitor network that models the interfacial properties of the electrode. The experimental results demonstrate that the resistance of the solution is approximately 150 Ω. The resistor-capacitor network that models the interfacial properties of the electrodes have a resistance and capacitance of 1 kΩ and 15 μF, respectively. A second set of experiments are performed to determine the electrical properties of the porous polycarbonate membrane that separates the chambers. The characteristics of the impedance data are similar to the case without the polycarbonate membrane. A curve fit of the impedance measurement allows us to separate the properties of the porous membrane with that of the solution and electrodes. The additional resistance and capacitance associated with the polycarbonate membrane are approximately 1.3 kΩ and 300 pF, respectively.

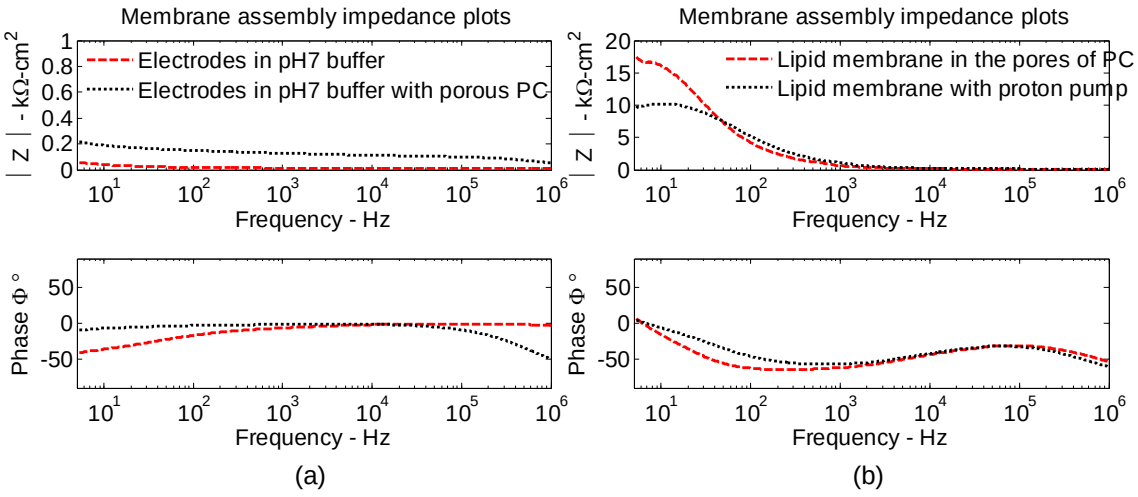

Figure 5.3: Plot (a): Impedance data measured using Ag/AgCl electrodes across pH7 buffer, pH7 buffer with polycarbonate membrane with 200 nm pores and 5-20% porosity, pH7 buffer with polycarbonate membrane carrying BLM and pH7 buffer with polycarbonate membrane carrying BLM reconstituted with ATPase proteins. Plot (b):Equivalent electrical circuit for the different components in the cell as interpreted from the impedance data

The third component of the BioCell is the bilayer membrane that is reconstituted on the porous polycarbonate substrate. Electrical impedance analysis of the cell with a reconstituted BLM on the substrate demonstrates that the low-frequency impedance of the

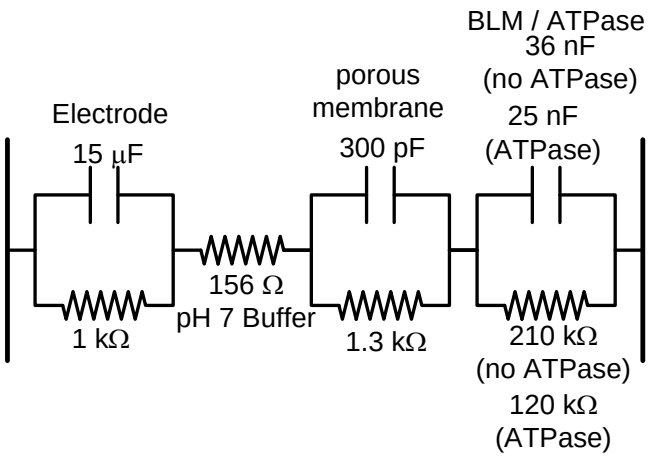

Figure 5.4: Equivalent electrical circuit for the different components in the cell as interpreted from the impedance data

cell increased from approximately 1 kΩ to almost 200 kΩ. The increase in impedance is due to the sealing properties of the BLM over the porous substrate. The electrical properties of the BLM membrane are added to the impedance model as shown in Figure 5.4. There are measurable variations in the electrical properties depending on the quality of the bilayer formation, but generally the values of the resistance lie in the 100-300 kΩ range and the values of the capacitance are on the order of 10-50 nF.

The final component of the BioCell are the ATPase transporters that insert into the BLM to form the conductive path for electrical power generation. Impedance analysis of the cell with ATPase in the BLM demonstrate a reduction in the membrane-BLM resistance and a variation in the capacitance. The reduction in the membrane-BLM resistance is consistent with the notion that the transporters are forming conductive pathways through the BLM. Typically a reduction by a factor of two in the membrane-BLM resistance is observed after the insertion of the ATPase into the BLM.

A network model for the complete BioCell is shown in Figure 5.4. The resistance and capacitance values of the various components are listed. The only variation in the network model is the presence or absence of ATPase in the BLM. This is shown in Figure 5.4 as a variable resistance and capacitance.

5.4 Baseline Power measurements

A set of control experiments starting with brand new silver-silver chloride pellet electrodes are performed. The pair is checked for factory calibration of zero millivolts(≈180 μV) in 0.1 M NaCl solution and washed with deionized water. The washed pair is then kept in pH7.0 buffer for 30 minutes and the potential difference between the electrodes is recorded. There is no potential difference observed between the pair and correspondingly zero current is measured in short circuit. These electrodes are washed again and used in a full cell. The electrodes are washed with deionized water to prevent the phosphate ions from the hydrolysis reaction accumulating and forming a phosphate salt in the high surface area interface between the electrolyte and electrode pellets.

The cell voltage for the trial shown in Figure 5.5 increased and stabilized at 94 mV in about 5 minutes. The potential difference dropped under load and returned back to the same value on removing the load as shown in Figure 5.5. The recharging ability of the full cell lasted for a few hours in all of the trials.

A set of electrical power analysis experiments are done with the electrodes in pH7.0 buffer to estimate the background current and power in the system on a used electrode. The baseline power analyses are conducted with the following configurations:

- Electrodes in pH7.0 buffer
- Electrodes in pH7.0 buffer on either side of the BLM supported on porous polycarbonate substrate
- Electrodes in pH7.0 and ATP in pH7.0 on different sides of the BLM supported on porous polycarbonate substrate

The first baseline measurement is performed to measure the background current due to the electrodes placed in pH7.0 buffer. The last two baseline experiments are done to quantify the current due to local charge separation measured ATPase in the membrane assembly. The potential difference between a pair of electrodes across a plain BLM drifted for 10-15 minutes before settling at value between 25 and 45 mV. The power sourced through an electrical load between new electrodes across the BLM on connecting an electrical load is less than 10nW . On an electrode that has been used in full cell, we observed that the potential

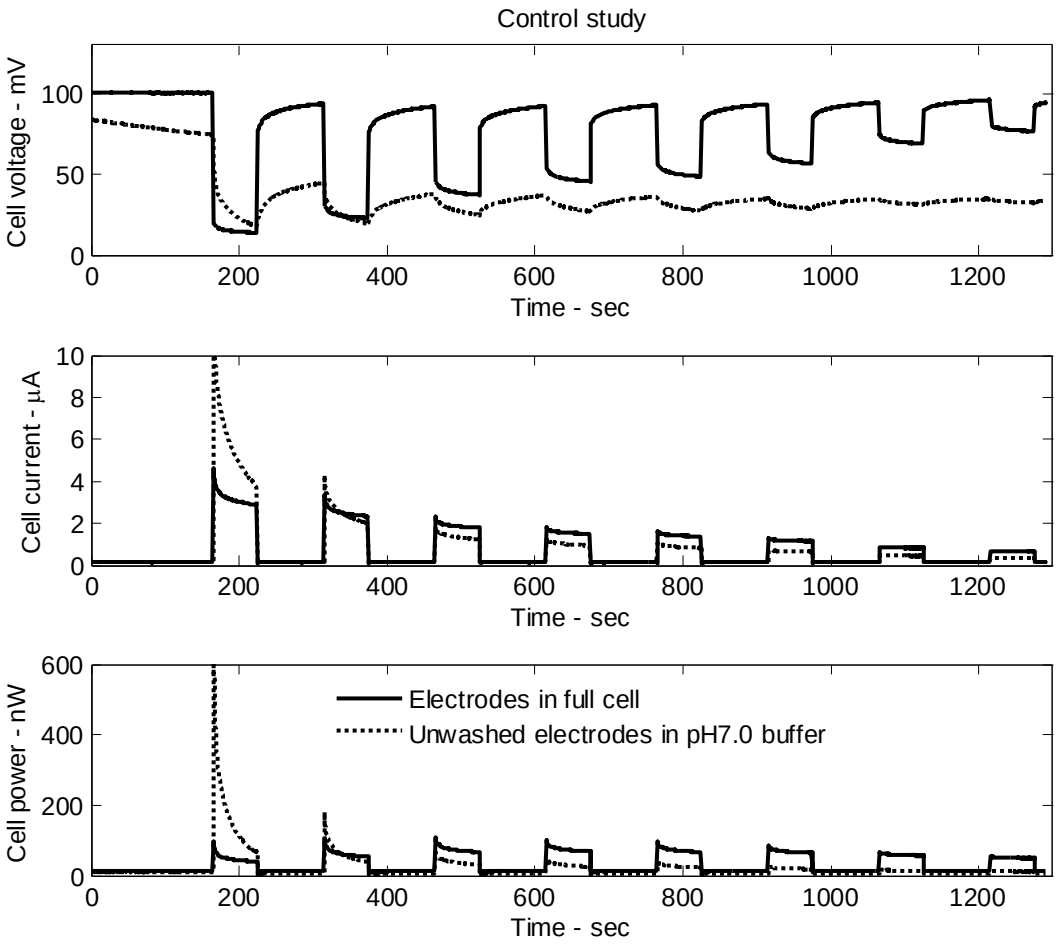

Figure 5.5: Measurement of power output for different loads applied in the following order - 4.7 kΩ, 10 kΩ, 22 kΩ, 33 kΩ,39 kΩ, 55 kΩ, 100 kΩ, 150 kΩ. shows the VI behavior under different resistive loads of a full cell compared with that of the same electrode removed from the cell and kept in pH7.0 buffer.

difference drops drastically when suspended in pH7 buffer after the experiment and the charge accumulated due to the biochemical reaction drains very quickly on connecting a resistor as shown in Figure 5.5. This potential decreases to 20-25 millivolts on storing for 30-45 minutes in pH7.0 buffer or in 0.1 M NaCl. Representative baseline measurements shown in the power characterization plot in Figure 5.7 are done between to trials to ensure that the electrodes had considerably lower charge accumulated from the previous run. On all the baseline curves, it is observed that the cell current is less than 0.5 μA and the cell voltage dropped appreciably from its open-circuit value.

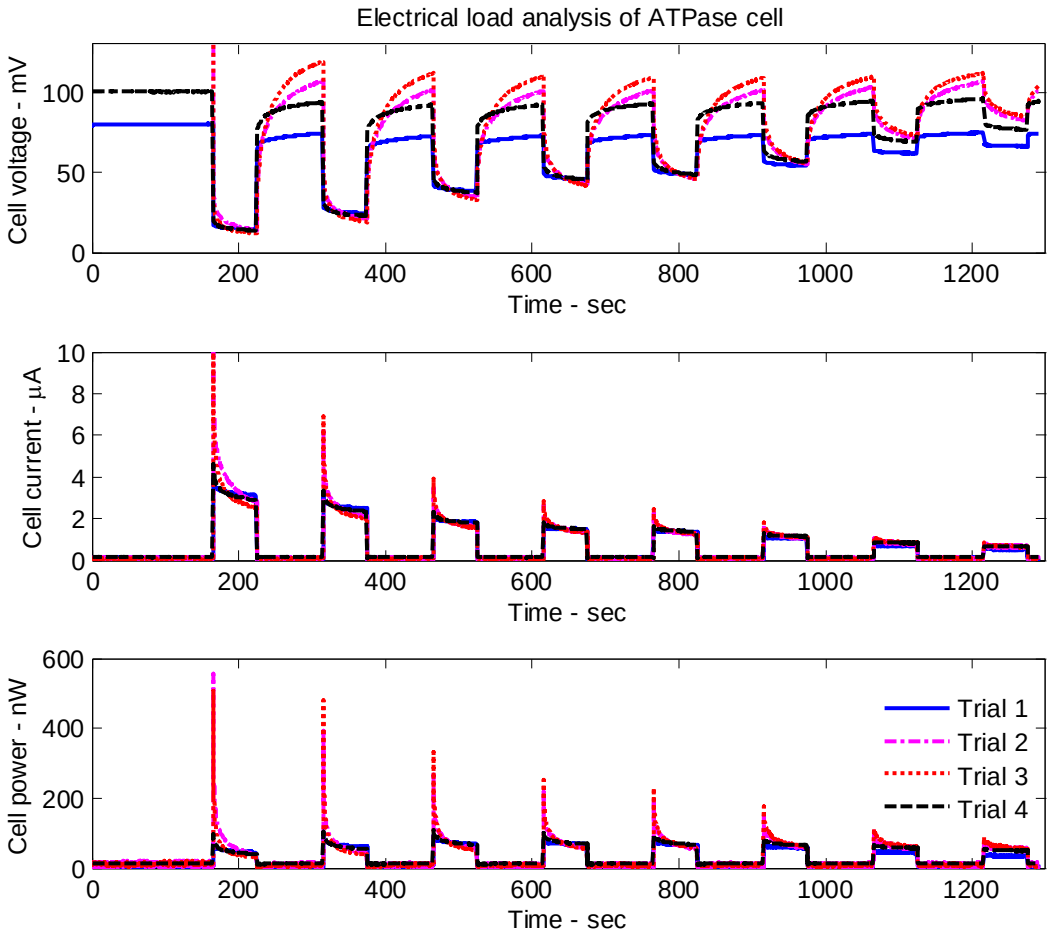

Figure 5.6: Measurement of power output for different loads applied in the following order - 4.7 kΩ, 10 kΩ, 22 kΩ, 33 kΩ,39 kΩ, 55 kΩ, 100 kΩ, 150 kΩ from different trials.

5.5 Power characterization of a full cell

Each full cell is reconstituted and allowed to reach its resting open circuit voltage (OCV). The resting OCV for a single cell with 10 μl of lipids is found to be between 80 and 90 mV for all trials. It can be observed from Figure 5.7 that the OCV is different for each of the reported trials. From our experiments in assembling a BioCell, we have observed this to be dependent on the quantity of the lipids added to the substrates. One of the reasons for the difference could be the formation of multiple bilayers in some of the pores which is an analogue of cells in series.

The current-voltage output measured on a single cell under load is shown in Figure

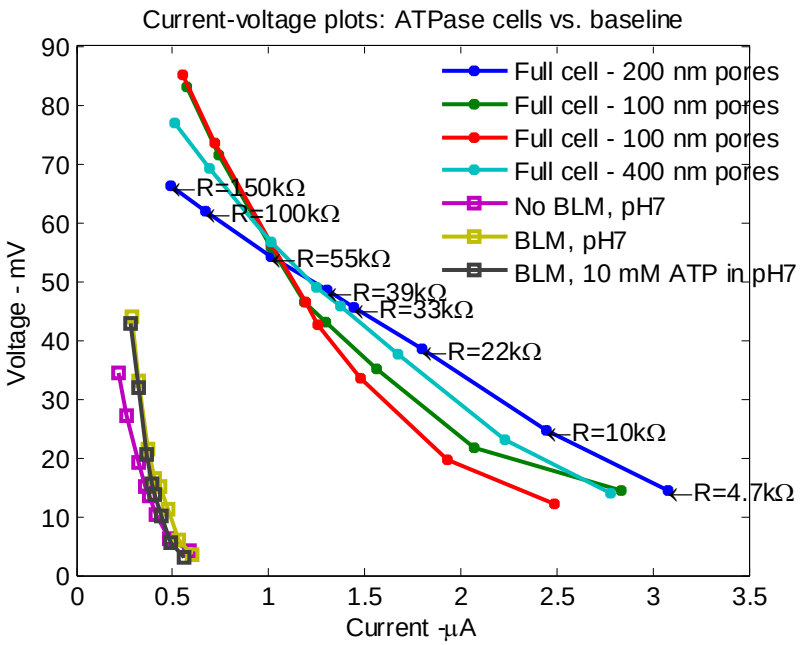

Figure 5.7: Power characterization plots. Current-voltage characteristics of the BioCell for different electrical loads compared with baseline data.

5.7 and the computed electrical power at the applied load is shown in Figure 5.8. The values reported in this plot are steady state values taken from plots similar to the ones shown in Figure 5.6. The plot in Figure 5.7 shows that the full cell is able to maintain a higher trans-membrane potential and generate higher current under load than the baseline cells. This corresponds to the higher power shown in Figure 5.8 compared with the baseline data. The higher power output from the cell is attributed to the biochemical reaction. It can be interpreted from the current-voltage characteristics shown in Figure 5.8 that a full cell behaves like a constant current power source with an internal resistance. The slope of the current-voltage curve is an estimate of the internal resistance and varies between 22 and 39 kΩ. It is reasonable to believe that the current recorded by the system is a combination of the electrons released by the phosphate ions due to ATP hydrolysis and the proton current through the medium. The SEM images and EDS data shown in Figures 5.10 and 5.11 of the electrodes show a definite presence of phosphorus in a washed electrode used in the biocell. This can be explained only by the formation of silver phosphate from the buffer.

In the presence of ATP in the medium, the ATPase pumps behave like a constant current power source. The schematic in Figure 5.9 shows the location of the current source in the equivalent network model postulated for the BioCell from impedance data. From the

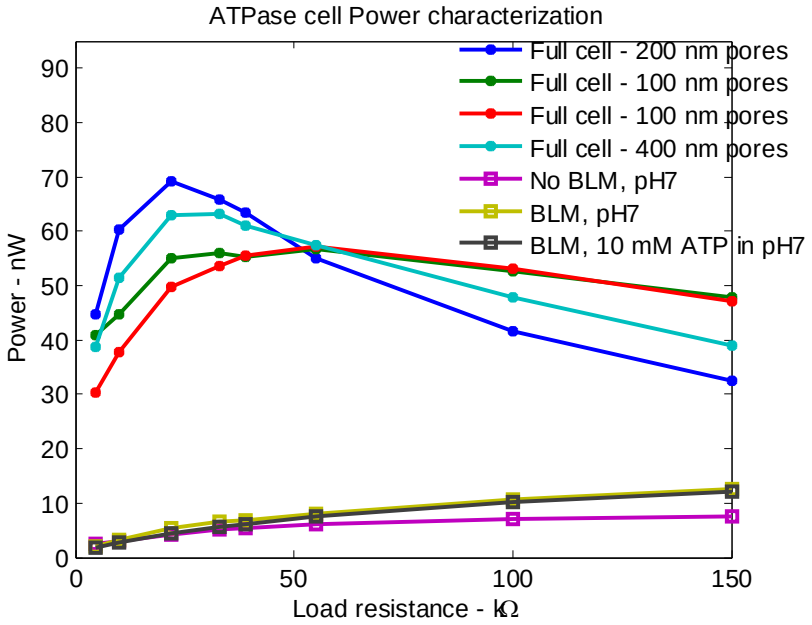

Figure 5.8: Power characterization plots. Plot of power developed by the Bio-Cell from different trials compared with baseline data

current-voltage data, the internal resistance of the cell, estimated between 22 kΩ and 39 kΩ differs from 120 kΩ resulting from the impedance data for the BLM and ATPase. It should be noted that the impedance measurements are done without ATP in the medium. The proton pumps in the absence of ATP will remain closed and hence have higher impedance. We attribute to the lower resistance from the current-voltage data to the functioning of ATPase pumps. Our assumption that the ionic conductance of the BLM with open proton pumps is higher is intuitive but has not been experimentally confirmed.

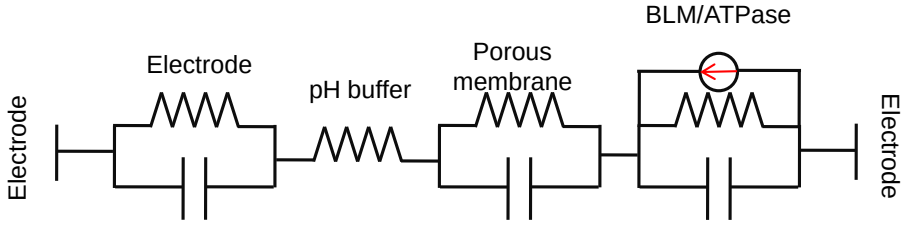

Figure 5.9: ATPase pumps in BLM as a constant power source

The fill factor for the single cell can be computed for this constant current source using the same formula used for a solar cell[69] as shown in Equation 5.1, where J_{pp}, V_{pp} are the current density, cell voltage at peak power and J_{sc}, V_{OC} are the short-circuit current

and the open-circuit voltage of the cell.

$$FF = \frac{J_{pp}V_{pp}}{J_{sc}V_{OC}} \tag{5.1}$$

The average fill factor (FF) for the working single cell is computed to be 0.35 and compares with the average values of 0.5-0.85 for a high performance solar cell [50, 83]. The fill factor can potentially be used as a performance metric to understand the effect of cell components on power output from the system. The specific power developed by a prototype single cell can be stated in terms of active membrane area and can be computed using the expression shown in Equation 5.2, where P is the peak power and A_m is the active membrane area, specified at a known quantity of ATPase reconstituted in the BLM.

$$P_{spA} = \frac{P}{A_m} \tag{5.2}$$

The polycarbonate disc measured 6.5 mm in diameter and had a porosity of 5-20%. The prototype ATPase cell with an effective BLM area of 4.15 mm^2 carrying 15 μl of ATPase proteins developed a steady state peak power output of 70 nW available as 40 mV and 1.8 μA at 22 kΩ electrical load. This corresponds to a specific power of 1.69 $\mu W/cm^2$ and a current density of 43.4 $\mu A/cm^2$. The average power output from the working cell is 62 nW available as 40 mV and 1.3 μA at 22 kΩ electrical load.

5.6 Chapter Summary

The BioCell uses biological components extracted from plant tissues reconstituted on polycarbonate substrate. The system is designed to support biochemical reaction in an artificial environment and harness the energy available from biological sources. Our results indicate that the electrical power seen in the external circuit is due to the presence of ATP in pH7 medium with ATPase reconstituted in the membrane and behaves like a constant current power source. The power available from biological sources will enable novel applications possible that are not possible earlier. This concept can also be extended to a conceptual demonstration of a device that can generate electrical power from ATP in living plants when plugged into the accessible regions of a plant without starving the host of its nutrients.

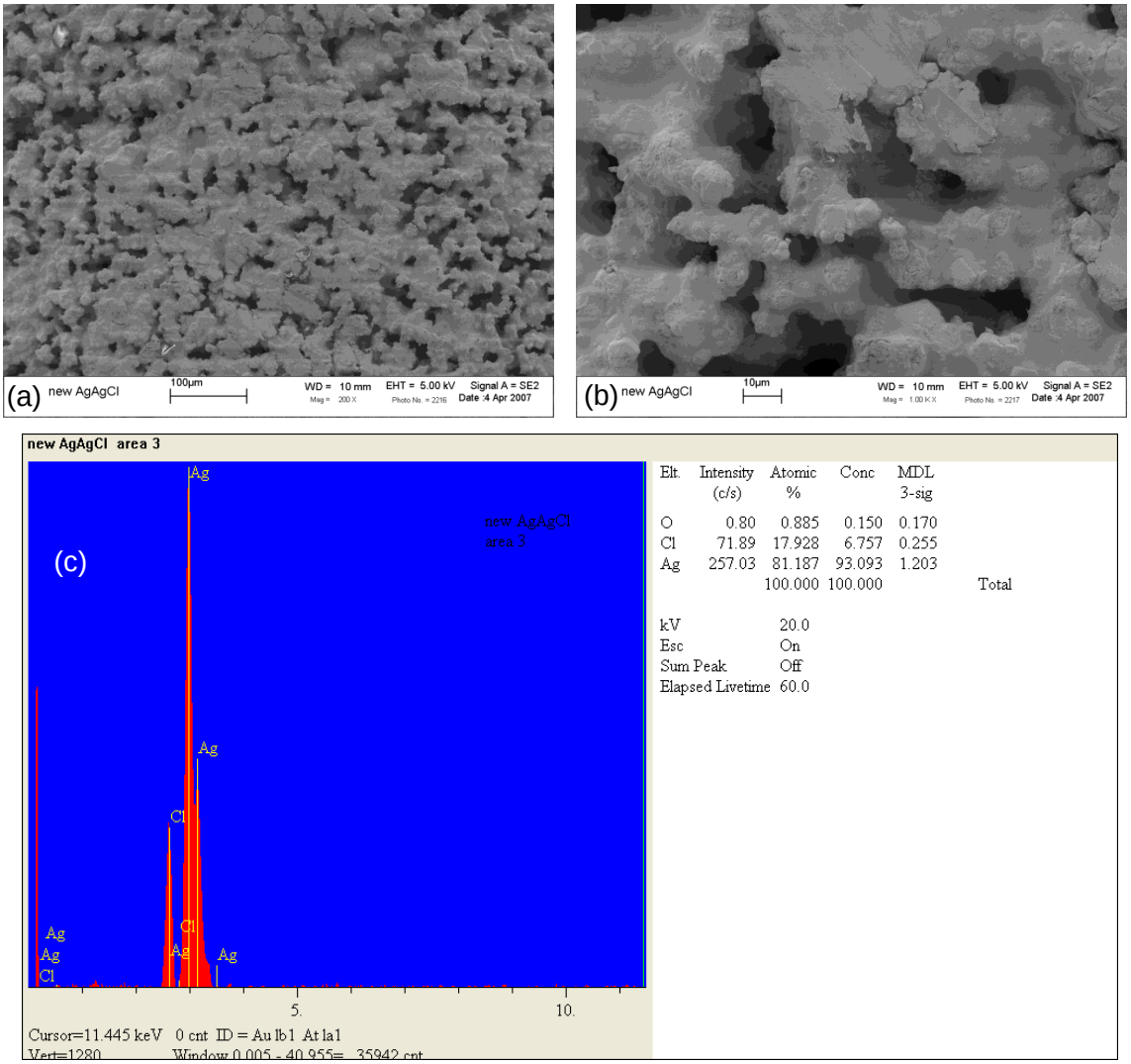

Figure 5.10: Scanning electron micrographs of new Ag/AgCl electrodes used in the BioCell for characterizing a BLM with ATPase as an electrical power source. The SEM images at 200X and at 1kX show a clear surface and the composition of the new electrodes from EDS in (c) show only Ag and Cl as the constituent elements

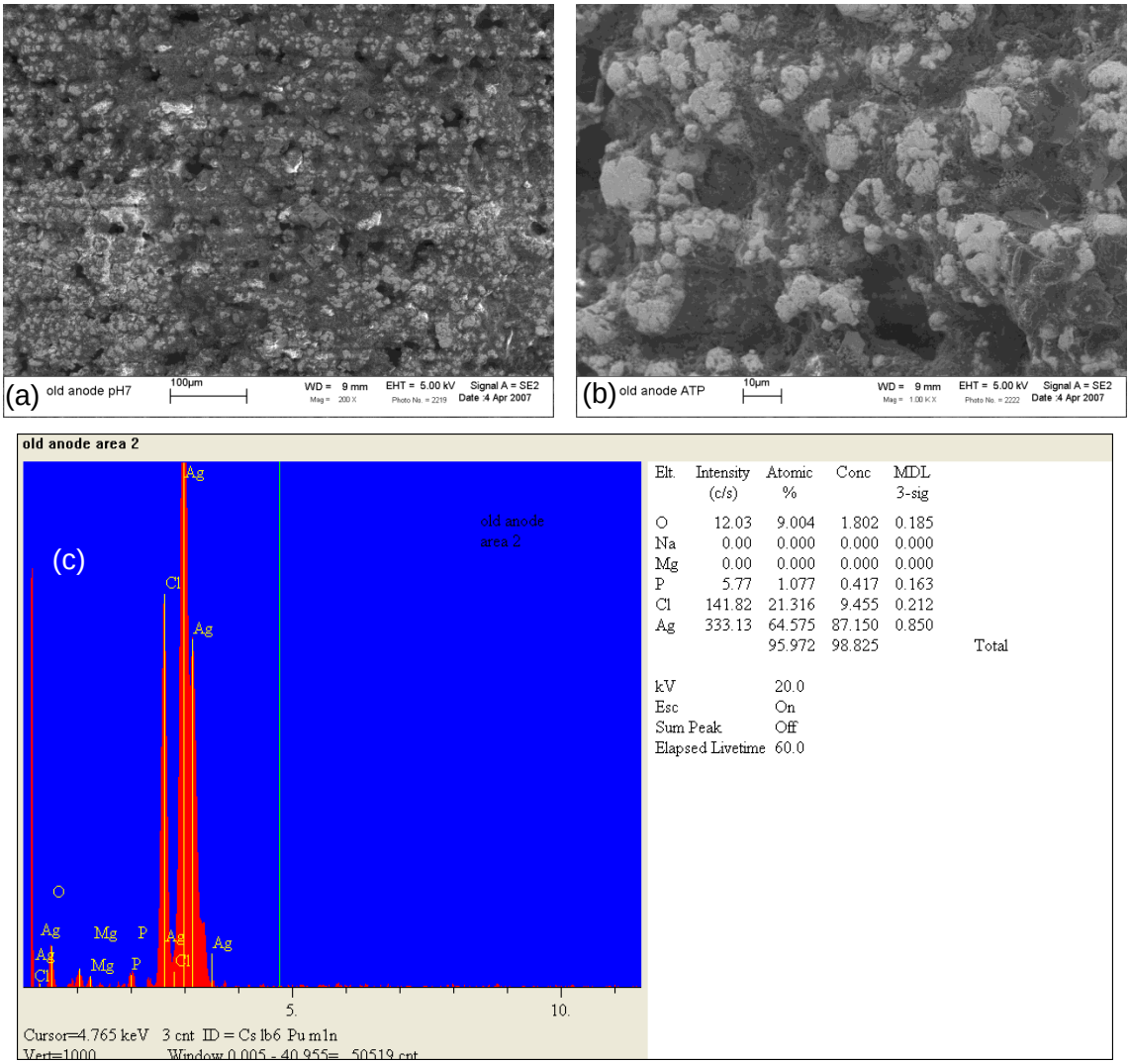

Figure 5.11: Scanning electron micrographs of old Ag/AgCl electrodes used in the BioCell for characterizing a BLM with ATPase as an electrical power source. (a) (b) The SEM images at 200 X and at 1 kX show visible degradation on surface of electrodes (c) The EDS data at the bright regions shows traces of Phosphorus and Magnesium which are introduced into the electrode surface due to ATP hydrolysis reaction

Chapter 6

Summary and Conclusion

The final chapter in this dissertation provides a synopsis of the most notable accomplishments. This is followed by significant contributions to the field of bio-inspired actuation and some future recommendations that can extend the work presented here.

6.1 Research Summary

Actuator materials under research and development are restricted to metals and polymers. Naturally occurring biological systems generate strain and motion and function as actuators. Inspired by bio-motion, this work expands the material and mechanism choice available to build an actuator and an actuation system. The ion transporter proteins extracted from plant cell membranes are incorporated in a synthetic substrate to transport fluid across a membrane barrier. The proteins are provided for this work by Dr. Cuppoletti's group at University of Cincinnati. The chemical stimulus used in the actuator to generate deformation is a proton and sucrose gradient applied across the membrane assembly. The SUT4 cotransporter used in this work is a proton sucrose symporter with a low affinity and high throughput for sucrose transport. The protein based membrane is used as an actuator for the first time to demonstrate deformation. The passive proton gradient applied to the SUT4 cotransporter is replaced by another protein transporter - H^+-ATPase that can generate the required transmembrane proton gradient using ATP hydrolysis. This is followed by a demonstration to use the proton pump for generating electrical power. The lab demonstration used a membrane similar to a living cell membrane to generate a membrane potential and to use it in an external electrical circuit.

6.2 Result Summary

6.2.1 Actuation experiments

The results from fabricating an actuator can be discussed under the following groups.

- **Characterizing the membrane assembly:** The membrane assembly consists of the planar BLM with protein transporters in the pores of a porous substrate. Porous polycarbonate membranes and lead silicate glass plates were used as substrates for forming the membrane assembly. with the transporters is characterized by impedance analysis. The specific impedance of the planar BLM is three orders of magnitude higher than the porous substrate. An average specific resistance of the membrane assembly is between 50-100 kΩ-cm^2. It is observed the specific resistance decreases on introducing a protein channel or a pump in the membrane. This is consistent with the presence of an ionophore in the membrane.

- **Transport properties of the membrane assembly:** The membrane assembly serves as the selectively conductive pathway for solute and fluid transport through the membrane. The SUT4 reconstituted in the membrane assembly responds to sucrose gradient in the presence of a pH gradient. The amount of fluid transported through the membrane varies with the sucrose concentration and the membranes balances the electrochemical proton gradient with sucrose potential. A fluid level meter is built to measure the fluid flux through the membrane that results from proton-sucrose cotransport. The amount of fluid transported is dependent on the amount of transporters in the membrane assembly. The flux rate is observed to maximize between 10-20 mM initial sucrose concentration. The symmetric, simplified four state carrier model is adopted to represent the flux through the membrane assembly. This model is applied to analyze the sensitivity of the membrane to sucrose concentration. The average maximum steady state flux observed is found to be 22 μl/(μg.cm^2) at 20 mM initial sucrose concentration with an initial flux rate of 1.25 μl/(μg.cm^2.min). The flux data follows the Michaelis-Menton relation for facilitated diffusion through the membrane assembly with a half-saturation constant of 4.9 mM. This is the first demonstration of a fluid transport through the protein transporter with the intent of using it in an actuator. The pH gradient required to drive fluid transport through

the membrane assembly is replaced by H-ATPase where the hydrolysis of ATP provides the required energy for driving fluid transport through the membrane. The acidification reaction due to ATPase triggers SUT4 and generates fluid flux through the membrane assembly. The effect of ATPase is analyzed by varying the amount of enzyme in the membrane and results indicate that the flux increases through the membrane assembly due to higher concentration of the enzyme.

- **Protein based actuator:** The characterization experiments on the membrane assembly demonstrated the usefulness of the transporter to generate fluid flux for an applied chemical potential. Two prototype actuators are built to demonstrate actuation using the fluid transport through the membrane assembly with proteins. The membrane assembly on the first prototype was supported on a porous polycarbonate substrate. The results demonstrate that the sucrose concentration is a control variable for the deformation produced in the actuator. The results were not evenly distributed in the first prototype, but yet demonstrated that actuation using transport through biological transporter is possible. The second prototype is fabricated with a membrane assembly supported on porous lead silicate glass. The results from the second prototype shows a linear relation between the deformation produced in the actuator to sucrose concentration. Maximum steady state deformation of 60-90 μm are achievable at 30 mM initial sucrose on one side of the membrane.

6.2.2 Chemoelectrical energy conversion

The H^+-ATPase enzyme is a proton pump that can generate an electrochemical potential across the membrane. The electrochemical gradient generated from the biochemical reaction using a ubiquitously available fuel source can be used to generate electrical power and possibly power low power electronic devices. In pursuit of understanding the engineering possibilities for the electrochemical gradient, a device called a Biocell is fabricated. The Biocell has a planar BLM with H^+-ATPase pumps supported on a porous polycarbonate membrane. The silver-silver chloride electrodes on both the sides of the membrane is used to transfer the proton gradient to an external circuit . Current-voltage characterization experiments reveal that the the single cell behaves like a constant current power source with an internal resistance of 22 kΩ-50 kΩ. The power density of the membrane is 2

μW/cm^2 which comparable to other power scavenging devices. The single cell arrangement also shows the possibility to stack the cells in series and in parallel and possibly power an electronic device.

6.3 Contributions

The actuator developed in this work will be the first of its kind to use a protein transporter to generate fluid flux and deform a flexible wall of a constrained chamber. The following is the list of my contributions:

- Fluid transport properties of a membrane assembly with SUT4 due to sucrose cotransport has been characterized. The transport experiments in a membrane assembly for different sucrose concentrations provided the characterization curves for fluid transport through the membrane assembly.

- A prototype actuator that uses SUT4 as the gating device for chemomechanical energy conversion has been fabricated. The deformation experiments using the membrane assembly with SUT4 showed that the deformation produced in the actuator can be controlled by changing the sucrose concentration in the system.

- Characterizing fluid transport through a membrane assembly powered by ATP hydrolysis reaction with the intent for using it in an actuator is a third major contribution. This demonstrates the use of H^+-ATPase protein to energize a cotransporter in the membrane assembly of an actuator using a biological fuel.

- Chemoelectrical energy conversion using a protein to generate electrical power starting from ATP as an alternative power source is proposed. The single cell has a measurable cell voltage and current at a power density of 2 μW/cm^2. Multiple single cells can be stacked in series and parallel to generate higher currents and voltage. This breaks a new ground in using the chemical energy available in living cells to generate electrical power.

6.4 Future directions

The work summarized in this document can be considered a starting point for a variety of project ideas. The very important and revolutionary ideas are summarized below.

- **Protein based actuator:**

  ▷ The protein transporter used in this work is a proton sucrose cotransporter. The proton motive force can be substituted by an electrical gradient to trigger the transporter to transport fluid through the membrane assembly. This will enable electrically modulating the fluid transported through the membrane and provide real-time control of the deformation in the actuator.

  ▷ Other protein transporters that can move fluid through the membrane assembly should be tested and compared with the response from SUT4. My recommendation will be a voltage controlled aquaporin that can move large quantities of water for an electrical signal applied to the membrane. This will be a hydraulic actuator in the true sense of the word as the protein transporter can directly control the amount of water transported through the membrane. That will be a direct one step method to generate fluid flux over using sucrose as an intermediate molecule for driving osmotic flux. The purity percentage of SUT4 can be improved to generate higher flux through the membrane that will generate higher strain in the actuator.

- **Biocell:**

  There are no bounds for what the engineering community can do once this technology matures into a product. The first project for a power scavenging concept like the biocell will be to design a device that generates electrical power from living plants without killing the host. A demonstration on using an ATPase pump with a cotransporter can be used to simultaneously quantify the electrical gradient developed and sucrose flux through the membrane. Thus a balance can be obtained for the concentration of ATPase and other transporters in the membrane to engineer a plant cell that can sustain the additional power sourced from the ATP synthesized within the cell. Using inputs from the work on plant kingdom, the device can be modified to work using animals as host for generating electrical power.

Bibliography

[1] Akala, E. O., Kopeckova, P., and Kopecek, J. (1998). Novel ph-sensitive hydrogels with adjustable swelling kinetics. *Biomaterials*, 19(11-12):1037–1047.

[2] Akle, B., Bennett, M., and Leo, D. J. (2006). Development of a novel electrochemically active membrane and 'smart' material based vibration sensor/damper. *Sensors and Actuators A: Physical*, 126(1):173–181.

[3] Angelova, M. I. and Dimitrov, D. S. (1986). Liposome electroformation. *Faraday Discuss. Chem. Soc.*, 81:303 – 311.

[4] Bangham, A. D. (1995). Surrogate cells or trojan horses. the discovery of liposomes. *BioEssays*, 17(12):1521–1878.

[5] Bangham, A. D., Hill, M. W., and Miller, N. C. A. (1974). *Methods in membrane biology - Preparation and use of liposomes as models of biological membranes, Ed Korn (ed.,)*, volume 1. Plenum Press, New York.

[6] Batalin, A. (1877). Mechanik der bewegung der insektfressenden pflanzen (mechanics of the movements of carnivorous plants). *Flora*, 60:145–154.

[7] Bennett, M. (2005). *Electromechanical Transduction in Ionic LiquidSwollen Nafion*$^{\mathrm{T}}$M *Membranes*. PhD thesis, Virginia Polytechnic Institute and State University, Blacksburg, VA - 24061, USA.

[8] Bertoncello, P., Nicolini, D., Paternolli, C., Bavastrello, V., and Nicolini, C. (2003). Bacteriorhodopsin-based langmuirschaefer films for solar energy capture. *IEEE Tansactions on Nanobioscience*, 2(2):124–132.

[9] Beuchler, M. A. (2005). Variational modeling of ionic polymer-based structures. Master's thesis, Virginia Polytechnic Institute and State University, Blacksburg, VA - 24061, USA.

[10] Beyenbach, K. W. and Wieczorek, H. (2006). Review: The v-type h^+ atpase: Molecular structure and function, physiological roles and regulation. *The Journal of Experimental Biology*, 209:577–589.

[11] Briskin, D. P. and Reynolds-Niesman, I. (1991). Determination of h+/atp stoichiometry for the plasma membrane h -atpase from red beet (beta vulgaris l.) storage tissue. *Plant Physiology*, 95:242–250.

[12] Britton, H. G. (1964). Permeability of the human red cell to labelled glucose. *J Physiol*, 170(1):1–20.

[13] Brown, W. H. (1916). The mechanism of movement and the duration of the effect of stimulation in the leaves of dionaea. *American Journal of Botany*, 3(2):68–90.

[14] Bush, D. R. (1989). Proton-coupled sucrose transport in plasmalemma vesicles isolated from sugar beet (beta vulgaris l. cv great western) leaves. *Plant Physiol.*, 89(4):1318–1323.

[15] Carpaneto, A., Geiger, D., Bamberg, E., Sauer, N., Fromm, J., and Hedrich, R. (2005). Phloem-localized, proton-coupled sucrose carrier zmsut1 mediates sucrose efflux under the control of the sucrose gradient and the proton motive force. *J. Biol. Chem.*, 280(22):21437–21443.

[16] Cheng, Y., Ogier, S. D., Bushby, R. J., and Evans, S. D. (2000). Discrete membrane arrays. *Reviews in Molecular Biotechnology*, 74:159–74.

[17] Cohen, F., Zimmerberg, J., and Finkelstein, A. (1980). Fusion of phospholipid vesicles with planar phospholipid bilayer membranes. ii. incorporation of a vesicular membrane marker into the planar membrane. *J. Gen. Physiol.*, 75(3):251–270.

[18] Crank, J. (1975). *The Mathematics of Diffusion*. Academic Press.

[19] Darwin, C. (1875). *Insectivorous Plants*. Murray Publishers, London.

[20] Delrot, S., Atanassova, R., Gomes, E., and Thevenot, P. (2001). Plasma membrane transporters: A machinery for uptake of organic solutes and stress resistance. *Plant Science*, 161:391–404.

[21] Dhoke.M.A, Ladha.P.J, Boerio.F.J, Lessard.L.B, Malinowska.D.H, Cuppoletti.J, and Wieczorek.D.S (15 October 2005). Porous membranes for reconstitution of ion channels. *Biochimica et Biophysica Acta (BBA) - Biomembranes*, 1716(2):117–125.

[22] Dobereiner, H.-G. (2000). Properties of giant vesicles. *Current Opinion in Colloid and Interface Science*, 5:256–263.

[23] Drachev, L. A., Jasaitis, A., Kaulen, A. D., Kondrashin, A. A., Liberman, E. A., Nemecek, I. B., Ostroumov, S. A., Semenov, A. Y., and Skulachev, V. P. (1974/05/24). Direct measurement of electric current generation by cytochrome oxidase, h+-atpase and bacteriorhodopsin. *Nature*, 249(5455):321–324.

[24] E, M. (1930). *Die Stoffbewegungen in der Pflanze*. Verlag Gustav Fischer, Jena, Germany.

[25] Elliott, W. H. and Elliott, D. C. (1997). *Biochemistry and Molecular Biology*. Oxford University Press, New York, New York, USA.

[26] Farinholt, K. (2005). *Modeling and Characterization of Ionic Polymer Transducers for Sensing and Actuation*. PhD thesis, Virginia Polytechnic Institute and State University, Blacksburg, VA - 24061, USA.

[27] Forterre, Y., Skotheim, J. M., Dumais, J., and Mahadevan, L. (2005). How the venus flytrap snaps. *Nature*, 433:421–425.

[28] Friedman, M. H. (1986). *Principles and Models of Biological Transport*. Springer-Verlag Berlin, Heidelberg, Germany.

[29] Fujiwara, H., Fujihara, M., Koyama, T., and Ishiwata, T. (2004). New aspect of the spontaneous formation of a bilayer lipid membrane. In Tokuyama, M. and Oppenheim, I., editors, *Slow Dynamics in Complex Systems, 3rd International Symposium*, volume (19)3 of *American Institute of Physics*, pages 724–726.

[30] Gerenscer, G. and Stevens, B. (1994). Thermodynamics of symport and antiport catalyzed by cloned or native transporters. *J. exp. Biol.*, 196:5975.

[31] Grimnes, S. and Martinsen, O. (2000). *Bioimpedance & Bioelectricity BASICS*. Academic press.

[32] Gyftopoulos, E. P. and Berreta, G. P. (1996). *Thermodynamics: Foundations and Applications*. Macmillan Publishing Company.

[33] Hamley, I. W. (2006). *Introduction to Soft Matter: Polymers, Colloids, Amphiphiles and Liquid Crystals*. John Wiley and Sons.

[34] Hearn, E. J. (1997). *Mechanics of Materials II, Chapter 7*. Butterworth-Heinemann, Burlington, MA, USA.

[35] Heath, J. R., Ries, R. S., Choi, H., Blunck, R., and Bezanilla, F. (2004). Black lipid membranes: Visualizing the structure, dynamics and substrate dependence of membranes. *Journal of Physical Chemistry B*, 108:16040–16049.

[36] Heimburg, T. (1998). Mechanical aspects of membrane thermodynamics: Estimation of the mechanical properties of lipid membranes close to the chain melting transition from calorimetry. *Biochemica et Biophysica Acta*, 1415:147–162.

[37] Heinz, E., Geck, P., and Wilbrandt, W. (11 February 1972). Coupling in secondary active transport : Activation of transport by co-transport and/or counter-transport with the fluxes of other solutes. *Biochimica et Biophysica Acta (BBA) - Biomembranes*, 255(2):442–461.

[38] Hill, B. S. and Findlay, G. P. (1981). The power of movement in plants: The role of osmotic machines. *Quaterly Review in Biophysics*, 14(2):173–222.

[39] Ho, D., Chu, B., and Montemagno, H. L. C. D. (2004). Protein-driven energy transduction across polymeric biomembranes. *Nanotechnology*, 15:1084–1094.

[40] Hodick, D. and Sievers, A. (1989). On the mechanism of trap closure of venus flytrap (dionaea muscipula ellis). *Planta*, 179:32–42.

[41] Hopkinson, D. P., DeVita, R., and Leo, D. J. (2006). Failure pressure of bilayer lipid membranes. In *Proceedings of SPIE Conference for Smart Structures & Materials/NDE*.

[42] Huang, P., K, K. S., J, J. C., SK, S. K. M., and Scarborough, G. A. (1996). Functional expression of the cystic fibrosis transmembrane conductance regulator in yeast. *Biochim Biophys Acta*, 1281:80–90.

[43] Ide, T. and Ichikawa, T. (2005). Short communication: A novel method for artificial lipid bilayer formation. *Biosensors and Bioelectronics*, 21:672–677.

[44] Iscla, I., Levin, G., Wray, R., Reynolds, R., and Blount, P. (2004). Defining the physical gate of a mechanosensitive channel, mscl, by engineering metal-binding sites. *Biophys. J.*, 87(5):3172–3180.

[45] Iwasa, T., Tokunaga, F., and Yoshizawa, T. (1980). A new pathway in the photoreaction cycle of trans-bacteriorhodopsin and the absorption spectra of its intermediates. *European Biophysics Journal*, 6(4):253–270.

[46] Jass, J., Tjarnhage, T., and Puu, G. (2000). From liposomes to supported, planar bilayer structures on hydrophilic and hydrophobic surfaces: An atomic force microscopy study. *Biophys. J.*, 79(6):3153–3163.

[47] Katachalsky, A. and Curran, P. F. (1965). *Nonequlibrium Thermodynamics in Biophysics*. Harvard University Press.

[48] Kataoka, K., Miyazaki, H., Bunya, M., Okano, T., and Sakurai, Y. (1998). Totally synthetic polymer gels responding to external glucose concentration: Their preparation and application to on-off regulation of insulin release. *Journal of the American Chemical Society*, 120(48):12694–12695.

[49] Kedem, O. and Katchalsky, A. (1961). A physical interpretation of the phenomenological coefficients of membrane permeability. *J. Gen. Physiol.*, 45(1):143–179.

[50] Kiess, H. and Rehwald, W. (1995). On the ultimate efficiency of solar cells. *Solar Energy Materials and Solar Cells*, 38(1-4):45–55.

[51] Klausner, R. D., Kleinfeld, A., Hoover, R., and Karnovsky, M. J. (1980). Lipid membrane domains in membranes. *Journal of Biological Chemistry*, 255:1286–1295.

[52] Kothera, C. (2005). *Characterization, Modeling, and Control of the Nonlinear Actuation Response of Ionic Polymer Transducers*. PhD thesis, Virginia Polytechnic Institute and State University, Blacksburg, VA - 24061, USA.

[53] Kuhn, C. (2003). A comparison of the sucrose transporter systems of different plant species. *Plant Biology*, 5:215–232.

[54] Lanyi, J. K. (1993). Pathways of proton transfer in the light-driven pump bacteriorhodopsin. *Cellular and Molecular Life Sciences (CMLS)*, 49(6-7):514–517.

[55] Lemoine, R. and Delrot, S. (1989). Proton-motive-force-driven uptake in sugar beet plasma membrane vesicles. *FEBS Newsletters*, 249(1):129–133.

[56] Lichtner, F. T. and Williams, S. (1977). Prey capture and factors controlling trap narrowing in dionaea droseraceae. *American Journal of Botany*, 64:881–886.

[57] Lino, B., Baizabal-Aguirre, V. M., and de la Vera, L. E. G. (1998). The plasma-membrane h+-atpase from beet root is inhibited by a calcium-dependent phosphorylation. *Planta*, 204:352–359.

[58] Lodish, H., Baltimore, D., Berk, A., Zipursky, L., Matsudaira, P., and Darnell, J. (1998). *Molecular Cell Biology*. Scientific American Books, Inc., New York, New York, USA.

[59] Luecke, H., Richter, H.-T., and Lanyi, J. K. (1998). Proton transfer pathways in bacteriorhodopsin at 2.3 angstrom resolution. *Science*, 280(6-7):1934–1937.

[60] Maurel, C. and Chrispeels, M. J. (2001). Aquaporins. a molecular entry into plant water relations. *Plant Physiol.*, 125(1):135–138.

[61] Montal, M. and Mueller, P. (1972). Formation of Bimolecular Membranes from Lipid Monolayers and a Study of their Electrical Properties. *PNAS*, 69(12):3561–3566.

[62] Morillon, R., Lienard, D., Chrispeels, M. J., and Lassalles, J.-P. (2001). Rapid movements of plants organs require solute-water cotransporters or contractile proteins. *Plant Physiology*, 127(3):720–723.

[63] Mueller, P., Rudin, D. O., Tien, H. T., and Wescott, W. (1963). Methods for the formation of single bimolecular lipid membranes in aqueous solutions. In *Journal of Physical Chemistry*, volume 67, pages 534–535.

[64] Mukherjee, S. and Maxfield, F. R. (2004). Membrane domains. *Annual Reviews in Cell Developmental Biology*, 839-866:839–866.

[65] Myrray, R. K., Granner, D. G., and Rodwell, V. W., editors (2006). *Harper's Illustrated Biochemistry*. Mcgraw Hill Medical, New York, 27th edition.

[66] Naumowicza, M., Petelskaa, A. D., and Figaszewskia, Z. A. (2005). Impedance analysis of phosphatidylcholine -cholesterol system in bilayer lipid membranes. *Electrochimica Acta*, 50:2155–2161.

[67] Needham, D. and Hochmuth, R. M. (1989). Electro-mechanical permeabilization of lipid vesicles. role of membrane tension and compressibility. *Biophys. J.*, 55(5):10011009.

[68] Needham, D. and Nunn, R. S. (1990). Elastic deformation and failure of lipid bilayer membranes containing cholesterol. *Biophysical Journal*, 58:997–1009.

[69] Nelson, J. (2003). *The Physics of Solar Cells (Properties of Semiconductor Materials)*. Imperial College Press, London.

[70] Newbury, K. (2002). *Characterization, Modeling, and Control of Ionic Polymer Transducers*. PhD thesis, Virginia Polytechnic Institute and State University, Blacksburg, VA - 24061, USA.

[71] Nikolelis, D. P., Raftopoulou, G., Nikoleli, G.-P., and Simantiraki, M. (2006). Stabilized lipid membrane based biosensors with incorporated enzyme for repetitive uses. *Electroanalysis*, 18(24):2467 2474.

[72] Onsager, L. (1931). Reciprocal relations in irreversible processes. ii. *Phys. Rev.*, 38(12):2265–2279.

[73] Paradiso, J. A. and Starner, T. (2005). Energy scavenging for mobile and wireless electronics. *IEEE Pervasive Computing*, 04(1):18–27.

[74] P.Hangarter, R. (2007). Plants in motion - insectivorous plants. Web.

[75] RCSB (2005). Research collaboratory for structural bioinformatics (rcsb)protein data bank. Website. http://www.rcsb.org/pdb - generated using RasWin Molecule viewer.

[76] Romer, W. and Steinem, C. (2004). Impedance analysis and single-channel recordings on nano-black lipid membranes based on porous alumina. *Biophysical Journal*, 86:955–965.

[77] Saccani, J., Castano, S., Desbat, B., and Blaudezy, D. (2003). A phospholipid bilayer supported under a polymerized langmuir film. *Biophysical Journal*, 85:3781–3787.

[78] Sackmann, E. (1996). Supported membranes: Scientific and practical applications. *Science*, 271:43–48.

[79] Sadeghipour, K., Salomon, R., and Neogi, S. (1992). Development of a novel electrochemically active membrane and 'smart' material based vibration sensor/damper. *Smart Materials and Structures*, 1(2):172–179.

[80] Schultz, S. G. and Curran, P. F. (1970). Coupled transport of sodium and organic solutes. *Physiol. Rev.*, 50(4):637–718.

[81] Schulze, W., Reinders, A., Ward, J., Lalonde, S., and Frommer, W. (2003). Interactions between co-expressed arabidopsis sucrose transporters in the split-ubiquitin system. *BMC Biochemistry*, 4(1):3.

[82] Segel, I. H. (1968). *Biochemical Calculations - How to Solve Mathematical Problems in General Biochemistry*. John Wiley Sons, Inc.

[83] Shah, A., Torres, P., Tscharner, R., Wyrsch, N., and Keppner, H. (1999). Photovoltaic technology: The case for thin-film solar cells. *Science*, 285(5428):692–698.

[84] Shahinpoor, M., Bar-Cohen, Y., Simpson, J. O., and Smith, J. (1998). Ionic polymer-metal composites (ipmcs) as biomimetic sensors, actuators and artificial muscles - a review. *Smart Materials and Structures*, 7(6):R15–R30.

[85] Shakya, R. and Sturm, A. (1998). Characterization of source- and sink-specific sucrose/h+ symporters from carrot. *Plant Physiol.*, 118(4):1473–1480.

[86] Sibaoka, T. (1969). Physiology of rapid movements in higher plants. *Annual Review of Plant Physiology*, 20:165–184.

[87] Sodano, H. A., Inman, D. J., and Park, G. (2005). Comparison of piezoelectric energy harvesting devices for recharging batteries. *Journal of Intelligent Material Systems and Structures*, 16(10):799–807.

[88] Sondergaard, T. E., Schulz, A., and Palmgren, M. G. (2004). Energization of transport processes in plants roles of the plasma membrane h^+-atpase. *Plant Physiology*, 136:24752482.

[89] Spanner, D. C. (1978). The munch hypothesis, freeze-substitution and the structure of sieve-plate pores. *Ann Bot*, 42(2):485–488.

[90] Stein, W. D. and Lieb, W. (April 1972). Carrier and non-carrier models for sugar transport in the human red blood cell. *Biochemical Biophysica Acta*, 265(2):187–207.

[91] Steinem, C., Janshoff, A., Ulrich, W. P., Sieber, M., and Galla, H. J. (March 1996). Impedance analysis of supported lipid bilayer membranes: A scrutiny of different preparation techniques. *Molecular and Cellular Biology Letters*, 1279(2):169–180.

[92] Stevens, T. H. and Forgac, M. (1997). Structure, function and regulation of vacuolar h^+-atpase. *Annual Reviews in Cell Developmental Biology*, 13:779–808.

[93] Sundaresan, V. B., Akle, B., and Leo, D. J. (2006). Investigation on micro-patterned gold-plated polymer substrate for a micro hydraulic actuator. In Armstrong, W., editor, *Smart Structures and Materials: Active Materials: Behavior and Mechanics*, volume 6170.

[94] Suzuki, A. and Tanaka, T. (1990). Phase transition in polymer gels induced by visible light. *Nature*, 346(6282):345–347.

[95] Tamm, L. K. and McConnell, H. M. (1985). Supported phospholipid bilayers. *Biophys. J.*, 47(1):105–113.

[96] Tanaka, T. (1978). Collapse of gels and the critical endpoint. *Phys. Rev. Lett.*, 40(12):820–823.

[97] Tanaka, T., Fillmore, D., Sun, S.-T., Nishio, I., Swislow, G., and Shah, A. (1980). Phase transitions in ionic gels. *Phys. Rev. Lett.*, 45(20):1636–1639.

[98] Tanaka, T., Nishio, I., Sun, S.-T., and Ueno-Nishio, S. (1982). Collapse of gels in an electric field. *Science*, 218(4571):467–469.

[99] Tien, H. T. (1985). Planar bilayer lipid membranes. In *Progress in Surface Science*, volume (19)3, pages 169–274.

[100] Tien, H. T. and Ottova, A. L. (2001). The lipid bilayer concept and its experimental realization: From soap bubbles, kitchen sink, to bilayer lipid membranes. *Journal of Membrane Science*, 189:83–117.

[101] Timoshenko, S. (1959). *Strength of Materials: Part II: Advanced Theory and Problems*. Robert E Krieger Publishing, FL, USA.

[102] Trojanowicz, M. and Mulchandni, A. (2004). Analytical applications of planar bilayer lipid membranes. *Anal Bioanal Chem*, 379:347–350.

[103] Truernit, E. (2001). Plant physiology: The importance of sucrose transporters. *Current Biology*, 11:R169–R171.

[104] Wagner, M. L. and Tamm, L. K. (2000). Tethered polymer-supported planar lipid bilayers for reconstitution of integral membrane proteins: Silane-polyethyleneglycol-lipid as a cushion and covalent linker. *Biophysical Journal*, 79:1400–1414.

[105] Walz, D. and Caplan, R. S. (1986). The thermostatics and thermodynamics of cotransport revisited a restatement of the zero law. *Biochimica et Biophysica Acta*, 859(2):151–164.

[106] Weise, A., Barker, L., Kuhn, C., Lalonde, S., Buschmann, H., Frommer, W. B., and Ward, J. M. (2000). A new subfamily of sucrose transporters, sut4, with low affinity/high capacity localized in enucleate sieve elements of plants. *Plant Cell*, 12:1345–1355.

[107] Weiss, T. F. (1996). *Cellular Biophysics*. The MIT Press, Cambridge, MA, USA.

[108] Williams, L. E., Lemoine, R., and Sauer, N. (2000). Sugar transporters in higher plants - a diversity of roles and complex regulation:review article. *Trends in Plant Science*, 5:283–290.

[109] Williams, S. E. and Bennett, A. B. (1982). Leaf closure in the venus flytrap: An acid growth response. *Science*, 218(4577):1120–1122.

[110] Wilner, B. (May 1960). Variable capacitance liquid level sensors. *The Review of Scientific Instruments*, 31(5):501–507.

[111] Yang, W. Y., Hahn, Y. B., Nahm, K. S., and Lee, Y.-S. (2001). Chemical modification of skeletonized vesicles via hydrolysis. *Bulletin - Korean Chemical Society*, 22 - 12:1291–1292.

[112] Ye, J.-S., Cui, H.-F., Wen, Y., Zhang, W. D., Ottova, A., Tien, H. T., Xu, G. Q., and Sheu, F.-S. (2005). Self-assembly of bilayer lipid membrane at multi-walled carbon

nanotubes toward the development of photo-switched functional device. *Electrochemistry communications*, 7:81–86.

[113] Yoda, A. and Hokin, L. E. (1970). Commun 40. *Biochim Biophys Res*, pages 880–884.

[114] Yuan, C., O'Connell, R. J., Feinberg-Zadek, P. L., Johnston, L. J., and Treistman, S. N. (2004). Bilayer Thickness Modulates the Conductance of the BK Channel in Model Membranes. *Biophys. J.*, 86(6):3620–3633.

[115] Zimmerberg, J., Cohen, F., and Finkelstein, A. (1980). Fusion of phospholipid vesicles with planar phospholipid bilayer membranes. i. discharge of vesicular contents across the planar membrane. *J. Gen. Physiol.*, 75(3):241–250.

Appendix A

Capacitance meter

The amount of fluid transported through the membrane assembly of the proposed actuation concept is expected to be few hundred microliters. The first step in designing the system is to quantify the fluid flux through the membrane for an applied chemical stimulus. The instrumentation for measuring small volumes and at small flow rates (few microliters/min) are very limited and commercially available options are probihitively expensive or not feasible. To name a few - tracer based techniques, optic fiber based flow meters require expensive setup and post processing to obtain results. Also, an instrumentation that provides real-time data, every second or at least every minute is not available. Electronic flow meters are not designed to work in the anticipated range. The fluid in the top chamber is conductive and it makes it even more harder for manufacturers to package a sensor and calibrate a signal conditioner that can give a flow rate or volume measurement directly. This served as a motivation for fabricating a flow measurement system using sophisticated instruments already available.

A possible approach to quantify flow rate in a chamber is to monitor the liquid level. A liquid level sensor has been used on non-conductive and conductive liquids. Variety of equipments use liquid level sensors. To name a few, aircraft fuel sensor is a liquid level sensor, automotive fuel level sensor and in chemical processing plants use level sensing to measure volume and flow rate. All these systems require extensive calibration and specified operating conditions for performing as required. Liquid level sensors are potentiometric or variable capacitance type. The potentiometric type has a float that moves over a variable resistor, changing the resistances in a bridge network. The level of the liquid is obtained as a

voltage signal. In the case of a capacitance based system, the coupled electrical properties of the liquid and the sensor forms the basis for detecting liquid level. The signal conditioning equipment required for measuring capacitance requires measuring complex impedance of the system. The real and imaginary parts of the impedance measured can be used to compute the capacitance of the liquid sensor interface. An impedance analyzer readily available in any smart structures lab will be the most suited equipment to perform such a task. Fortunately CIMSS has two impedance analyzers - HP4192A and HP4194 capable of measuring not just impedance, but also capacitance directly. Furthermore, coming from Hewlett-Packard stable, they have built-in HPIB capabilities and hence can communicate over HPIB/GPIB/IEE488.2 bus to a laptop computer for recording real-time data. The instrument to measure volume and flux rate for the chemomechanical actuator had all the required sophisticated components, except for a sensor element.

A.1 Sensor configuration

The motivation and the required components to assemble an instrument is ready. A survey of materials is done to find available sensor elements. The sensor elements used in capacitance meters for measuring liquid level of conductive liquids always have an insulated wire and a conductive electrode that is kept immersed in the liquid. Using a wire insulation in a sensor element to measure small quantities of level change will be impaired by the wetting properties of the liquid. In the presence of conducting salts in the liquid, accumulation in the pores of the insulation will pose additional problems. To overcome this obstacle, an equivalent electrical network model is developed to analyze the feasibility of using a two metal electrodes as the sensor element. The inertness of platinum to aqueous medium made it an obvious first choice. Before discussing the sensor arrangement, a discussion on the principle of capacitance based sensing will ease the transition.

A.2 Capacitance based level sensing

The principle of capacitance based sensing is based on the complex impedance of an electrical network. The theory discussed here can be found in a variety of instrumentation textbooks and electrical catalogues. A good reference for understanding capacitance based liquid level sensing will be the article by Wilner[110]. The theory based on electric networks, nowadays

a common knowledge, is applied to the experimental setup to explain the working of a capacitance based liquid level measurement.

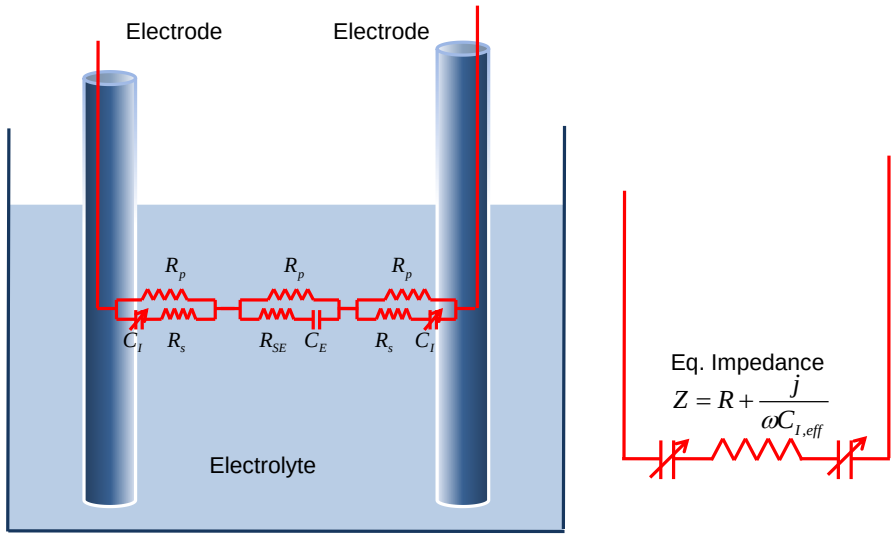

Figure A.1: Circuit equivalent: Capacitance based liquid level meter

A schematic of the experimental setup to measure liquid level is shown in Figure A.1. The capacitance measured in the capacitance meter is due to the dielectric properties of the electrode-liquid interface. The electrical double layer serves as the capacitor and the metal electrodes and the electrolyte serve as electrical conductors. A change in liquid level changes the capacitance of the interface. For a conductive fluid, the dielectric properties are dependent on the amount of dissolved ions at all concentrations and on the amount of non-electrolytes at significantly higher concentrations. For the two electrodes immersed in a conductive electrolyte to measure the liquid level, an equivalent electrical network can be used as shown in Figure A.1. Assuming that the series resistance is small at the interface and the parallel resistance is large, the double layer can be represented as a capacitor. It is represented as a variable capacitor a change in liquid level will change the capacitance of the interface. The electrolyte can be considered to behave like a conductor and the interfacial capacitance only will contribute to the capacitance measured in the network. The actual value of the interfacial capacitance is difficult to measure using the impedance analyzer due to the limitation in reliably measuring the complex impedance at frequencies of interest. But from the equivalent impedance, it can be observed that the resistor plays a minimal role in the network impedance at low frequencies. Two cylindrical wire configuration is

chosen to minimize the wetting area and hence to minimize the error introduced. Deriving a mathematical expression for the capacitance as function of the depth of immersion for a two cylindrical wires is also not directly feasible. Experimental calibration of the capacitance response is done to use this system for level measurement.

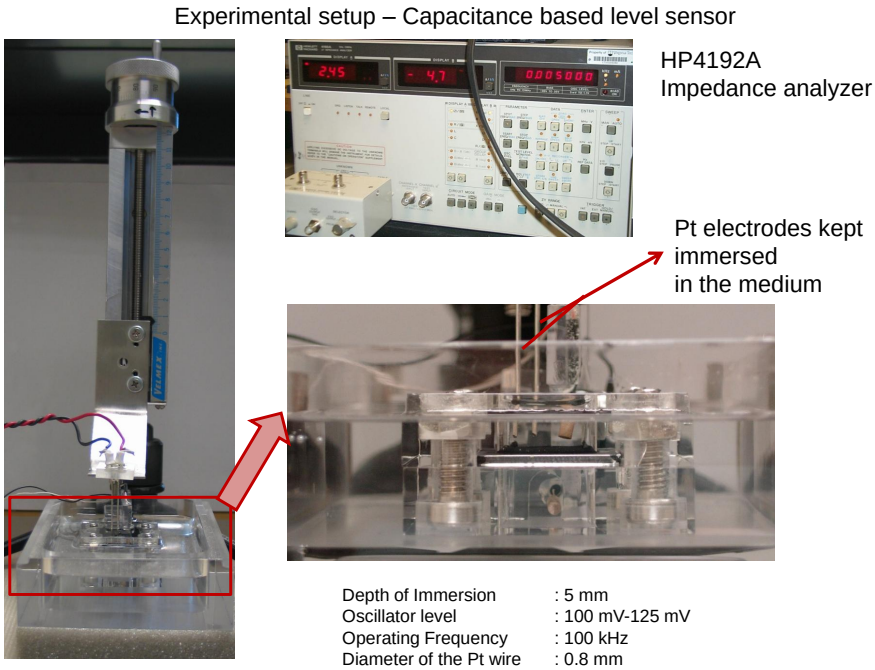

Figure A.2: Experimental setup: Capacitance meter calibration

A.3 Experimental setup

The capacitance meter used to measure volumetric flux through the membrane into a chamber is shown in Figure A.2. The Pt electrodes are mounted on a custom made fixture and attached to a micrometer slide. The two wires are connected to HP4192A impedance analyzer and a LabView program is written to communicate with the analyzer. The program sets the operating frequency and continuously requests for data on channel A and channel B of analyzer. The GPIB requests to the analyzer are handled by NI VISA 2.4 instrument driver and converted to the appropriate units in the VI program. The VI program can also set other relevant parameters like oscillator voltage, circuit mode and duration of data acquisition on the analyzer. The calibration experiments were done pH4.0 buffer, pH7.0 buffer, pH7.0 buffer with 10 mM, 20 mM, 50 mM and 500 mM sucrose concentration. It is

obesrved that the change in capacitance for the same depths of immersion were within 10% limits and on the following electrolytes for the same depths of immersion. The capacitance measured between electrodes is dependent on the pH of the medium. A litmus test was performed to confirm that the pH in the top chamber did not from pH7.0. Though this test is a qualitative test, it still assures that the change is capacitance is not due to a change in pH in the medium.

The impedance analyzer is operated in RC series circuit mode and capacitance measurements are taken at different frequencies (10 kHz, 50 kHz, 80 kHz, 100 kHz, 150 kHz) and at different depths of immersion of the Pt electrodes. The measurements from the impedance analyzer at lower frequencies (upto 50 kHz) are constantly drifting and is unreliable. This is due to instrument drift and is not observed in capacitance measurements at 100 kHz for different depths of immersion. Thus 100 kHz is chosen as the operating frequency for quantifying the level of liquid in the chamber.

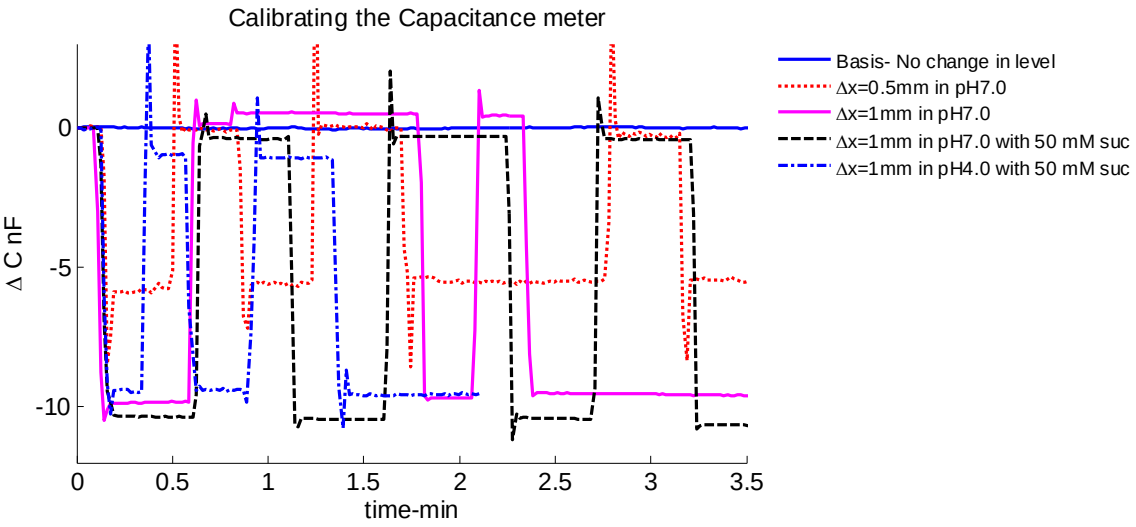

Figure A.3: Capacitance values from the meter

Once the operating frequency is chosen, the electrodes are immersed to 5 mm in the electrolyte in top chamber. The pH7.0 buffer is filled in the assay cup held in the transport experiment fixture shown in Figure 3.7. The impedance analyzer is set up to perform the data acquisition and the LabView program is started. The first test is to check if the capacitance can remain stable without any change in position in the electrodes. From the results shown in Figure A.3, there is no change in the measured capacitance

when there depth of immersion remains constant. After this preliminary test, the level of the electrode is slowly varied by turning the micrometer. The slide is brought down by 0.5 mm and an increase in capacitance is observed. This increase is due to the additional depth of immersion in the medium. The slide is raised and the capacitance decreases as the liquid drops behind the electrode. This procedure is repeated for different electrolytes and it is observed that the change in capacitance for different electrolyte is with 10% limits for 1 mm change in depth of immersion. The change in volume in the top chamber is computed by multiplying the change in level with the cross-sectional area of the chamber. The change in capacitance from 6 trials on pH7.0 buffer is shown in Figure A.4 and 95% confidence interval data limits are very convincing that the meter will have a high degree of repeatability to measure change in depth. The key to the success of this capacitance meter is the sophistication and high degree of accuracy with which the imepdance analyzer can measure imedance.

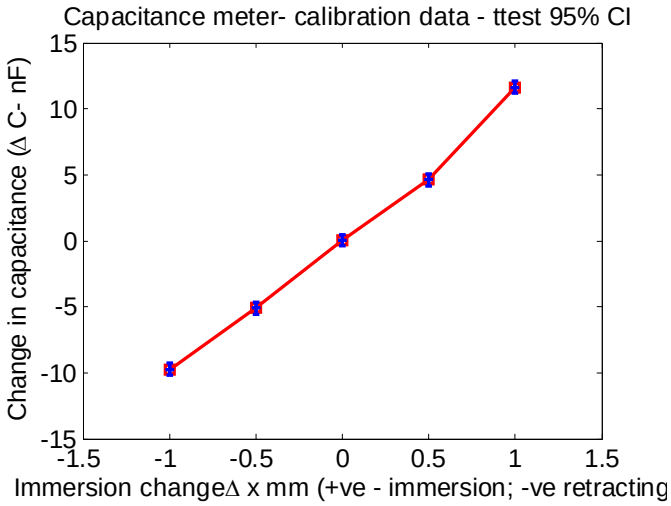

Figure A.4: Capacitance meter:Result

Appendix B

Copyright approval

Vishnu Baba S

From: Roger Hangarter [rhangart@indiana.edu]
Sent: Thursday, April 05, 2007 4:50 PM
To: Vishnu Baba S
Subject: Re: Plants-in-motion

Vishnu;

I am pleased that you enjoy the material on my website. You are certainly welcome to use my movies in your presentation and to reference them in your dissertation. I put them on the web for people to be able to use them in non-profit educational activities.

Good luck with your dissertation.

Best regards,
Roger

Roger P. Hangarter Office phone 812-855-5456
Indiana University FAX 812-855-6082
Myers Hall 352 email: rhangart@indiana.edu
915 E. 3rd St.
Bloomington, IN 47405-7107
http://bio.indiana.edu/~hangarterlab
http://plantsinmotion.bio.indiana.edu

On Apr 5, 2007, at 4:45 PM, Vishnu Baba S wrote:

> Hello Prof. Hangarter,
> I am graduate student in Mechanical Engg at Virginia Tech. I am
> writing to
> you to express my appreciation for the fantastic images and movies
> available
> in your website under "Plants in Motion".
> My dissertation involves using biological transport for
> Chemomechanical and
> chemo electrical energy conversion. I was wondering if it will be
> possible
> for me to use your two or three of your Nastic motion videos and
> reference
> your work in my PhD dissertation document with your consent. If
> yes, can you
> please send me a document that expresses your consent for the same.
> I can send you a draft copy of a pdf file with an embedded movie if
> you can
> permit me to use your movies.
> Thanks and Regards,
> Vishnu
>
>

Vita

Vishnu Baba Sundaresan was born on February 18, 1979 to Sundaresan Ganesan and Radha Sundaresan in Karur, India. Vishnu grew up in the south indian state of Tamil Nadu and did most of his schooling in Coimbatore. He attended PSG College of Technology and earned his Bachelor of Engineering in 2001. During his undergraduate course, he attended various internships in Coimbatore and Bangalore, India. Upon the completion of his Bachelors degree, he moved to Bangalore to work for Robert Bosch India for a few years which included a brief period with Gasoline Systems Division, Robert Bosch GmbH, Stuttgart, Germany. Vishnu moved to the United States in Jan 2003 for his Graduate program and started working with Dr. Donald J. Leo for his direct doctoral degree from Fall 2003. He won the Best Student Paper award for his work on Chemoelectrical energy conversion of adenosine triphospate in the SPIE Smart structures conference held in San Diego in March 2007. Vishnu defended his doctoral degree on 15$^{\text{th}}$ May 2007 to earn his Ph.D. in Mechanical Engineering.

Address: Center for Intelligent Material Systems and Structures
310 Durham Hall
Blacksburg, VA 24061-0261

This dissertation was typeset with LaTeX 2_ε[1] by Vishnu Baba Sundaresan.

[1] LaTeX 2_ε is an extension of LaTeX. LaTeX is a collection of macros for TeXwhich is a trademark of the American Mathematical Society. The macros used in formatting this dissertation were written by Greg Walker and updated by Vishnu Baba Sundaresan and Jamil Renno, Department of Mechanical Engineering, Virginia Polytechnic Institute and State University.